Special Research Paper

# SEISMIC DRIFT OF REINFORCED CONCRETE STRUCTURES

By

K. SHIMAZAKI

&

Mete A. SOZEN

# SEISMIC DRIFT OF REINFORCED CONCRETE STRUCTURES

By

Kazushi Shimazaki

and

Mete A. Sozen

## Synopsis

Nonlinear displacement response of reinforced concrete structures is investigated by a parameteric study of single-degree-of-freedom systems with appropriate hysteresis properties. Strength, stiffness, and the type of ground motion are the main variables considered. It is shown that a set of dimensionless parameters defining the three variables can be used to determine nonlinear displacement response from linear-response spectral values. The evaluation of this relation by data from 34 tests shows satisfactory results. This conclusion leads to a simple method for estimating maximum seismic drift.

## Key Words

Reinforced Concrete, Earthquake Response, Ground Motions
Nonlinear Systems, Response Spectra, Energy Spectra,
Earthquake-Resistant Design, Single-degree-of-freedom System

# ACKNOWLEDGMENTS

The first writer participated in this study while he was a visiting scholar at the University of Illinois supported by Hazama-gumi, Ltd., Tokyo, Japan, in connection with the U.S.-Japan Cooperative Research Program Utilizing Large-Scale Testing Facilities.

The first writer gratefully acknowledges Professor Watabe, Tokyo Metropolitan University, Building Constructor's Society, Tokyo, Japan, and Dr. Fujita and Mr. Miyazaki of Hazama-Gumi, Ltd., Tokyo, Japan, about their efforts for visiting and their support.

The first writer also wishes to record his appreciation for the generous help at the early stage of this study by Professor French of the University of Minnesota and Mr. Rothe, former graduate research assistants, and for valuable suggestions from A. Schultz, S. Wood, and other assistants.

D. Bever, is thanked for typing this report. The CDC Cyber 175 computer system of Computing Services Office and the DEC LSI/23 computer system of the Civil Engineering Department of the University of Illinois were used for the computations. Support was provided by the National Science Foundation, grant CEE-81-14977.

# TABLE OF CONTENTS

# LIST OF TABLES

# LIST OF FIGURES

# SEISMIC DRIFT OF REINFORCED CONCRETE STRUCTURES

## 1. INTRODUCTION

Distortion of a reinforced concrete structure caused by strong ground motion is an important factor in the planning and proportioning of reinforced concrete structural systems. Most of the generalizations about seismic response may be related to Newmark's observations of nearly constant response ranges of acceleration, velocity, and displacement, and how the magnitudes of these ranges can be modified on the basis of tolerable ductility limits. Early tangible evidence for Newmark's initial observations related to earthquake response rests in two studies (Sheth 1959, Veletsos 1960) of dynamic response using elasto-plastic models with equal and constant loading/unloading slopes. Recently, Otani (1981) re-evaluated the effect of differences in hysteresis models on response. His results generally confirmed Newmark's insights but indicated that for systems with periods less than 0.15 sec. the required ductility tended to be more than that anticipated.

In 1975, Kato and Akiyama (1975) returned to Housner's energy input concept (Housner 1956) for ground-motion intensity to structural damage. This work led to methods of design with energy as the basic principle (Akiyama 1980). In an evaluation of structural response in relation to dissipated energy, Suzuki and Takeda (1981) noted that the nonlinear displacement response of a single-degree-of-freedom system had different characteristics in regions of constant-acceleration and constant-velocity response.

The work presented in this paper builds on ideas from the above sources to arrive at simple generalizations about the relationship of nonlinear to linear displacement response for reinforced concrete structures. The first part of this paper reports the results of a parametric study to investigate the effects of strength, stiffness, and type of ground motion on nonlinear displacement response. It is shown that nonlinear displacement response of analytical models with force-displacement properties similar to those of reinforced concrete under cyclic loads can be related simply and satisfactorily to linear-response spectral values using dimensionless parameters for strength, initial stiffness, and the type of ground motion. This conclusion leads to a simple method for estimating maximum seismic drift. The report also contains an evaluation of this method using data from 34 tests.

# 2. GROUND MOTION

## 2.1 Ground Motion Records

Nine earthquake records indicated in Table 2.1 were selected for response studies.

Table 2.2 shows reported geological properties of the sites where the records were obtained. Accelaration data for motions 8 and 9 were obtained from the files at the Building Research Institute, Tsukuba, Japan. Data for the other seven motions were obtained from U.S.G.S.

Because most of the spurious information in ground-motion records tends to be concentrated in the extreme low- and high-frequency components of the signal, Trifunac (1973) recommended that a record filtered to eliminate those components would provide a good representation of the actual motion. All nine sets of ground-motion data were filtered using the procedure proposed by Hodder (1983). Hodder's procedure was selected because it is easy to use and because its results are in close agreement with those obtained using the lengthier procedure proposed by Sunder and Connor (1982).

Main features of Hodder's filtering process are shown in Fig.2.1. Components below 24.5 Hz are passed and those above 25.5 Hz are stopped by the filter. In the transition zone from 24.5 Hz to 25.5Hz, the signal components are modified by:

$$\sin^2 \left[\frac{\pi}{2} \frac{25.5 - f}{25.5 - 24.5}\right] = \sin^2 \left[\pi * (25.5 - f)/2.0\right] \qquad (2.1)$$

where f is the frequency of the signal component considered.

For the high-pass filter, the transition zone starts at a frequency ($f_s$ + 0.15) and ends at a frequency of $f_s$. The frequency $f_s$ is the larger of 0.1 Hz and $3/T_L$, where $T_L$ is the duration of the record. In this study, frequency $f_s$ was 0.1 Hz for all records. In the 0.15-Hz range of transition, the signal component is multiplied by:

$$\sin^2 \left[\frac{\pi}{2} \frac{f - f_s}{0.15}\right] = \sin^2 \left[\pi * (f - f_s) / 0.3\right] \qquad (2.2)$$

Filtered acceleration records and computed velocity and displacement histories are shown in Fig. 2.2 through 2.10 for twenty seconds of each record. Velocity and displacement responses are obtained by integration using the linear acceleration procedure. Initial velocity was set at a value chosen to avoid a nonzero value for calculated displacement after strong motion. To determine the initial velocity, acceleration records were first integrated with respect to time assuming zero initial velocity and displacement. Then the displacement response after the defined end of strong motion was approximated by a straight line fitted using the least squares method. The slope of that line was chosen to be the initial velocity. Thus there was no calculated increase in average ground displacement after end of strong motion. Initial displacement was set at zero.

Calculations to obtain the beginning and end time of strong motion were made using the modified method suggested by Noayyad and Mohraz (1982). The end of the strong motion was defined to be the time after which the slope of the cumulative root mean square function (RMS) as given in Eq. 2.3 stopped exceeding 1.0 cm/sec /sec.

$$RMS(t) = \left[\frac{1}{t} \int_0^t \ddot{x}_g(u)\, du\right]^{1/2} \qquad (2.3)$$

To obtain the beginning time, the same procedure was repeated starting at the end of the record and proceeding backwards. The durations of strong motion so determined are shown in Table 2.1.

## 2.2 Response Spectra

Calculated displacement and energy response spectra for the nine ground motions are shown in Fig. 2.2 through 2.10. Response spectra were calculated using the Nigam-Jennings method (1964) based on the first fifteen seconds of each acceleration record. The same method of integration of the equation of motion was used for energy response spectra. The entire method is described below.

Equation of motion of a linearly elastic SDOF system is:

$$m\ddot{x} + c\dot{x} + kx = -m\ddot{x}_g \qquad (2.4)$$

where

$m$ : mass

$c$ : coefficient of viscous damping

$k$ : stiffness constant

$x, \dot{x}, \ddot{x}$ : displacement, velocity, and acceleration of mass with respect to base

$\ddot{x}_g$ : acceleration of base

Equation 2.4 is written in terms of forces. It can also be written as a statement of energy balance during a very short time increment $\Delta t$.

$$m\ddot{x}(t) \cdot \Delta x + c\dot{x}(t) \cdot \Delta x + kx(t) \cdot \Delta x = - m\ddot{x}_g (t) \cdot \Delta x \qquad (2.5)$$

To show the relation of Eq. 2.5 to familiar forms of energy, it may be integrated over a time period, t, recognizing that $\Delta x = x \cdot \Delta t$ with $\Delta t$ approaching zero,

$$m\int_0^t \ddot{x}\dot{x}dt + c\int_0^t \dot{x}^2 dt + k\int_0^t \dot{x}x dt = -m\int_0^t \ddot{x}_g \dot{x} dt \qquad (2.6)$$

Integrating by parts,

$$\frac{m}{2}\left[\dot{x}(t)\right] + \frac{k}{2}\left[x(t)\right] + c\int_0^t \dot{x}^2 dt = -m\int_0^t \ddot{x}_g \dot{x} dt \qquad (2.7)$$

The terms in Eq. 2.7 are interpreted as:

Kinetic Energy + Potential Energy + Dissipated Energy = Input Energy

The energy response spectrum can also be obtained from the Fourier Amplitude Spectrum (Takizawa 1977). The approach is described below because it helps identify the relationship of the Energy Response Spectrum to the Fourier Amplitude Spectrum, because it helps explain characteristics of the energy response spectrum, and because it will be used to explain changes in input energy with increase in period related to nonlinear response.

The relationship between the energy response and Fourier amplitude spectra is derived below starting from definitions of the Fourier transform (Eq. 2.8)

$$\ddot{X}_g(\omega) = \int_{-\infty}^{\infty} \ddot{x}_g(t)\, e^{-i\omega t}\, dt \qquad (2.8a)$$

$$\dot{X}(\omega) = \int_{-\infty}^{\infty} \dot{x}(t)\, e^{-i\omega t}\, dt \qquad (2.8b)$$

and Parseval's identity (Eq. 2.9)

$$\int_{-\infty}^{\infty} f(t)\, \overline{g(t)}\, dt = \frac{1}{2\pi} \int_{-\infty}^{\infty} F(\omega)\, \overline{G(\omega)}\, d\omega \qquad (2.9)$$

where, the bar denotes the complex conjugate and $F(\omega)$ and $G(\omega)$ are Fourier transform of $f(t)$ and $g(t)$.

As indicated by Eq. 2.7, response energy is defined as the integral, from time zero when ground motion starts to a time t when strong ground motion is assumed to have stopped, of the product of mass, the ground acceleration, and the relative velocity of the mass. Ground acceleration is assumed to be zero before and after the period of strong ground motion. The range of the integral may be extended from minus to plus infinity without changing the value of the integral for response energy, RE.

$$RE = - m \int_{-\infty}^{\infty} \ddot{x}_g\, \dot{x}\, dt \qquad (2.10)$$

Equation 2.10 may be expressed in its complex form.

$$RE = - m \ \text{Real} \left[ \int_{-\infty}^{\infty} \ddot{x}_g\, \dot{\bar{x}}\, dt \right] \qquad (2.11)$$

The form of Eq. 2.11 makes it possible to use Parseval's identity to transfer the response energy expression from the time to the frequency domain to obtain Eq. 2.12

$$RE = -\frac{m}{2\pi} \quad \text{Real}\left[ \int_{-\infty}^{\infty} \ddot{X}_g(\omega)\dot{\bar{X}}(\omega)\, d\omega \right] \tag{2.12}$$

Recognizing that the conjugate velocity term may be defined as the product of the conjugate acceleration term and the velocity transfer function in the frequency domain.

$$\dot{\bar{X}}(\omega) = -i\omega H(\omega)\bar{\ddot{X}}_g(\omega) \tag{2.13}$$

Eq. 2.12 is rewritten

$$RE = \frac{m}{2\pi} \quad \text{Real}\left[\int_{-\infty}^{\infty} i\omega H(\omega)\ddot{X}_g(\omega)\, \bar{\ddot{X}}_g(\omega)\, d\omega\right] \tag{2.14}$$

It is seen that the product of the acceleration term and its conjugate in Eq. 2.14 eliminates the imaginary components of the two terms. Equation 2.14 may be rewritten as

$$RE = \frac{m}{2\pi} \left[\int_{-\infty}^{\infty} \text{Real}\left[i\omega H(\omega)\right] \left|\ddot{X}_g(\omega)\right|^2 d\omega \right. \tag{2.15}$$

Expanding the transfer function,

$$RE = \frac{m}{2\pi} \left\{\int_{-\infty}^{\infty} \text{Real}\left[\frac{i\omega}{\omega_o^2 - \omega^2 + 2i\beta\omega_o\omega}\right] \left|\ddot{X}_g(\omega)\right|^2 d\omega\right\} \tag{2.16}$$

where, $\omega_o$ is the frequency of the system ($\sqrt{k/m}$) and $\beta$ is the damping factor.

The real part of the term in brackets is obtained by multiplying both the numerator and the denominator by the term $((\omega_o^2-\omega^2)-2i\beta\omega_o\omega)$ to obtain Eq. 2.17

$$RE = \frac{m}{2\pi} \int_{-\infty}^{\infty} \frac{2\beta\, \omega_o\, \omega^2}{(\omega_o^2 - \omega^2)^2 + 4\beta^2\omega_o^2\omega^2} \left| \ddot{X}_g(\omega) \right|^2 d\omega \qquad (2.17)$$

Equation 2.17 is symmetrical with respect to a line drawn at origin perpendicular to the $\omega$ axis. The range of integration may be changed to extend from zero to infinity if the entire right-hand side of the equation is doubled.

$$RE = \frac{m}{2\pi} \int_{0}^{\infty} \frac{4\beta\omega_o\, \omega^2}{(\omega_o^2 - \omega^2)^2 + 4\beta^2\omega_o^2\omega^2} \left| \ddot{X}_g(\omega) \right|^2 d\omega \qquad (2.18)$$

Equation 2.18 is rewritten using the definition of a "weighting function", $W(\omega)$

$$W(\omega) = \frac{4\beta\omega_o\omega^2}{\pi\left[(\omega_o^2 - \omega^2)^2 + 4\beta^2\omega_o^2\omega^2\right]} \qquad (2.19)$$

to yield a compact form of Eq. 2.15 for response energy

$$RE = \frac{m}{2} \int_{0}^{\infty} W(\omega) \left| \ddot{X}_g(\omega) \right|^2 d\omega \qquad (2.20)$$

Fig. 2.11 shows the shape of Eq. 2.19 with various damping factors.

In reference to Eq. 2.20, it may be said that the energy spectrum is a square of the Fourier spectrum (or the power spectrum) smoothed with a velocity transfer function used as a weighting function, and it is independent of the Fourier phase spectrum.

In the time-domain approach, the input energy for an oscillator of given stiffness and viscous damping, the left-hand side of Eq. 2.5 is evaluated numerically for calculated acceleration, velocity, and displacement responses

for any specified part of a given ground-motion record. The maximum energy, $E_m$, determined during this process is the spectral value for the period and damping factor of the oscillator. The input energy is not a monotonically increasing function, and the maximum value may not be observed at the end of strong motion, so that calculated energy spectrum is not necessarily the same as one obtained by Eq. 2.20. In a damped system it may be assumed that the maximum value occurs at the end of strong motion. The difference between the maximum energy response and the response at the end may be disregarded. Figure 2.12 is a energy spectra obtained by Eq. 2.20 for the El Centro 1940 N-S record. Comparing it with the input energy in Fig. 2.6, it may be concluded that the differences are not objectionable.

A convenient form for presenting energy response is the equivalent velocity, $V_m$.

$$V_m = \sqrt{2E_m/m} \tag{2.21}$$

where $E_m$ is maximum input energy and m is mass of the oscillator.

The dominant features of the energy spectra represented by the equivalent velocity are (Fig. 2.2 through 2.10):

1. Response energy increases at a steady rate with increase in period from the origin up to a certain characteristic period, to be designated TG in this report.

2. Response energy tends to remain constant with increase in period from TG to a certain period above TG.

3. Response energy tends to decrease at a low rate as period increases above TG.

4. The equivalent velocity, $V_m$, becomes asymptotic to the maximum ground velocity, $|\dot{x}_g|_{max}$, at a period of infinity. However, $V_m$ goes to zero at a period of infinity if Eq. 2.20 is used, because the Fourier amplitude spectrum is zero at that period.

Midorikawa (1984) has noted that the rate of variation of the term $V_m$ (item 3 above) with period depends on the location of the strong-motion instrument in relation to the development of the fault. If the fault develops processing toward the instrument lacation, $V_m$decreases slowly with increase in period. If the fault develops progressing away from the instrument location, $V_m$ decreases at a faster rate with increase in period.

## 2.3 Characteristic Period for the Ground Motion

Akiyama (1980) has suggested that the energy response spectrum can be represented ideally by two straight lines with the first line going through the origin and the second representing a "flat" bound enveloping the energy response spectrum of $\beta = 0.10$. The period at the intersection of these two portions, TG, usually occurs at a value comparable to the period at the intersection of the constant-acceleration and constant-velocity response regions. In this paper, it will be called the characteristic period of the ground motion. The characteristic periods for the ground motions selected are indicated in Fig. 2.2 through 2.10 and in Table 2.1.

The ground motion at the surface of a certain site can be obtained from the motion at the base rock by multiplying the transfer function in the frequency domain using the equivalent linear method (Kanai 1951, Schnabel 1972). The response spectrum at the base rock may be obtained from the Ohsaki spectrum (Hisada 1978) as a function of magnitude and epicental distance of

earthquakes. The Ohsaki spectrum suggests that the characteristic period vary with the magnitude and epicental distance of the earthquake. Figure 2.13 shows the Ohsaki spectrum.

Because the transfer function depends on the property of ground, and that property varies with strain depending on the intensity of ground motion, the intensity is another important factor for determining TG. For evaluating the intensity of ground motion as a peak velocity, Hisada (1978) recommended to use Kanai's empirical expression.

$$V_{peak} = 10^{0.61M - \log_{10}X - Q} \qquad (2.22)$$

where,

$P = 1.66 + 3.60/ X$

$Q = 0.631 + 1.83/ X$

M : Magnitude

X : Focal distance in km

This equation shows the intensity of the ground motion as a function of its magnitude and focal distance.

Accordingly, the characteristic period, TG, is given as a function of type of earthquake (magnitude, epicentral distance and focal distance) and property of a ground. The characteristic period, TG, is not likely to be constant at a certain site.

To show the variation of TG with type of earthquake, one example is given below.

Fig. 2.14 shows the calculated amplification function (Absolute value of the complex transfer function) at an alluvium site in Sendai, Japan (Sibuya 1980).

The approximate fundamental site period can be calculated from Eq. 2.23.

$$T_1 = \frac{4H}{V_s} \qquad (2.23)$$

where H is the thickness of the layer and $V_s$ is the shear velocity of the layer.

Assuming the mean value of $V_s$ to be approximately 200m/sec. in the 23m layer, Eq. 2.23 gives 0.45 sec. as $T_1$. This value corresponds to the second peak in Fig. 2.14. The first peak at about 0.18 sec. may correspond to the second mode period which is approximately one-third of the first mode period in theory. The equivalent damping of the soil is assumed as a complex damping (not viscous damping), the amplification of higher modes does not decrease so much.

Here, we consider two earthquakes;

I. $M = 7$, $\Delta = 150$ km

II. $M = 7$, $\Delta = 10$ km

The Ohsaki response spectrum is constructed simply using only the point C in Fig. 2.13. In the arithmetric scale it is assumed to vary as shown in Fig. 2.17a with the break point corresponding to point C. The simplifided Ohsaki spectra are constructed for a peak velocity of 10 cm/sec. Multiplying the amplification function shown in Fig. 2.14 leads to Fig. 2.15c and 2.15d depending on the earthquake. TG of Type I earthquake differs from that of Type II earthquake; the former corresponds to the first mode period, while the latter corresponds to the second mode period.

For a soft site with only a few layers of soil having different stiffnesses, however, the amplification function has a single peak at long period range. At that period, the Ohsaki spectra indicate constant velocity response with

incresing period independent of epicentral distance and magnitude, so that TG is likely to be a function primarily of the soil properties for such a site.

# 3. HYSTERESIS MODELS

The five hysteresis models used are illustrated in Fig. 3.1.

Hysteresis model 1 is the well-known elasto-plastic model with constant slope for loading and unloading. Even though it is a poor representation of the actual response for most structural engineering materials, it is useful because it represents a reasonable upper bound for energy dissipation.

Hysteresis model 2, used to represent reinforced concrete by Clough and Johnston (1966), differs from model 1 because of changes in the stiffness of the loading slope.

Hysteresis model 3, used by Otani (1981) as a simplified version of the Takeda hysteresis (Takeda 1970) for reinforced concrete, is similar to model 2 except for the unloading slope which varies with loading history as indicated by Eq. 3.1.

$$k_r = k_y \left| \frac{x_m}{x_y} \right|^{-\alpha} \tag{3.1}$$

$k_r$ : unloading stiffness

$k_y$ : yielding stiffness

$x_m$ : maximum displacement

$x_y$ : yielding displacement

$\alpha$ : constant defining unloading stiffness.

Hysteresis model 4 was used to represent the slip phenomenon of reinforced concrete members or structures. This is a simplified version of the Takeda-Slip model (Takeda 1977) with zero stiffness during slip and differs from model 3 only by the portions representive slip.

Hysteresis model 5 may be considered to be a variant of model 1. The main

difference is the "slip"; loading in either direction does not start unless the point on the displacement axis corresponding to the immediately previous unloading is reached.

Relative energy dissipation capabilities of the first four models may be compared by using the equivalent viscous-damping values defined by Jacobsen (1960).

For model 1, the equivalent viscous damping is given by Eq. 3.2.

$$\beta_1 = 2 * (1 - 1/\mu)/\pi \qquad (3.2)$$

$\beta_1$ : equivalent viscous damping for hysteresis model 1

$\mu$ : ratio of maximum to yield displacement

This value is considered the maximum value so the capability of hysterical energy dissipation.

For models 2 and 3,

$$\beta_{2,3} = (1 - \mu^{\alpha-1})/\pi \qquad (3.3)$$

$\beta_{2,3}$ : equivalent viscous damping for hysteresis models 2 and 3.

For model 4,

$$\beta_4 = (1 - \mu^{\alpha-1})/2\pi \qquad (3.4)$$

$\beta_4$ : equivalent viscous damping for hysteresis model 4.

Variations of the equivalent viscous-damping factors with the ductility ratio are compared in Fig. 3.2 for the first four models. The damping factors plotted refer to constant-amplitude cycles and are not directly relevant to earthquake response, but they do provide a measure of the relative capabilities of the hysteresis systems to dissipate energy. Although a comparable value cannot be calculated directly for model 5, it is plausible to assume that model 5 has less energy-dissipation capability than the other four models.

# 4. CALCULATED DISPLACEMENT RESPONSE

## 4.1 Parametric Study for Nonlinear Response

To study the trends of calculated displacement response, calculations were made for a number of single-degree-of-freedom oscillators in the same manner as previous studies (Veletsos 1960).

Dynamic response was determined using Newmark's beta method (Newmark 1959), with beta set at 1/6. At instants of slope-change of the assumed hysteresis, iterations were continued until both the equation of dynamic equilibrium and the overall hysteresis relationship were satisfied. Response was determined for a duration of fifteen seconds for each ground-motion record. Time interval was the smaller of 0.01 sec. and $T_o/20$, where $T_o$ is the initial period of the oscillator. The damping factor, which varied linearly with the stiffness, was assumed to have an initial value of 0.02.

The organization of the parametric studies is illustrated by the arrangement of Fig. 4.1. Two different initial stiffnesses were considered. Calculations for oscillators with an initial period of 0.3 sec are summarized in the top row of three plots and those for oscillators with an initial period of 1.0 sec are summarized in the bottom row of three plots. Response was determined for the three typical ground motions attributed to short, medium, and long characteristic periods, leading to the six plots in Fig. 4.1. Each plot includes five curves, one for each of the hysteresis models discussed. For each hysteresis model, calculations were made successively for a series of single-degree-of-freedom oscillators of decreasing strength, 100%, 90%, 80%, .... 20%, 10%, 5% of linear response at a damping factor of 0.02. The

horizontal line in each figure represents the displacement corresponding to linear response.

The abscissas in Fig. 4.1 refer to the base shear strength coefficient, $C_y$, which defines the force at the initial break point (yielding) of the assumed force-displacement relationship as a ratio of the assumed weight of the oscillator. The ordinates are given in mm. Because of the low displacements calculated, displacement data for the Castaic record were plotted with a different scale.

For each combination of period and ground motion, the trends of the five curves obtained for different hysteresis models can be said to be generally similar. The curves for models 1-4 are more consistent with each other than with the curve for hysteresis model 5. The magnitudes of the response displacement for an oscillator of given strength are different for different hysteresis models. For the 0.3-sec. oscillator, the relative magnitudes of the displacement curves are in an order consistent with the equivalent damping implied by the hysteresis models, especially for the El Centro and Hachinohe motions. This result is attributed to the fact that the assumed shapes of the force-displacement relationship have more influence on energy dissipation if the displacement attained is large and the yield displacement is small.

## 4.2 Normalized Nonlinear Response

The data in Fig. 4.1 have been presented without modification to account for differences in intensity of the acceleration records. To permit direct comparisons among the displacement responses calculated for the three ground motions, a normalizing scheme was devised. Displacements and base shear strength coefficients were plotted as ratios of corresponding linear-response

quantities calculated for a damping factor of 0.02.

Displacement, DR, and strength, SR, ratios are defined below.

$$DR = D_n/D_S \tag{4.1}$$

$$SR = C_y/(A_S/g) \tag{4.2}$$

where,

$D_S$, $A_S$ : displacement and acceleration responses for a linear oscillator with initial period $T_o$

$D_n$ : displacement resopnse for a nonlinear oscillator with initial period $T_o$

$C_y$ : base shear strength coefficient (shear strength/weight)

$g$ : acceleration of gravity

Figure 4.2, shows the relationship between normalized displacement and base shear strength for model 2, 3, and 4. Each plot compares the response to the three ground motions for oscillators having the same initial period.

For oscillators with a 0.3-sec. initial period in the top row, the displacement ratio varies at different rates with the strength ratio, the rate depending on the ground motion and on the hysteresis model. Because the plotted quantities have been normalized with respect to spectral response, it is assumed that the observed differences depending on the ground motions are caused by the differences in frequency content and, possibly, sequence rather than by differences in acceleration magnitudes.

The displacement data in Fig. 4.2 refer to cases with base shear strength less than that required for linear response with a damping factor of 0.02. In every case up to a strength ratio of unity, calculated response extended beyond the break point in the assumed force-displacement relationship. As a result of increasing displacement, the effective period increased and, in keeping with

the assumed hysteresis model, the capability to dissipate energy or the area included in the largest hysteresis loop increased. Accordingly, if the initial period of the oscillator is above the characteristic ground period TG, an increase in the effective period does not cause an increase or causes a small decrease in the energy demand. Under those conditions, the oscillator is able to dissipate the energy with little or even no further increase in displacement above that for linear response. However, if the initial period of the oscillator is below TG, and increase in the effective period is likely to result in an increase in the energy demand. The displacement response has to increase to dissipate the energy. Because the energy dissipated depends on the strength of the system as well as on displacement, the required increase in the displacement ratio is a function of the strength ratio; the increase in the displacement ratio decreases with increase in the strength ratio.

However, it should be noted that the maximum displacement is not a direct function of the input energy. The input energy is a sum of a damping energy ($E_d$) and a hysteresis energy ($E_h$), and the hysteresis energy is related to the integral of displacement response, and not to maximum displacement response. These will be discussed in a later section.

## 4.3 Displacement Response for Reinforced Concrete Structures

The rationalization presented in the previous section suggests that the displacement ratios may be normalized to reflect the effect of the type of ground motion using the hypothesis that oscillators having similar period ratios, TR = $T_o$/TG (initial period of the oscillator/characteristic period for the ground motion), will have similar variations of the displacement ratio, DR, with the strength ratio, SR. Figure 4.3, tests this hypothesis for model 3

which has led to satisfactory results for determining maximum displacement response of reinforced concrete structural models (Saiidi 1979). Each one of the six plots in Fig. 4.3 compares variations of the displacement ratio, DR, with the strength ratio, SR, for equal values of the period ratio, TR, ranging from one-third to twice the period TG. In general, the data in the six plots indicate that the choice of the period ratio, TR, is appropriate for organizing the results of calculated displacements. There are some discordances. At TR = (4/3), data for Hachinohe tend to lie high. At TR = (2/3), the values for El Centro separate from the other two for low strength ratios. The calculated spectral response curves for Hachinohe (Fig. 2.10) show that it has very low response in the range 1.4 to 1.9 sec. Idealizing the displacement spectrum promises to improve consistency in Fig. 4.3.

A simple subjective procedure was used for determining the idealized response spectra by using the calculated response spectra for a damping factor of 0.02 as shown in Fig. 4.4. First, a line passing through the origin was chosen to provide a reasonable fit to the calculated curve between the periods TG and 2TG (Line AB in Fig. 4.4). It was assumed that the idealized spectrum for a damping factor of 0.02 would be line CD obtained by doubling the ordinates of line AB (Shibata 1976). The idealized spectrum in the period range (TG/3) to TG was assumed to vary as the square of the period and have the ordinate 2DG at TG. The idealized spectra used are shown in Table 4.1 for nine ground motions.

Relationships between displacement and strength ratios based on idealized spectral response are shown in Fig. 4.5 for all nine ground motion records. The data plotted in Fig. 4.5 demonstrates that the parameters selected for normalizing displacement response are appropriate.

Figure 4.6 shows the effect of hysteresis models for the same period ratios used in Fig. 4.5. Responses were calculated for El Centro 1940 N-S record. It is seen that, for $T_O \geq TG$, responses calculated for the five hysteresis models tend to cluster together. For $T_O < TG$, response results for models 2, 3, and 4 tend to be the same but those for models 1 and 5 are perceptibly different from the rest and from each other.

From the trends of the normalized data in Fig. 4.5 and sensitivity to hysteresis models observed in Fig. 4.6, the nonlinear response for reinforced concrete structures may be divided into two regions on a plane defined by TR and SR.

I. TR + SR > 1.0.

The displacement ratio is likely to be approximately unity and independent of the shape of a hysteresis model. Therefore, displacement response can be satisfactorily estimated using the spectral response value for a damping factor of 0.02.

II. TR + SR < 1.0.

Displacement ratio will vary with the strength ratio. Displacement may be estimated by using the curves in Fig. 4.5. However, it is necessary to know the type of hysteretic response. For reinforced concrete systems not valuerable to prematave shear or bond failures, models 2 and 3 would be plausible.

## 4.4 Maximum Nonlinear Displacement Response

Previously the nondimensionalized response calculations were presented only for Model 3 because it is believed that it represents reinforced concrete structures failing in flexure reasonably well. In order to study the

applicability of the trends observed to other structures having different hysteresis relationships, it is relevant to look at displacement response calculated on the basis of Models 1, 2, 4, and 5 which are shown in Fig. 4.7 through 4.10.

From the data presented in these figures it is seen that for ranges where period ratios exceeding one, the data tend not to exceed unity for all four types of hysteresis models. Clearly, in that range of period ratios the trends observed below would apply to systems made of other materials that have hysteretic response relationships in the range of the relationships considered.

For period ratios less than unity, it is observed a different sensitivity to the strength ratio for the different hysteresis models. This observation can be summarized as indicated in Fig. 4.11. The data in Fig. 4.11 refer to all five hysteresis models for cases with the three period ratios less than one. The points on the plot, given for each hysteresis model individually, represent the strength ratio for a given period ratio above which the displacement ratio exceeds unity. In effect, then, the locations of the points represents the domain above which the displacement ratio is likely to be equal to or less than unity.

It is seen that a simple generalization can be made about the first four models. That represents the broken straight line connecting a strength ratio of one to a period ratio of one. Data within the triangle defined by that line would be considered to be in the range where the displacement ratio may exceed one.

The variation, however, depends on the hysteresis model and the plotted data do not vary linearly. These plotted data may be represented by Eq. 4.3.

$$SR = 0.9\ e^{-TR/\alpha} + 0.1 \qquad (4.3)$$

where $\alpha$ is a constant that depends on the hysteresis model.

Curve No. 1 with $\alpha = 0.3$ in Fig. 4.11 represents the variation of first four models. The trend of Model 5 can be represented by curve No. 2 with $\alpha = 0.9$.

It is also interesting to note that Model 5 is more sensitive than Model 1 and that in general the sensitivity of the various hysteretic models varies in relation to their designation.

## 4.5 Nonlinear Response to Synthetic Ground Motions

The description up to previous section leads to a simple conclusion; nonlinear displacement response of a certain system is a function of the energy spectrum, which is a smoothed Fourier amplitude spectrum according to Eq. 2.20. This means nonlinear response appears to be independent of the Fourier phase spectrum. Nonlinear response analyses using simulated motions having random Fourier phase spectra are studied below to investigate the above hypothesis, because it is beleaved to be an indirect verification.

Three synthetic ground motions are used to calculate nonlinear responses. These were generated to meet target velocity response spectra of 0.02 damping factor with random Fourier phase spectra. (Watabe 1978). Smoothed Castaic, El Centro, and Hachinohe response spectra were selected for the target spectra. The Jennings Model (Jennings 1968) was applied for the envelope function of the acceleration histories.

Acceleration, velocity, and displacement histories are shown in Fig. 4.12

through 4.14 as well as the displacement and energy response spectra. These motions were filtered by the same method used for the ground motion in the range of 0.1 Hz to 25.5 Hz.

The calculated results in the relation of the dimensionless parameters based on smoothed response spectra, which are in the same parameter as one in Fig. 4.5, are shown in Fig. 4.15 through 4.17 for hysteresis model 1, 3, and 5. Each one of six plots in each figure includes twelve curves, three for the synthetic ground motions and nine for the ground motions used previous section.

For each figure, any period ratio or hysteresis model, the trends of the twelve curves are quite similar, and there is no special difference between curves for the synthetic ground motions and for the ground motions.

From these results, it may be said that the main parameter of the ground motion to maximum nonlinear displacement is a Fourier amplitude spectrum; in contrast, a Fourier phase spectrum may be irrelevant. In other words, the design method based on smoothed response spectra (or design response spectra) can be said to be a well-grounded method.

## 4.6 Discussion of Calculated Results

(1) Displacement Response by the Energy Concept.

It has been stated that the differences of the nonlinear displacement response for a certain system, which has a certain initial period and hysteresis rules, could be explained by the concept of the input energy. If the input energy relates to maximum displacement directly and changes of dissipated energy is caused only by hysteresis energy, the tendency of the variation of displacement response may be explained by "the equivalent linear method", which considers increasing displacement with increasing "effective

period" and decreasing displacement with increasing effective damping (See Appendix A). However, as shown in Appendix A, the explanation by "the equivalent linear method" is not sufficient. The maximum displacement response is not a direct function of the input energy. The input energy ($E_m$) is a sum of damping energy ($E_d$) and hysteresis energy ($E_h$), and the hysteresis energy is relates to integrated displacement response ($x_a$), and not to the maximum displacement ($x_{max}$), which is the directly "visible" value. Let the ratio of the hysteresis energy ($E_h$) to the apparent absorbed energy (Area A of Fig. 4.18) be written as $R_a$, the accumulation ratio, defined by Eq. 4.4.

$$R_a = \frac{E_h}{A} = \frac{E_h}{Q_y ( x_{max} - x_y / 2 )} \tag{4.4}$$

Furthermore:

$$E_m = E_h + E_d \tag{4.5}$$

Accordingly:

$$x_{max} = \frac{E_h}{R_a Q_y} + \frac{1}{2} x_y$$

$$= \frac{E_m - E_d}{R_a Q_y} + \frac{1}{2} x_y \tag{4.6}$$

Equation 4.6 shows that if $E_h$ (or $E_m$ and $E_d$) and $R_a$ are given by a function of the strength ratio, SR, the maximum displacement can be given by a function of SR.

If the hysteresis energy and the accumulation ratio may to be assumed as constant, the maximum displacement response can be obtained by a simple function of the strength ratio as a ratio of the elastic response

spectrum: displacement ratio, DR. For model 1, Akiyama (1980) showed that the accumulation ratio (in his study, the ratio was defined by the ratio of ductility, not the ratio of energy) might be assumed as a constant value of four from numerical analyses mainly for El Centro record. This result leads to Eq. 4.7.

$$DR = \frac{1}{8} \left( \frac{1}{SR} + 7SR \right) \tag{4.7}$$

This equation seems to correspond to the case of $T_O > TG$ for this study. Equation 4.7 does not exceed one in case of SR > 0.14, however, this equation underestimates DR to the higher SR and excessively overestimates DR to the lower SR especially under 0.1 of SR comparing to this study.

(2) Input Energy ($E_m$)

According to Akiyama (1980), the energy input of an elasto-plastic system (Model 1) can be obtained from the mean value of the energy spectrum between the initial period of the system and a period larger than the initial representing the effective period of the system after yielding. Thus, the energy input for the inelastic system will be obtained as a smoothed Fourier spectrum with a flat weighting function between the two periods. On the other hand, Kikuda and Suzuki (1984) have shown that the input energy of the bilinear slip model (Model 5) can be approximated using a triangular weighting function from the Fourier spectrum. In fact, the weighting function should vary over the period range in such a way as to indicate the "amount of dwell" at each period. Therefore, it is difficult to specify the same weighting function universally. Nevertheless, the idea used by Akiyama and Kikuta provides an explanation of the energy input of a nonlinear system.

Berg (1960) concluded that nonlinear systems have smaller energy response than linear systems having the same initial period. This conclusion is consistent with the results of nonlinear systems having a period, $T_o$, more than TG.

Because, the input energy for the range of $T_o$ > TG decreases with increasing period. That is to say that inelastic deformation means the width of the filter spreads to the long-period range, which is a direction of decreasing input energy, so that the input energy decreases.

On the other hand, for the system of $T_o$ < TG, the energy input increases within some degree of decreasing strength. However, if the system is weaker than a certain strength, then the input energy will decrease. For the almost zero-strength system, the input energy is constant value ($V_e = [\dot{X}_g]_{max}$)

independent of the initial period.

Figure 4.19 shows the energy input (the energy response spectra) into the system of model 3 for El Centro record. The tendencies explained up to here are observed in this figure.

(3) Energy Dissipated by Viscous Damping

In the numerical model of a SDOF oscillator, energy is dissipated by two assumed sources: viscous damping and hysteresis. The first one, set proportional to stiffness, dominates if the response is in the linear range and the second one dominates if the response is well in the nonlinear range. The results illustrated in Fig. 4.20 were developed to get a measure of the relative role of energy dissipated by the assumed viscous damping. Responses were calculated for the El Centro 1940 N-S component.

The vertical axis is the ratio of the damping energy to the input energy, and the horizontal axis is the strength ratio. The smaller the strength ratio is, the larger is the degree of nonlinearity. Calculated ratios are not unity at strength ratios of one because the input energy is defined as a maximum value during the motion and includes the potential energy stored in the system temporarily.

In Fig. 4.20, the bounds to the damping ratio are seen to vary from a linear to a square function of the strength ratio depending on the hysteresis model. Furthermore, the ratio is almost insensitive to the period ratio.

(4) Hysteresis Energy ($E_h$)

The energy dissipated by hysteresis is the difference between the input energy and the energy dissipated by the assumed viscous damping.

Figure 4.21a shows variations of hysteresis energy with the strength ratio at period ratios of 1/3 and 3/3 calculated for El Centro 1940 N-S

component. Even if the system period is above TG, the hysteresis energy does not decrease with decreasing strength ratio in spite of decreasing input energy because the energy dissipated by damping is decreasing at a rapid rate as discussed above. Changes in the displacement ratio with the strength ratio are also plotted in Fig. 4.21b for the same period ratios. On comparing the two figures, it can be said that the displacement ratio is not proportional to hysteresis energy in some cases. For example, at SR = 0.3 for $T_o$ = 3/3 TG, the displacement ratio of models 2 and 3 decrease while the hysteresis energy increases.

Changes of the hysteresis energy for model 1 are relatively small because for this model the system dwell at its initial period for a longer time than for the other model.

(5) Accumulation Ratio ($R_a$)

If the system yields only in one direction and reaches its maximum displacement, the maximum displacement should be a linear proportion of the hysteresis energy. However, earthquake response is a cyclic phenomenon, thus, the energy is dissipated by successive excursions into the yield range in both directions. Furthermore, for model 2 through 4, the energy is dissipated not only by yielding but also by small amplitude hysteresis. Accordingly, the difference between the hysteresis energy and the apparent maximum energy (Area A of Fig. 4.18) is an important factor for the maximum displacement response.

Figure 4.22 shows variation of the accumulation ratio (Eq. 4.4) with the strength ratio at period ratios of 1/3 and 3/3 for Castaic, El Centro and Hachinohe records. In general, the ratio is given by a similar curve at the same period, and the larger value is given by the larger energy-dissipating-ability model. On the other hand, at the same strength ratio, the ratio is larger at the period ratio of 1/3 than that at the period ratio of 3/3. The

reason seems to be a difference of nonlinearity; the displacement ratio or the ductility factor. Figure 4.23 shows changes of the ratio $R_a$ with the ductility factor. It can be said that the tendency of six figures is almost the same except for model 1.

Each figure shows that the accumulation ratio increases with increasing ductility factor and reaches to a certain value depending on the hysteresis model at three or four ductility factors. It is about four for model 2 and two for model 5. Models 3 and 4 take the value between them. However, the ratio of model 1 is unsteady, and it seems that there is no united rule in the changes. In Figure 4.22 the accumulation ratio for model 1 is very small at higher strength ratio. Displacement response of model 1 has a tendency to shift into one direction when the system has a larger strength ratio (Fig. 4.24). In this case, the accumulation ratio does not increase in spite of increasing ductility factor. On the other word, even if model 1 has large energy-dissipation ability under steady state conditon, if the system vibrates only one direction shifted, the ability during the response becomes small. Accordingly, it can be said that the accumulation ratio is a function of both the ability of energy-dissipation and the degree of the shift.

The displacement response of model 1 at the period ratio of 3/3 is the response shifted little comparatively, and in this case, the accumulation ratio for the large energy-dissipation-ability model is larger than that for small-energy-dissipation ability model (Fig. 4.23) and the maximum displacement response (or the displacement ratio) indicates inverse tendencies (Fig. 4.21b). These results contradict with the general observation that the maximum displacement response for the system of $T_O > TG$ is not sensitive to the assumption of hysteresis models (Fig. 4.6). The explanation of this contradiction is the displacement response shifted.

The degree of displacement response shifted varies depending on earthquakes and the strength ratio of its system. However, in average, the system of the larger energy-dissipation ability has a tendency of the larger shift. This may be explained simply as follows. If the energy is supplied in the same amount to both positive and negative directions alternately, model 1 can dissipate the opposite-side energy only to return to the former point while model 5 needs to go through the same amount of displacement on the opposite side. Figure 4.25 and 4.26 show the hysteresis relation of each five model for El Centro record at 1/3 and 4/3 period ratio. The strength ratio is 0.3 for each figure. The phenomenon explained is observed in each figure. Refering to Fig. 4.6, at $T_o$ = 4/3 TG, the maximum displacement response for each hysteresis model is almost same. For certain, according to Fig. 4.26, the maximum displacement response is almost same value; however, the response in opposite side is different; model 1 is almost zero while model 5 deforms nearly the same as the maximum displacement.

(6) Displacement Response

The expected maximum displacement response can be estimated by Eq. 4.6 as a function of the strength ratio, however, as described, the factors in Eq. 4.6 are not simply increased or decreased functions of the strength ratio. Some of them vary not only with hysteresis models but also with the type of ground motion. Especially, the accumulation ratio for model 1 is unsteady under the parameter used in this study. Thus, this study could not represent the numerical equation to estimate the maximum deformation of a certain SDOF system for a certain ground motion using the factors in Eq. 4.6 and the parameters used in this study.

However, the investigation in this section provides the explanation why the displacement response of a system differs or does not differ depending on its

strength ratio or hysteresis rules at a certain initial period. For example, the difference between model 1 and the other models at $T_o$ = 1/3 TG is mainly caused by differences of the input energy (or hysteresis energy, Fig. 4.21(a)) and the differences between the other models are mainly caused by differences of the accumulation ratio. Or in case of $T_o$ > TG, the reason why the displacement is almost constant in spite of decreasing strength ratio can be explained by increasing accumulation ratio and why in spite of different hysteresis model can be explained by the difference of the degree of shift.

# 5. COMPARISON WITH EXPERIMENTAL RESULTS

The variation of the displacement response with the intensity and characteristics of the ground motion and strength and stiffness properties of the structure indicated in the previous chapters were tested by using experimental data from a total of 34 reinforced concrete test structures. The test structures and ground motions for the tests are summarized in Table 5.1.

Overall features of each type of test structure are described briefly below. Unless otherwise noted, tests were carried out in earthquake simulation facilities. All structures were ideally planar and were subjected to one horizontal component of the earthquake record.

Takeda (1970): Tests of single reinforced concrete columns carrying a concentrated mass on top. Fig. 5.1.

Gulkan (1971): Tests of 1-story, 1-bay frames with concentrated masses. Test structures of series HE were one-half of test structures of series FE. Fig. 5.2.

Otani (1972): 1-bay 3-story reinforced concrete frames with masses at each story. Fig. 5.3.

Aristizabal (1976): Ten-story coupled-wall structures. Fig. 5.4.

Cecen (1979): Three-bay ten-story frames with a uniform distribution of story

heights and masses. Fig. 5.5.

Healey (1978): Three-bay ten-story frame with tall first and top stories. Similar to structure shown in Fig. 5.6.

Moehle (1978): Three-bay ten-story frame with a missing beam. Fig. 5.6.

Abrams (1979): Three-bay frames and walls working in parallel to resist lateral loads. Fig. 5.7.

Moehle (1980): Three-bay nine-story frame-wall combinations with the wall stopped at various heights. Fig. 5.8.

Morrison (1981): Single-degree-of-freedom models of slab-column connections. Fig. 5.9.

Kitagawa (1984): One-bay two-story reinforced concrete frame. Fig. 5.10.

Okamoto (1982): A large scale seven-story reinforced concrete test structure including frames and walls tested by applied lateral forces. Fig. 5.11.

Aktan (1984): A one-fifth scale model of the structure reported by Okamoto.

Wolfgram (1983): One-tenth scale models of the structure reported by Okamoto. These models did not have floor slabs. Fig. 5.12.

Most of the experimental data have been obtained using multi-degree-of-freedom (MDOF) structures. It is well known that lateral displacement of planar building structures is dominated in the linear range by the lowest translational mode. This has been shown to be substantially correct even after general yielding of the structure (Saiidi 1979). With the help of the procedures used by Okamoto (1982) and Rothe (1983), results from MDOF systems were modified to compare them directly with calculations based on SDOF systems. In this process, the mode shape was assumed to be the shape at maximum displacement of the test structure.

The characteristic period $T_o$ of each test structure was interpreted to be that calculated using one half the gross-section stiffness.

Most of the test structures were subjected to more than one earthquake simulation. Displacement response considered for this study was that from the first run in which general yielding occurred.

Figure 5.13a shows the distribution of the test results with respect to strength and period ratios shown in Table 5.1. All but nine of the results were in region I as described in Section 4.3. According to the trends described in Chapter 4, specimen that would be located in region I by their strength and period ratios would be likely to develop displacement responses not exceeding those based on two-percent spectral response for $T_o$, the characteristic period. Experimentally measured displacements which exceeded the two-percent spectral-response displacements are identified by solid rectangles in Fig. 5.13a.

Variations of the measured displacement ratios with strength ratios are shown in two plots, Fig. 5.13b and 5.13c, with the data separated depending on

the period ratio, ($T_O$/TG). It is observed that for $T_O$ exceeding TG, the displacement ratios did not exceed the two-percent response-spectrum values. For $T_O$ less than $T_G$, the displacement ratio was found to be sensitive both to the strength and period ratios. These trends were consistent with the conclusions drawn in Chapter 4.

# 6. REINFORCED CONCRETE BUILDING

## 6.1 Applications

The results represented in this study provide a basis for estimating drift of reinforced concrete buildings. Use of the procedure in practice would require the following steps.

1. Estimation of the normalized response spectra.

Based on the assumption of TG and on estimated maximum input energy (or response velocity), the normalized spectrum would be estimated. (one calculation method is presented in the next section.)

2. Initial period of the system.

The initial period represented in this paper is not the period corresponding to uncracked section. This period may be assumed to be approximately $\sqrt{2}$ times the calculated value for the uncracked section or the value obtained from a simple relationship such as T = 0.1N, where N is the number of stories.

3. Modification to SDOF system.

MDOF system would be modified to SDOF system with adequate mode shape (Okamoto 1982, Rothe 1983). Based on the overview of test results, this mode shape is almost linear for a frame-wall system, top heavy for a coupled-wall system and for frame system it would be a bottom heavy shape.

4. Zoning using SR and TR.

If TR > 1.0, the system is in "Region I",

If TR < 1.0, the region of the system would be determined based on estimated SR.

5. Displacement of SDOF system.

If system is in "Region I", the maximum displacement is the spectra value of $\beta = 0.02$, otherwise, the maximum displacement may be estimated by interpolating from the curves in Fig. 4.5.

6. Drift of the buildings.

The mode shape used in Step 3, will provide the distribution of deflection over the height of the building.

It should be noted that this method is based on the constant mode shape and on the system which can sustain a substantial portion of its strength in the nonlinear range, so that if the system is too weak to maintain the constant mode shape or cannot maintain its strength, this method is not applicable. Furthermore, as this method is based on the fixed base, it cannot apply to the certain structures which are not able to ignore the soil-structure interaction such as nuclear power plants or very high rise buildings.

## 6.2 Calculation of the Displacement Response Spectrum for a SDOF System

If the characteristic period, TG, and the corresponding response energy are known for a given site, displacement response spectrum may be determined from them through the following procedure.

It is well-known that the response energy spectrum, which is insensitive to damping, is approximately the same as the Fourier amplitude spectrum. It is also known that the Fourier amplitude spectrum provides a fairly good estimate of the velocity response spectrum at zero damping (Hudson 1962). Therefore, there is a relationship between the response energy spectrum and the velocity response spectrum. However, this relationship is not well defined because the velocity spectrum does very with the effect of damping. To investigate this

relationship for the nine actual and three simulated motions considered, the data in Fig. 6.1 were developed.

The vertical axis in the figure represents the displacement for each motion corresponding to a period of TG determined from the calculated response spectrum at 2%. The horizontal axis represents the displacement that will be determined from considering the energy spectrum as directly a velocity spectrum.

It is found that the relationship between those two calculations is not one to one but rather that the displacement determined directly is approximately 90% of the displacement determined from the response energy spectrum. Then, the spectral displacement may be expressed as described by Eq. 6.2 in accordance with the assumptions made earlier.

$$S_d = 0.9 \frac{1}{2\pi} \frac{T^2}{TG} V_m \qquad TG/3 \leqq T \leqq TG$$

$$S_d = 0.9 \frac{T}{2\pi} V_m \qquad TG \leqq T \leqq 2TG \tag{6.2}$$

Equation 6.2 is drawn in Fig. 6.2 by a solid line.

The maximum nonlinear displacement response of the system, whose initial period is above TG, is less than the linear response spectrum value while for the system whose initial period is less than TG, it is not guaranteed. The maximum displacement ratio of the system can be read off from the Fig. 4.5 under the condition that the lower boundary of the strength ratio is 0.1. It is nine at one-third period ratio and three at two-thirds period ratio. These results lead to the one-broken line in Fig. 6.2 as the maximum nonlinear

displacement response for a SDOF system. The displacement response of the system whose initial period is between TG/3 and TG is in the shadowed area, and the deformation depends on its strength.

## 6.3 Calculation for A MDOF System.

The maximum displacement response of a MDOF system at top can obtain by multiplying a mode participation coefficient. The participation coefficient varies depending on type of structure; mass distribution, story height distribution, and mode shape. Here, in order to calculate practically, some assumptions are represented as follows:

1. linear mode shape (Wall-Frame system),
2. uniform mass distribution,
3. $T_o = 1.4 * (0.1N)$, where N is number of stories,
4. 3.3 m uniform story height.

Based on the above assumptions, the participation coefficient $\beta$ can be obtained by Eq. 6.3.

$$\beta = \frac{\{\phi\}^T[M]\{1\}}{\{\phi\}^T[M]\{\phi\}} = \frac{3N}{2N+1} \qquad (6.3)$$

where,

$\phi_i$ : mode shape amplitude at level i provided that $\phi_{top} = 1.0$,

[M] : mass matrix.

Eq. 6.3 shows that $\beta$ varies 1.0 to 1.5 for N = 1 to N = $\infty$.

As a value of $V_m$, the value of El Centro (1200 mm/sec) can be assumed for a "design motion." Accordingly, the displacement response of buildings can be

obtained by multiplying Eq. 6.2 and Eq. 6.3 and the overall drift ratio of the building having an initial period above TG is

$$\text{Drift} = \frac{S_d}{\text{Height}} = \frac{0.9 \frac{1}{2\pi} 1200\ 1.4\ (0.1N)}{3300\ N} \frac{3N}{2N+1}$$

$$= 0.0073 \frac{3N}{2N+1}$$

$$= 0.0073 \sim 0.0109 \quad (N = 1 \sim \infty) \qquad (6.4)$$

This results indicates that the drift of the building is approximately 1% to the "design motion" if its initial period is above TG, but depending on its height (number of stories).

In order to investigate the difference of the drift ratio depending on site and number of story, some practical calculations were shown in Table 6.1. Buildings were assumed 2, 5, and 10 story and located at the site whose TG is 0.35, 0.55, or 1.15 sec. In case of $T_o$ < TG, the yielding base shear coefficient of the building was assumed as 0.2. If an acceptable story drift for a "design motion" such as El Centro record would be 1%, low story buildings at site of TG = 0.55 sec. such as at El Centro are quite critical, when they don't have enough strength ratio to keep in Region I.

It is interesting that this result is corresponding to that severe damaged reinforced concrete structures during 1978 Miyagi-ken-oki earthquake located at medium ground site. (Sibuya 1980).

# 7. SUMMARY AND CONCLUSION

In order to investigate the possibility of developing a simple procedure for determining seismic drift of reinforced concrete buildings, a parametric study was made using single-degree-of-freedom oscillators with hysteresis properties simulating the behavior of reinforced concrete systems. The main variables considered were initial stiffness, strength, and type of ground motion. Scope of the variable combinations included in the study is summarized by Fig. 4.1. The two initial periods, 0.3 and 1.0 sec., reflect the stiffnesses. The ground motions selected are assumed to be representative of motions for hard, medium, and soft ground. Nonlinear response was calculated for a series of oscillators of decreasing strength in each case. The straight horizontal lines in each figure represent maximum linear response for the initial period of the oscillator at a damping factor of 0.02.

Values of strength and calculated displacement were normalized by expressing them as strength and displacement ratios or as ratios of the pertinent linear-response (damping factor = 0.02) values defined by Eq. 10 and 11. Trends of displacement ratios with strength ratios (Fig. 4.2) indicated that the period ratio, or the ratio of the initial period of oscillator to characteristic period of the ground motion TG determined using the energy spectrum, could be used to organize the data for the types of ground motion considered. Plots of displacement vs. strength ratio organized accordingly (Fig. 4.5) demonstrated that the nonlinear-response displacement was essentially the same as the displacement obtained from a linear-response calculation with a damping factor of 0.02, provided the sum of the strength and

period ratios was not less than one. Furthermore, in this region the nonlinear-response displacement is not sensitive to the hysteresis models assumed. If the sum is less than one, the displacement may be estimated by interpolation from the data in Fig. 4.5. However, in this region, as the response is sensitive to the hysteresis model, more detail modeling and calculation are recommended.

A total of 34 test results of dynamic tests for reinforced concrete systems were rearranged and it was shown these test results were satisfied this relationship.

After all, the appreciation of this method to reinforced concrete structures was indicated with some calculations.

As a conclusion, it can be said that these two generalizations provide the basis of a simple procedure for estimating drift for reinforced concrete structures. As a minimum, they will help identify whether the drift estimate can be accomplished using a linear-response spectrum or whether more detailed modeling and calculations are required.

# References


1. Abrams, D. P. and M. A. Sozen (1979), "Experimental Study of Frame-Wall Interaction in Reinforced Concrete Structures Subjected to Strong Earthquake Motion," Civil Engineering Studies, SRS No. 460, University of Illinois, Urbana.

2. Akiyama, H. (1980), "Aseismic Ultimate Design of Building Structures (In Japanese)," Tokyo University Press, Tokyo.

3. Aktan, A. E. and V. V. Bertero (1984), "Earthquake Response of a 1/5th-Scale Model of a 7 Story Reinforced Concrete Frame-Wall Structural System," Proceedings of the Eighth World Conference on Earthquake Engineering, Vol. VI, pp. 651-658, San Francisco.

4. Aristizabal-Ochoa, J. D. and M. A. Sozen (1976), "Behavior of Ten Story Reinforced Concrete Walls Subjected to Earthquake Motions," Civil Engineering Studies, SRS No. 431, University of Illinois, Urbana.

5. Berg, G. V. and S. S. Thomaides (1964), "Energy Consumption by Structures in Strong Motion Earthquakes," Proceedings of the 2nd World Conference on Earthquake Engineering, Tokyo, pp. 681-697.

6. Cecen, H., (1979), "Response of Ten-Story Model Frames to Simulated Earthquakes," Ph.D. Thesis, University of Illinois, Department of Civil Engineering, Urbana.

7. Clough, R. W. and S. B. Johnston (1966), "Effect of Stiffness Degradation on Earthquake Ductility Requirements," Proceedings of the Second Japan Earthquake Engineering Symposium, pp. 227-232.

8. Gulkan, P. and M. A. Sozen (1971), "Response and Energy-Dissipation of R/C Frames Subjected to Strong Base Motions," Civil Engineering Studies, SRS No. 377, University of Illinois, Urbana.

9. Healey, T. J. and M. A. Sozen (1978), "Experimental Study of Dynamic Response of a Ten-Story Reinforced Concrete Frame with a Tall First Story," Civil Engineering Studies, SRS No. 450, University of Illinois, Urbana.

10. Hisada, T., Y. Ohsaki, M. Watabe, and T. Chiba (1978), "Design Spectra for Stiff Structure on Rock," Proceedings of 2nd International Conference on Microzonation for Safer Construction, Vol. IV.

11. Hodder, S. B. (1983), "Computer Processing of New Zealand Strong-Motion Accelerograms," Proceedings of the Third South Pacific Regional Conference on Earthquake Engineering, New Zealand, Vol. I, pp. 36-53.

12. Housner, G. W. (1956), "Limit Design of Structures to Resist Earthquakes," Proceedings of the First World Conference on Earthquake Engineering, California, pp. 5-1 to 5-13.

13. Hudson, D. E. (1962), "Some Problems in the Application of Spectrum Techniques to Strong Motion Earthquake Analysis," Bulletin of the Seismological Society of America, Vol. 52, No. 2, pp. 417-430.

14. Jacobsen, L. S. (1960), "Damping in Composite Structures," Proceedings of the Second World Conference on Earthquake Engineering, Tokyo and Kyoto, Vol. II, pp. 1029-1044.

15. Jennings, P. C., G. W. Housner, and N. C. Tsai (1969), "Simulated Earthquake Motions for Design Purposes.", Proceedings of the Fourth World Conference on Earthquake Engineering, Vol. 1, pp. A1-145 to A1-160.

16. Kanai, K. (1951), "Relation Between the Nature of Surface Layer and the Amplitude of Earthquake Motions", Bulletin of Earthquake Research Institute, University of Tokyo, Japan.

17. Kato, B. and H. Akiyama (1975), "Energy Input and Damages in Structures Subjected to Severe Earthquakes (In Japanese)," Transaction of the Architectural Institute of Japan, Tokyo, Vol. 235, pp. 9-18.

18. Kikuta, S. and H. Suzuki (1984), "Earthquake Energy Input into Hysteretic Structural Systems," Summaries of Technical Papers of Annual Meeting, Structure, Architectural Institute of Japan.

19. Kitagawa, Y., T. Kubota, T. Kaminosono, and T. Kubo (1984), "Correlation Study on Shaking Table Tests and Pseudo-Dynamic Test by R/C Models," Proceedings of the Eighth World Conference on Earthquake Engineering, Vol. VI, pp. 667-674, San Francisco, CA.

20. Midorikawa S., and H. Kobayashi (1984) "Intensity of Strong Ground Motions Observed Near Fault (In Japanese)", Summaries of Technical Papers of Annual Meeting, Structure, Architectural Institute of Japan, pp. 611-612.

21. Moayyad, P. and B. Mohraz (1982), "A Study of Power Spectral Density of Earthquake Accelerograms," Southern Methodist University.

22. Moehle, J. P. and M. A. Sozen (1978), "Earthquake Simulation Tests of a Ten Story Reinforced Concrete Frame with a Discontinued First-Level Beam," Civil Engineering Studies, SRS No. 451, University of Illinois, Urbana.

23. Moehle, J. P. and M. A. Sozen (1980), "Experiments to Study Earthquake Response of R/C Structures with Stiffness Interruptions," Civil Engineering Studies, SRS No. 482, University of Illinois, Urbana.

24. Moehle, J. P. (1984), "Strong Motion Drift Estimates for R/C Structures," Journal of Structural Division, ASCE, Vol. 110, No. 9, pp. 1988-2001.

25. Mori, A. W. and C. B. Crouse (1981), "Strong Motion Data from Japanese Earthquakes," World Data Center A for Solid Earth Geophysics, Report SE-29, U.S. Department of Commerce, Boulder, CO.

26. Morrison, D. G. and M. A. Sozen (1981), "Response of Reinforced Concrete Plate-Column Connections to Dynamic and Static Horizontal Loads," Civil Engineering Studies, SRS No. 490, University of Illinois, Urbana.

27. Newmark, N. M. (1959), "A Method of Computation for Structural Dynamics," Journal of Structural Division, ASCE, Vol. 85, No. ST3, pp. 67-94.

28. Nigam, N. C. and P. C. Jennings (1984), "Calculation of Response Spectra from Strong Motion Earthquake Records," Bulletin of the Seismological Society of America, Vol. 59, No. 2, pp. 909-922.

29. Okamoto, S., S. Nakata, Y. Kitagawa, M. Yoshimura and T. Kaminosono (1982), "A Progress Report on the Full-Scale Seismic Experiment of a Seven-Story Reinforced Concrete Building - Part of the US-Japan Cooperative Program," Building Research Institute Research Paper, No. 94, Ministry of Construction, Japan.

30. Otani, S. and M. A. Sozen (1972), "Behavior of Multistory Reinforced Concrete Frames During Earthquakes," Civil Engineering Studies, SRS No. 392, University of Illinois, Urbana.

31. Otani, S. (1980), "Hysteresis Models of Reinforced Concrete for Earthquake Response Analysis," Journal of the Faculty of Engineering (B), University of Tokyo, Tokyo, Vol. 36, No. 2, pp. 125-159.

32. Porcella, R. L. (1984), "Geotechnical Investigations at Strong-Motion Stations in the Imperial Valley, California," Open-File Report 84-562, United States Department of the Interior Geological Survey, Menlo Park, CA.

33. Rothe, D. H. and M. A. Sozen (1983), "A SDOF Model to Study Nonlinear Dynamic Response of Large- and Small-Scale R/C Test Structures," Civil Engineering Studies, SRS No. 512, University of Illinois, Urbana.

34. Saiidi, M. and M. A. Sozen (1978), "Simple and Complex Models for Nonlinear Seismic Response of Reinforced Concrete Structures," Civil Engineering Studies, SRS No. 465, Department of Civil Engineering, University of Illinois, Urbana.

35. Schnabel, P. B., J. Lysmer and H. B. Seed (1972), "SHAKE, A Computer Program for Earthquake Response Analysis of Horizontally Layered Sites," EERC 72-12, Earthquake Engineering Research Center, University of California, Berkeley, CA.

36. Sheth, R. M. (1959), "Effect of Inelastic Action on the Response of Simple Structures to Earthquake Motions," M.S. Thesis, University of Illinois, Department of Civil Engineering, Urbana.

37. Shibata, A. (1975), "Equivalent Linear Models to Determine Maximum Inelastic Response of Nonlinear Structures for Earthquake Motions," Proceedings of the Fourth Japanese Earthquake Engineering Symposium.

38. Shibata, A. and M. A. Sozen (1976), "Substitute-Structure Method for Seismic Design in R/C," Journal of the Structural Division, ASCE, Vol. 102, No. SST1, pp. 1-18.

39. Shibuya, J., H. Kimura and T. Shiga (1980), "Effects of Local Site Conditions on Damage to Buildings During an Earthquake," Proceedings of the Seventh World Conference on Earthquake Engineering, Istanbul, Vol. 2, pp. 199-206.

40. Shiga, T., A. Shibata, J. Shibuya and J. Takahashi (1980), "Performance of the Building of Faculty of Engineering, Tohoku University, During the 1978 Miyagi-ken-Oki Earthquake, "Proceedings of the Seventh World Conference on Earthquake Engineering, Vol. 7, pp. 357-364.

41. Sunder, S. S. and J. J. Conner (1982), "A New Procedure for Processing Strong-Motion Earthquake Signals," Bulletin of the Seismological Society of America, Vol. 72, No. 2, pp. 643-661.

42. Suzuki, T. and T. Takeda (1981), "The Relationship Between the Strength and elastic Deformation of Buildings Based on Energy Concept (In Japanese)," Proceedings Kanto District Symposium, Architectural Institute of Japan, Tokyo, pp. 89-92.

43. Takeda, T., M. A. Sozen and N. N. Nelson (1970), "Reinforced Concrete Response to Simulated Earthquakes," Journal of Structural Division, ASCE, Vol. 96, No. ST12, pp. 2557-2573.

44. Takeda, T. and H. Edo (1977), "Elastoplastic Frame Response Analysis for Reinforced Concrete Structures (In Japanese)," Summaries of Technical Papers of Annual Meeting, Structure, Architectural Institute of Japan.

45. Takizawa, H. (1977), "Energy Response Spectra of Earthquake Motion (In Japanese)," Proceedings of the 14th Symposium on Natural Disaster Science.

46. Trifunac, M. D. and F. E. Udwadia and A. G. Brady (1973), "Analysis of Errors in Digitized Strong-Motion Accelerograms," Bulletin of Seismological Society of America, Vol. 63, No. 1, pp. 157-187.

47. Valera, J. E. (1973), "Soil Conditions and Local Soil Effects During the Managua Earthquake of December 23, 1972," Managua, Nicaragua Earthquake of December 23, 1972, EERC Conference Proceedings, Vol. 1, pp. 232-264.

48. Veletsos, A. S. and N. M. Newmark (1960), "Effect of Inelastic Behavior on the Response of Systems," Proceedings of the Second World Conference on Earthquake Engineering, Tokyo and Kyoto, Vol. II, pp. 895-912.

49. Watabe, M., O. Chiba and M. Tohdo (1979), "Generation of Simulated Three Dimensional Earthquake Ground Motions," Transactions of the 5th International Conference on Structural Mechanics in Reactor Technology, K 1/2, West Berlin.

50. Wolfgram, C. E. (1983), "Experimental Modeling and Analysis of Three One-Tenth-Scale Reinforced Concrete Frame-Wall Structures," Ph.D. Thesis, University of Illinois, Department of Civil Engineering, Urbana.

Table 2.1. Ground Motions

| Ground Motion | Earthquake and Site | Strong Motion Duration, sec (total Duration) | Maximum Values Acc. g | Vel. mm/s | Dis. mm | TG sec |
|---|---|---|---|---|---|---|
| Castaic N21E | San Fernando Earthquake 2/9/71<br>Castaic Old Ridge Route, CA. | 1.02- 8.02<br>(61.76) | -0.182<br>0.317 | -153.1<br>162.6 | -25.9<br>9.4 | 0.35 |
| Managua S00W | Esso Refinery Earthquake 12/23/72<br>Esso Refinery, Managua, Nicaragua | 1.34- 7.50<br>(45.68) | -0.302<br>0.324 | -294.8<br>252.1 | -66.6<br>44.2 | 0.37 |
| Hollister N89W | Hollister Earthquake 4/8/61<br>Hollister City Hall, CA. | 0.40- 9.98<br>(40.48) | -0.115<br>0.179 | -166.0<br>92.8 | -45.0<br>8.0 | 0.45 |
| Taft N21E | Kern County Earthquake 7/21/52<br>Taft Lincoln School Tunnel, CA. | 3.44-20.68<br>(54.36) | -0.155<br>0.141 | -97.3<br>141.4 | -37.0<br>32.0 | 0.50 |
| El Centro S00E | Imperial Valley Earthquake 5/18/40<br>El Centro Site Imperial Valley Irrigation District, CA. | 1.38-26.30<br>(53.74) | -0.270<br>0.348 | -251.4<br>336.0 | -71.5<br>71.6 | 0.55 |
| Los Angeles N00W | San Fernando Earthquake 2/9/71<br>8244 Orion Blvd., CA. | 3.36-14.82<br>(59.48) | -0.179<br>0.255 | -258.5<br>272.7 | -83.9<br>126.5 | 0.57 |
| Santa Barbara S48E | Kern County Earthquake 7/21/52<br>Santa Barbara Courthouse, CA. | 1.50-15.42*<br>(70.46) | -0.131<br>0.066 | -187.9<br>172.1 | -42.5<br>52.4 | 0.95 |
| Miyagi NS | Miyagi-Ken-Oki Earthquake 6/12/78<br>Tohoku University, Sendai, Japan | 2.46-17.69<br>(20.00) | -0.213<br>0.264 | -322.4<br>354.6 | -96.5<br>81.7 | 0.95 |
| Hachinohe EW | Tokachi-Oki Earthquake 5/16/68<br>Hachinohe Habour, Hachinohe, Japan | 0.98-24.44<br>(30.00) | -0.183<br>0.183 | -331.9<br>287.9 | -76.6<br>104.0 | 1.15 |

* Data in first five sec. of original record were ignored.

Table 2.2. Geological Properties of the Recorded Sites

| Record | Location | Geological Property | Reference |
|---|---|---|---|
| Castaic | Castaic Old Ridge Route | Sand Stone | Moayyad et al, 1982 |
| Managua | Esso Refinery | Over 20m of Silty Sand | Valera, 1973 |
| Hollister | Hollister City Hall | Recent Unconsolidated Alluvium over Partly Consolidated Gravels, and well Consolidated Marine Sandstone and Shale | Moayyad et al, 1982 |
| Taft | Taft Lincoln School | Quaternary Alluvium, Sand and Gravel Veneer over 600m Consolidated Gravel, Sand and Clay | Moayyad et al,1982 |
| El Centro | El Centro Valley Irrigation District | Alluvium over 250m Alternate Layer of Sand and Clay | Porcella, 1984 |
| Los Angeles | 8244 Orion Blvd. 1st FL. | Deep Cohesionless Soil 165m Deep | Moayyad et al, 1982 |
| Santa Barbara | Santa Barbara Court | Apporx. 180m of Pleistocene Cemented Alluvium over Sand, Silt and Clay | Moayyad et al, 1982 |
| Miyagi | Tohoku University | Gravelly Loam (at Top of a Hill) | Shiga et al, 1980 |
| Hachinihe | Hachinohe Habour | 30m of Sandy Soil over very Stiff Clay to Claystone | Mori et al, 1981 |

Table 4.1 Smoothed Response Spectra Used

| Ground Motions | | $T_o$ | | | | | |
|---|---|---|---|---|---|---|---|
| | | 1/3 TG | 2/3 TG | 3/3 TG | 4/3 TG | 5/3 TG | 6/3 TG |
| Castaic | Displ. (mm) | 3.9 | 15.7 | 35.3 | 47.1 | 58.8 | 70.6 |
| | Acc. (g) | 1.16 | 1.16 | 1.16 | 0.87 | 0.70 | 0.58 |
| Managua | Displ. (mm) | 6.96 | 27.8 | 62.9 | 83.8 | 104.9 | 125.8 |
| | Acc. (g) | 1.85 | 1.85 | 1.85 | 1.39 | 1.11 | 0.93 |
| Hollister | Displ. (mm) | 3.87 | 15.5 | 34.7 | 46.3 | 57.9 | 69.5 |
| | Acc. (g) | 0.69 | 0.69 | 0.69 | 0.52 | 0.41 | 0.35 |
| El Centro | Displ. (mm) | 11.0 | 44.0 | 99.0 | 132.0 | 165.0 | 198.0 |
| | Acc. (g) | 1.32 | 1.32 | 1.32 | 0.99 | 0.79 | 0.66 |
| Los Angeles | Displ (mm) | 12.0 | 48.1 | 108.3 | 144.4 | 180.5 | 216.6 |
| | Acc. (g) | 1.34 | 1.34 | 1.34 | 1.01 | 0.81 | 0.67 |
| Taft | Displ. (mm) | 4.63 | 18.4 | 41.5 | 55.4 | 69.1 | 83.0 |
| | Acc. (g) | 0.67 | 0.67 | 0.67 | 0.50 | 0.40 | 0.33 |
| Santa Barbara | Displ. (mm) | 11.7 | 46.5 | 104.5 | 139.4 | 174.1 | 209.0 |
| | Acc. (g) | 0.47 | 0.47 | 0.47 | 0.35 | 0.28 | 0.23 |
| Miyagi | Displ. (mm) | 29.3 | 117.0 | 263.2 | 351.0 | 438.5 | 526.3 |
| | Acc. (g) | 1.17 | 1.17 | 1.17 | 0.88 | 0.70 | 0.59 |
| Hachinohe | Displ. (mm) | 30.9 | 123.5 | 278.0 | 371.0 | 464.0 | 557.0 |
| | Acc. (g) | 0.78 | 0.78 | 0.78 | 0.58 | 0.47 | 0.39 |

Table 5.1. Dynamic Tests

| No. | Structures | Structure Type (No. of Stories) | $T_i$ (sec) | Ground Motion | Max. Acc. (g) | Time Scale | Reference |
|---|---|---|---|---|---|---|---|
| 1 | T2 | SDOF | 0.079 | El Centro | 1.28 | 1/8 | Takeda 1970 |
| 2 | T5 | SDOF | 0.079 | Taft | 2.70 | 1/10 | |
| 3 | FE1 | Frame ( 1 ) | 0.045 | Taft | 2.20 | 1/5 | Gulkan 1971 |
| 4 | FE2 | Frame ( 1 ) | 0.045 | Taft | 4.20 | 1/5 | |
| 5 | HE1 | Frame ( 1 ) | 0.028 | El Centro | 1.18 | 1/5 | |
| 6 | HE2 | Frame ( 1 ) | 0.028 | El Centro | 1.54 | 1/5 | |
| 7 | O-D1 | Frame ( 3 ) | 0.147 | El Centro | 0.24 | 1/2.5 | Otani 1972 |
| 8 | O-D2 | Frame ( 3 ) | 0.147 | El Centro | 0.86 | 1/2.5 | |
| 9 | O-D3 | Frame ( 3 ) | 0.147 | El Centro | 0.61 | 1/2.5 | |
| 10 | A-D1 | Coupled Wall ( 10 ) | 0.185 | El Centro | 0.5 | 1/2.5 | Aristizabel-Ochoa |
| 11 | A-D2 | Coupled Wall ( 10 ) | 0.185 | El Centro | 0.44 | 1/2.5 | 1976 |
| 12 | A-D3 | Coupled Wall ( 10 ) | 0.185 | Taft | 0.46 | 1/2.5 | |
| 13 | A-M1 | Coupled Wall ( 10 ) | 0.185 | El Centro | 0.91 | 1/2.5 | |
| 14 | H1 | Frame ( 10 ) | 0.205 | El Centro | 0.36 | 1/2.5 | Cecen 1979 |
| 15 | H2 | Frame ( 10 ) | 0.205 | El Centro | 0.17 | 1/2.5 | |
| 16 | MF1 | Frame ( 10 ) | 0.205 | El Centro | 0.40 | 1/2.5 | Healey 1978 |
| 17 | MF2 | Frame ( 10 ) | 0.205 | El Centro | 0.38 | 1/2.5 | Moehle 1978 |
| 18 | FW1 | Frame-Wall ( 10 ) | 0.167 | El Centro | 0.51 | 1/2.5 | Abrams 1979 |
| 19 | FW2 | Frame-Wall ( 10 ) | 0.170 | El Centro | 0.48 | 1/2.5 | |
| 20 | FW3 | Frame-Wall ( 10 ) | 0.170 | Taft | 0.47 | 1/2.5 | |
| 21 | FW4 | Frame-Wall ( 10 ) | 0.167 | Taft | 0.42 | 1/2.5 | |
| 22 | FNW | Frame ( 9 ) | 0.23 | El Centro | 0.39 | 1/2.5 | Moehle 1980 |
| 23 | FSW | Frame-Wall ( 9 ) | 0.18 | El Centro | 0.34 | 1/2.5 | |
| 24 | FHW | Frame-Wall ( 9 ) | 0.18 | El Centro | 0.41 | 1/2.5 | |
| 25 | FFW | Frame-Wall ( 9 ) | 0.18 | El Centro | 0.32 | 1/2.5 | |

Table 5.1. (Continued)

| No. | Structures | Structure Type (No. of Stories) | $T_i$ (sec) | Ground Motion | Max. Acc. (g) | Time Scale | Reference |
|---|---|---|---|---|---|---|---|
| 26 | M-D1 | SDOF (Column-Slab) | 0.069 | El Centro | 0.99 | 1/2.5 | Morrison 1981 |
| 27 | M-D2 | SDOF (Column-Slab) | 0.071 | El Centro | 0.86 | 1/2.5 | |
| 28 | M-D3 | SDOF (Column-Slab) | 0.069 | El Centro | 1.30 | 1/2.5 | |
| 29 | DR20 | Frame ( 2 ) | 0.18 | Miyagi | 0.48 | 1/2 | Kitagawa 1984 |
| 30 | PSD3 | Frame-Wall ( 7 ) | 0.41 | M-Taft | 0.33 | 1/1 | Okamoto 1982 |
| 31 | MO247 | Frame-Wall ( 7 ) | 0.21 | Miyagi | 0.42 | $1/\sqrt{5}$ | Aktan 1984 |
| 32 | NS1 | Frame-Wall ( 7 ) | 0.094 | Miyagi | 0.59 | 1/5 | Wolfgram 1983 |
| 33 | NS2 | Frame-Wall ( 7 ) | 0.094 | Miyagi | 0.59 | 1/5 | |
| 34 | NS3 | Frame-Wall ( 7 ) | 0.094 | Miyagi | 0.49 | 1/5 | |

Table 5.2 Calculated Normalized Ratios

| No. | Structure | Period Ratio TR | Strength Ratio SR | Displacement Ratio DR |
|---|---|---|---|---|
| 1 | T2 | 1.61 | 0.21 | 0.94 |
| 2 | T5 | 2.22 | 0.10 | 0.73 |
| 3 | FE1 | 0.63 | 0.16 | 1.65 |
| 4 | FE2 | 0.63 | 0.15 | 1.91 |
| 5 | HE1 | 0.28 | 0.26 | 2.20 |
| 6 | HE2 | 0.28 | 0.39 | 3.40 |
| 7 | O-D1 | 0.94 | 0.52 | 0.73 |
| 8 | O-D2 | 0.94 | 0.14 | 0.65 |
| 9 | O-D3 | 0.94 | 0.17 | 0.70 |
| 10 | A-D1 | 1.18 | 0.22 | 0.94 |
| 11 | A-D2 | 1.18 | 0.22 | 0.98 |
| 12 | A-D3 | 1.30 | 0.22 | 0.80 |
| 13 | A-M1 | 1.18 | 0.14 | 0.90 |
| 14 | H1 | 1.27 | 0.26 | 0.84 |
| 15 | H2 | 1.27 | 0.67 | 0.74 |
| 16 | MF1 | 1.32 | 0.31 | 0.70 |
| 17 | MF2 | 1.27 | 0.26 | 0.78 |
| 18 | FW1 | 1.06 | 0.38 | 0.99 |
| 19 | FW2 | 1.08 | 0.28 | 0.95 |
| 20 | FW3 | 1.19 | 0.33 | 0.65 |
| 21 | FW4 | 1.17 | 0.38 | 0.62 |
| 22 | FNW | 1.46 | 0.31 | 0.78 |
| 23 | FSW | 1.15 | 0.27 | 0.84 |
| 24 | FHW | 1.15 | 0.26 | 0.86 |
| 25 | FFW | 1.15 | 0.26 | 0.89 |
| 26 | M-D1 | 0.44 | 0.27 | 1.91 |
| 27 | M-D2 | 0.45 | 0.39 | 0.77 |
| 28 | M-D3 | 0.44 | 0.34 | 0.97 |
| 29 | DR20 | 0.52 | 0.26 | 2.20 |
| 30 | PSD3 | 1.29 | 0.25 | 0.95 |
| 31 | MO247 | 0.70 | 0.29 | 0.85 |
| 32 | NS1 | 0.68 | 0.42 | 0.88 |
| 33 | NS2 | 0.68 | 0.51 | 0.77 |
| 34 | NS3 | 0.68 | 0.51 | 0.70 |

Table 6.1. Estimated Drift of R/C Buildings

| TG | (sec) | 0.35 | 0.55 | 1.15 |
|---|---|---|---|---|
| 2 Story $T_0$=0.28 | TR | 0.80 | 0.51 | 0.24 |
| | SR | 0.11 | 0.14 | 0.30 |
| | DR | 1.2 | 3.0 | 3.0 |
| | Drift | 1/120 | 1/85 | 1/160 |
| 5 Story $T_0$=0.71 | TR | 2.10 | 1.29 | 0.62 |
| | SR | - | - | 0.30 |
| | DR | 1.0 | 1.0 | 1.1 |
| | Drift | 1/100 * | 1/100 | 1/150 |
| 10 Story $T_0$=1.41 | TR | 4.00 | 2.56 | 1.23 |
| | SR | - | - | - |
| | DR | 1.0 | 1.0 | 1.0 |
| | Drift | 1/95 * | 1/95 * | 1/95 |

* Because $T_0$ exceeds 2TG, these values are considered to be out of range of confident projection for the method of analysis presented. For $T_0$ higher than 2TG, displacement response should be less than those tabulated for the types of ground motion considered.

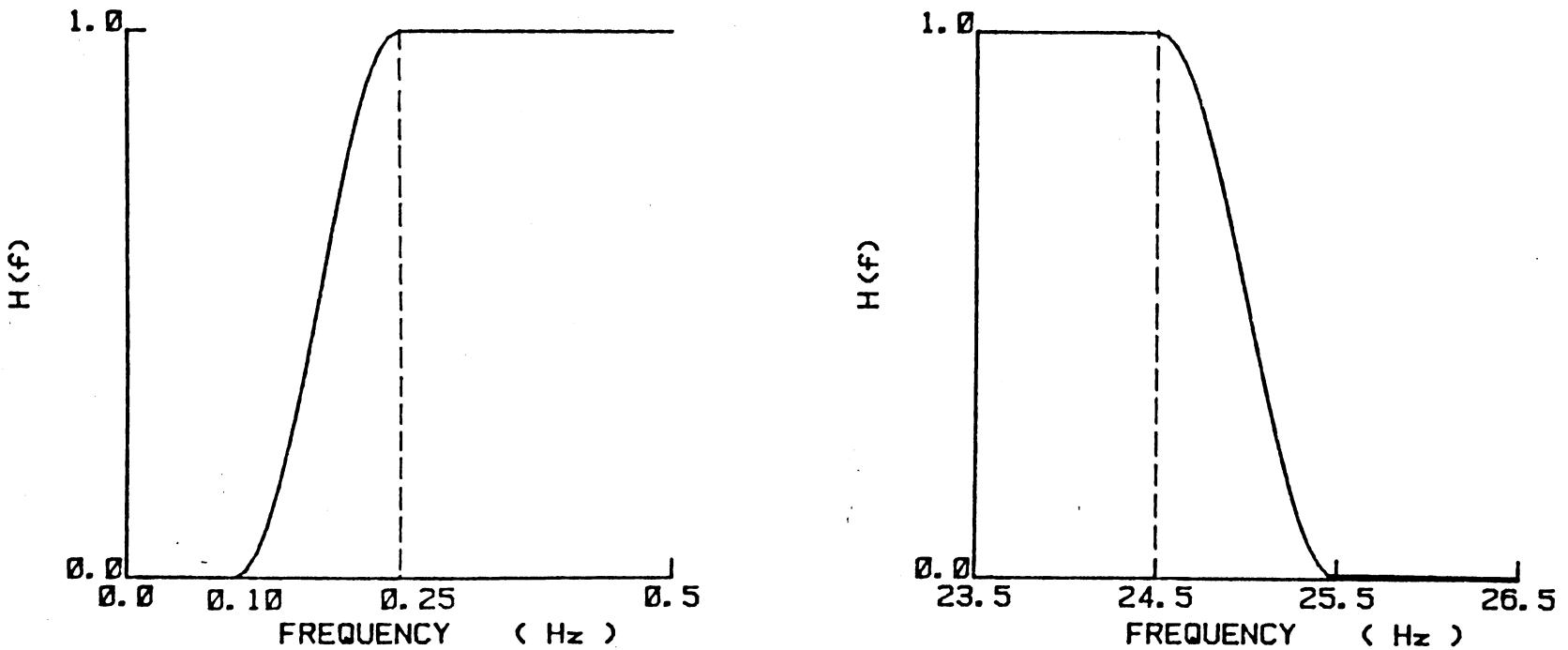


Fig. 2.1 Frequency Ranges for the Filter Used

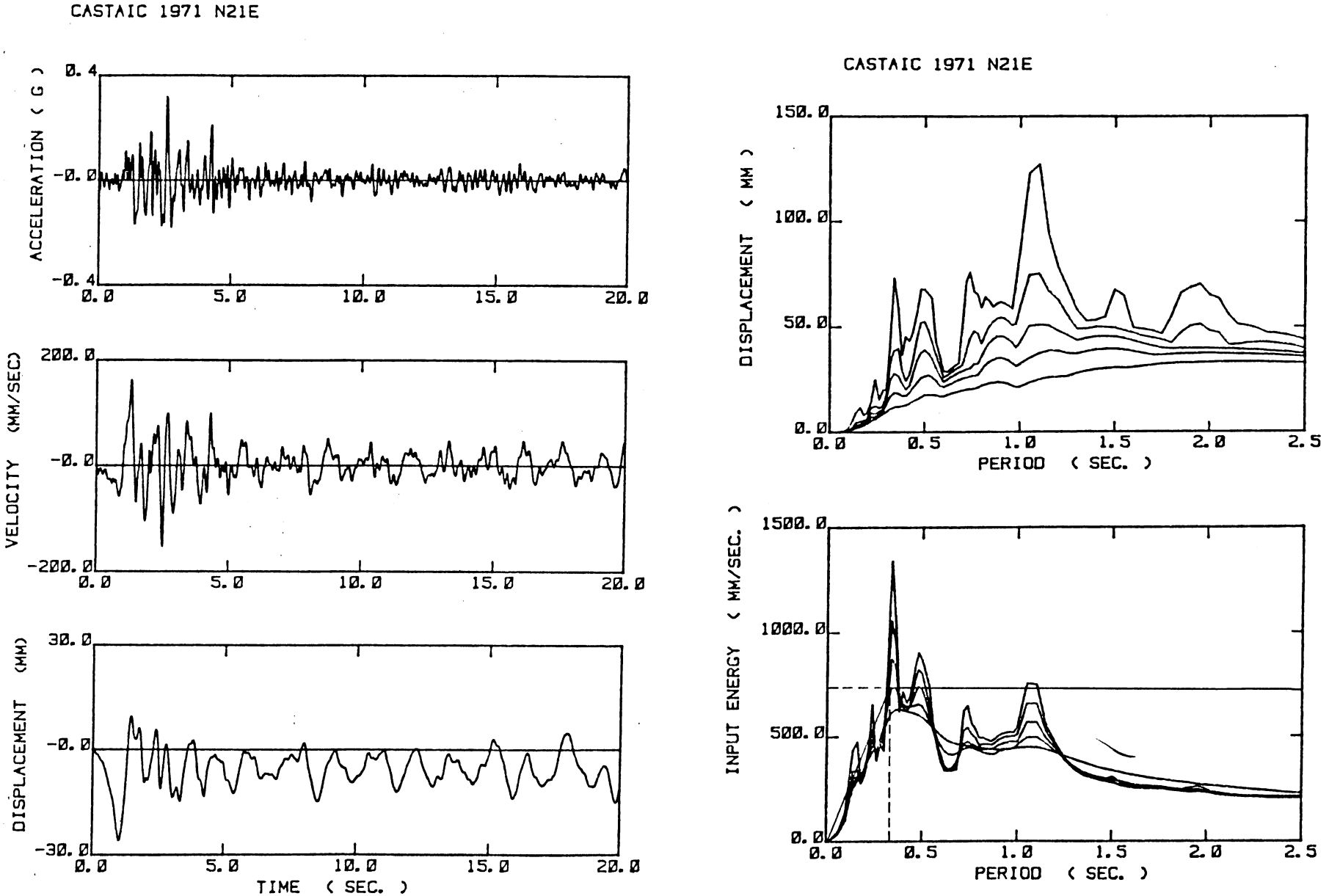


Fig. 2.2 Castaic 1971 N21E Ground Motion Record and Response Spactra

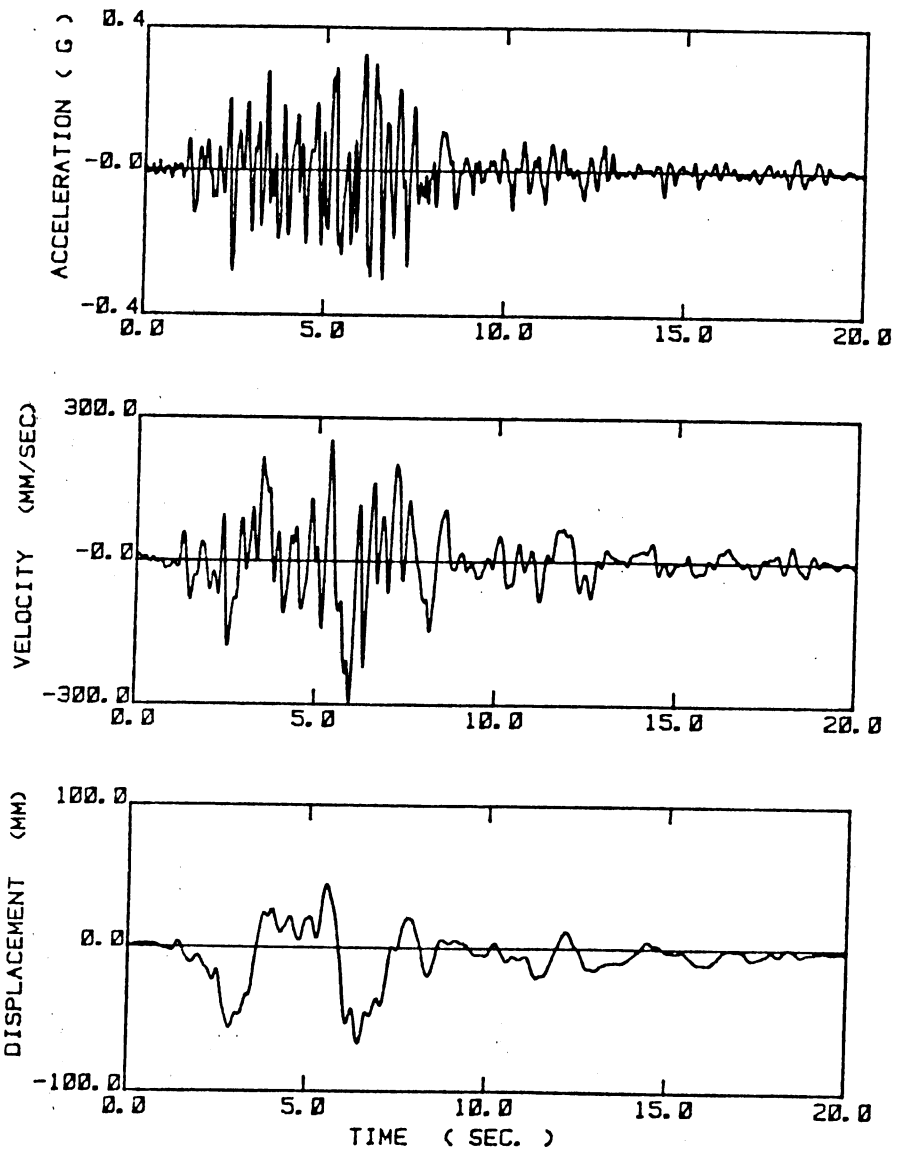


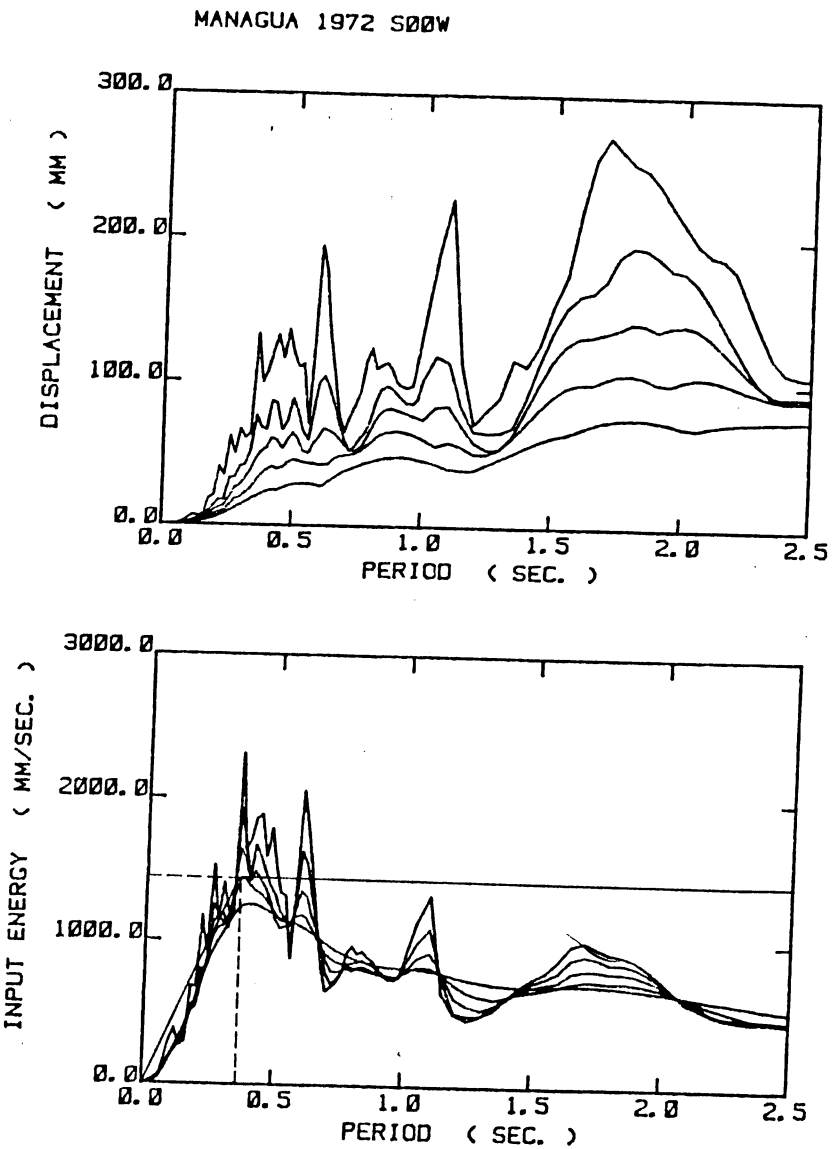


Fig. 2.3 Managua 1972 S00W Ground Motion Record and Response Spectra

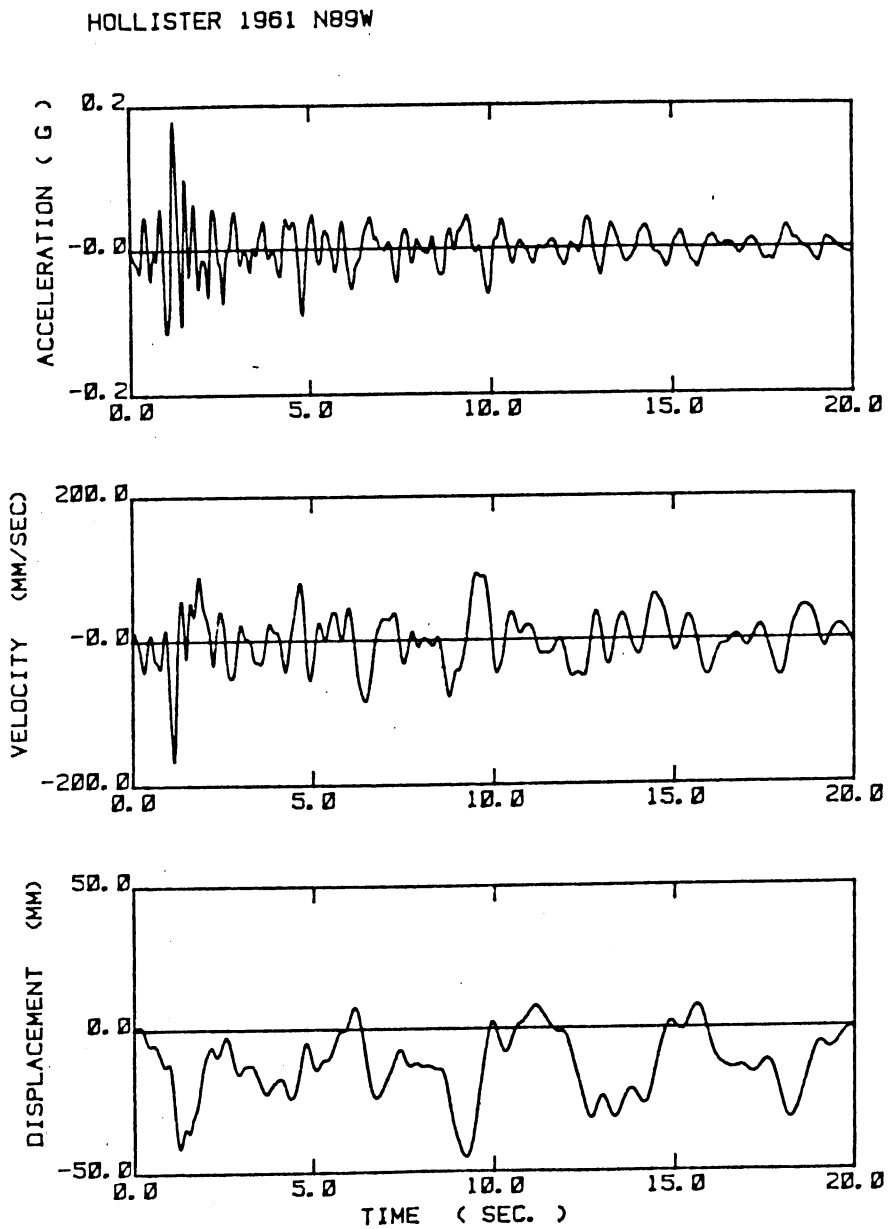


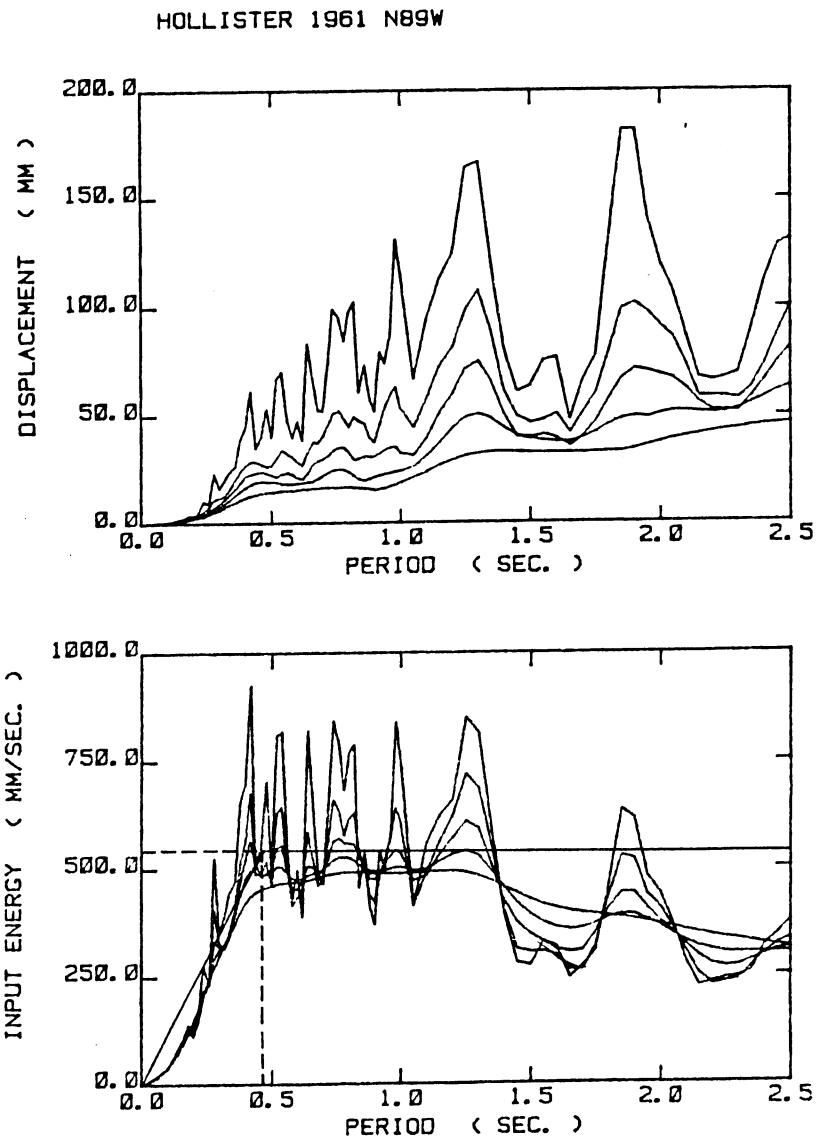


Fig. 2.4 Hollister 1961 N89W Ground Motion Record and Response Spectra

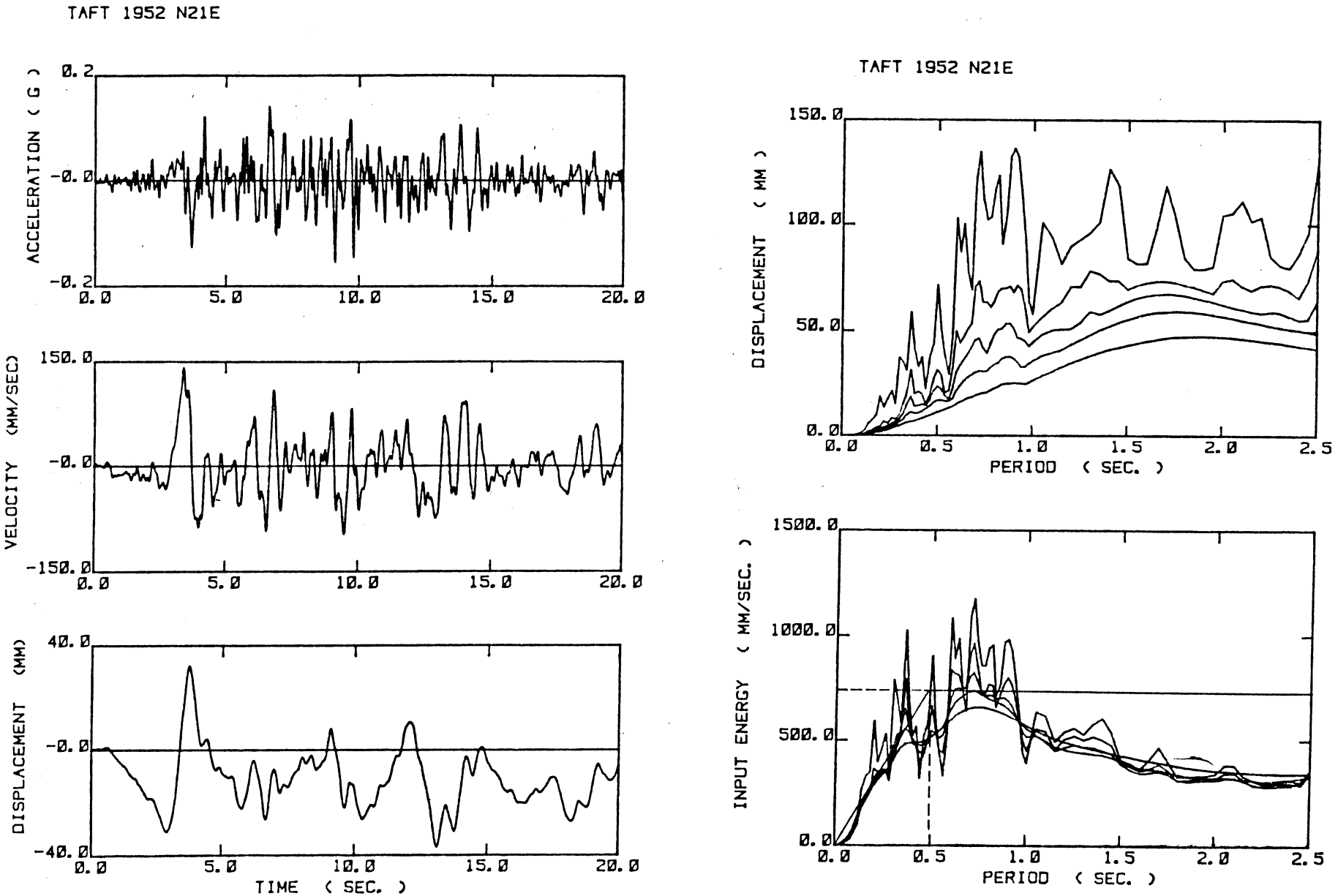


Fig. 2.5 Taft 1952 N21E Ground Motion Record and Response Spectra

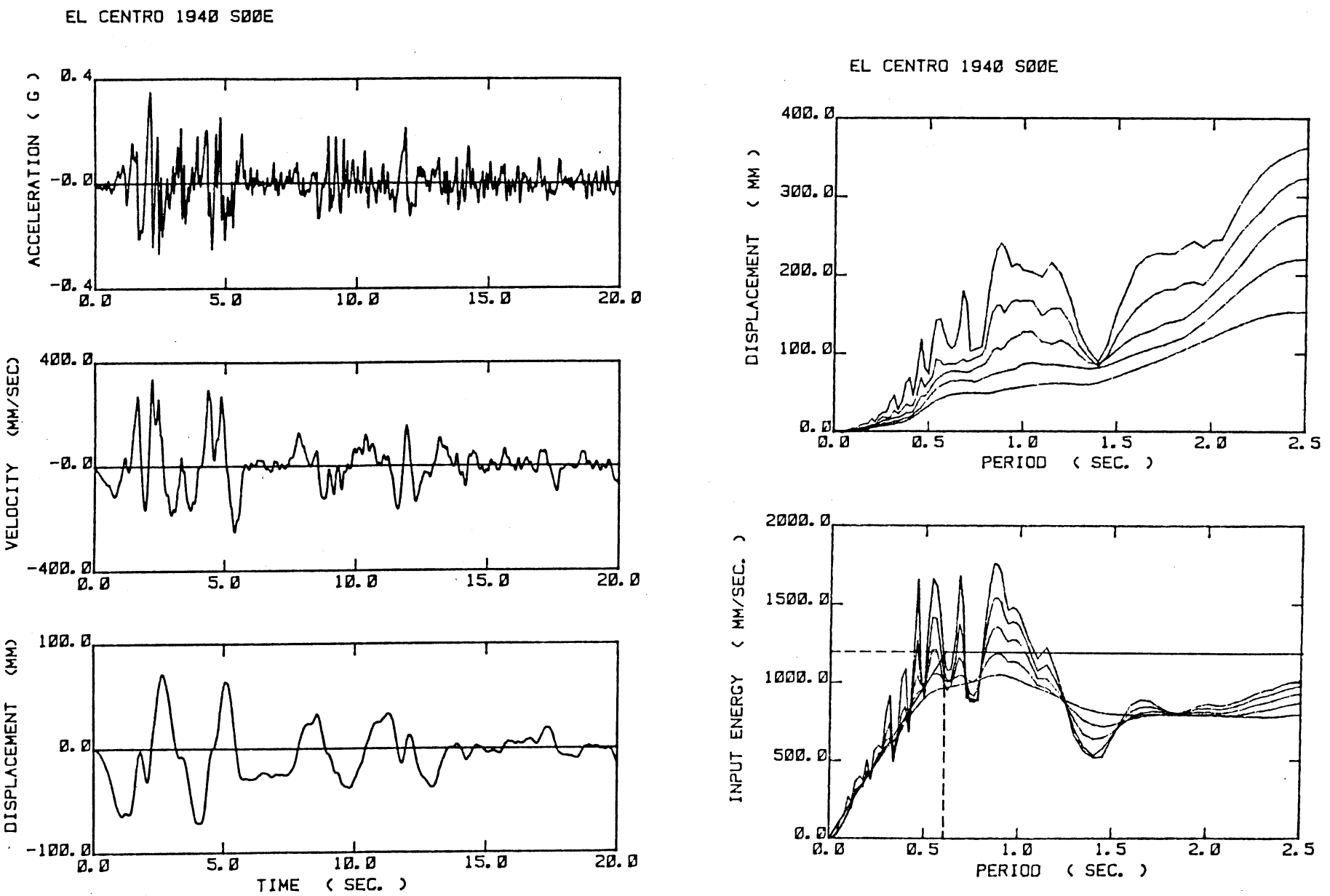


Fig. 2.6 El Centro 1940 S00E Ground Motion Record and Response Spectra

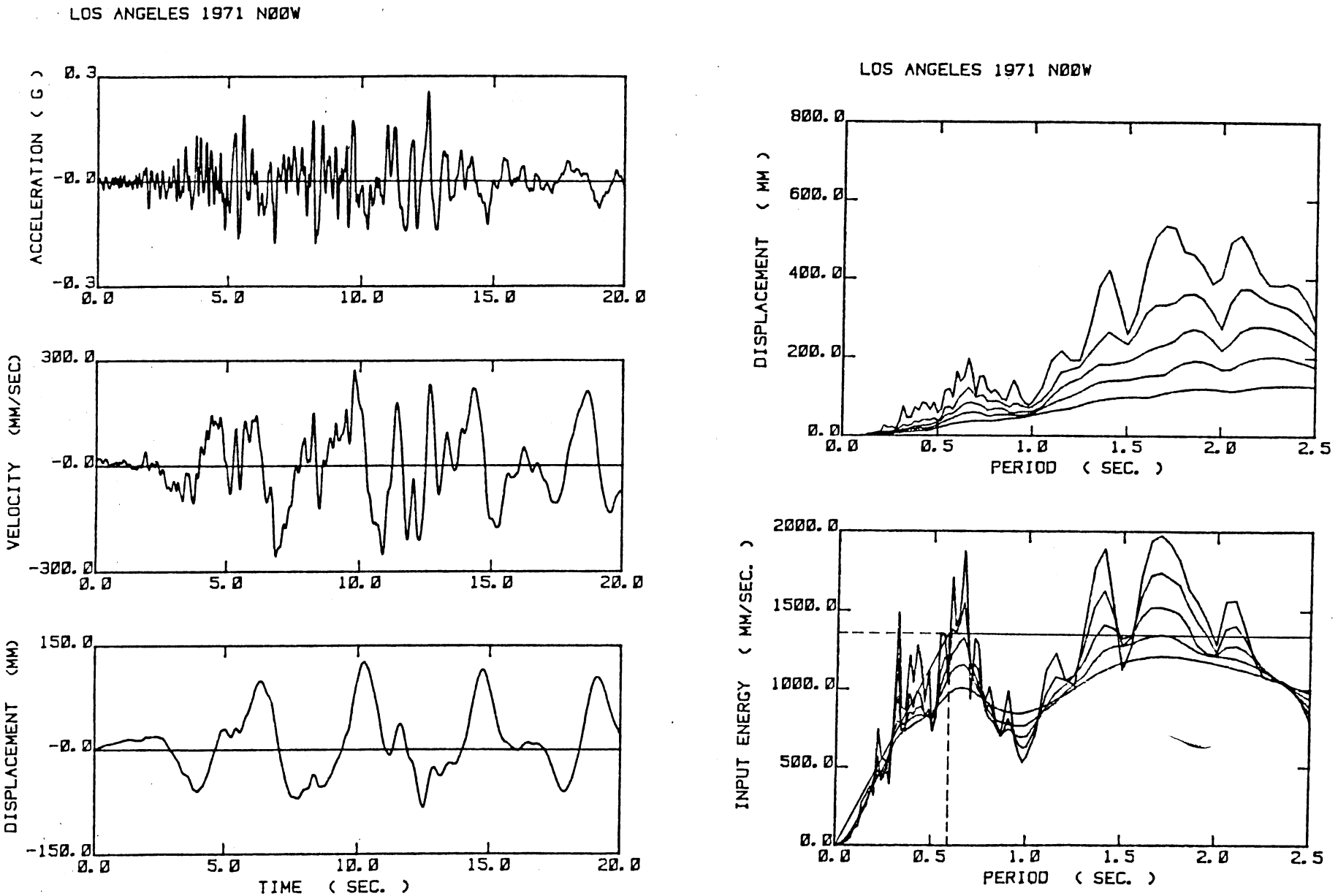


Fig. 2.7 Los Angeles 1971 N00W Ground Motion Record and Response Spectra

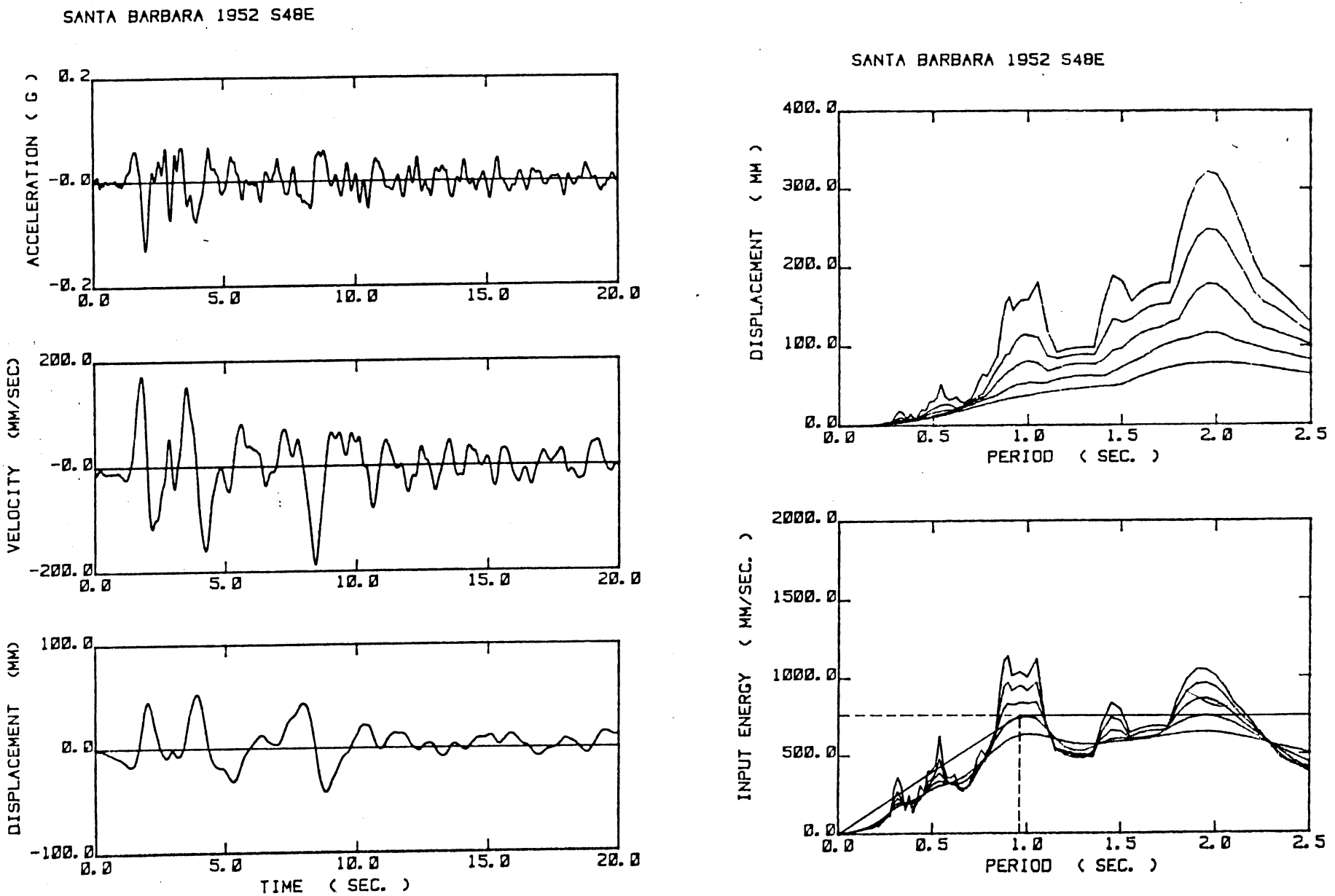


Fig. 2.8 Santa Barbara 1952 S48E Ground Motion Record and Response Spectra

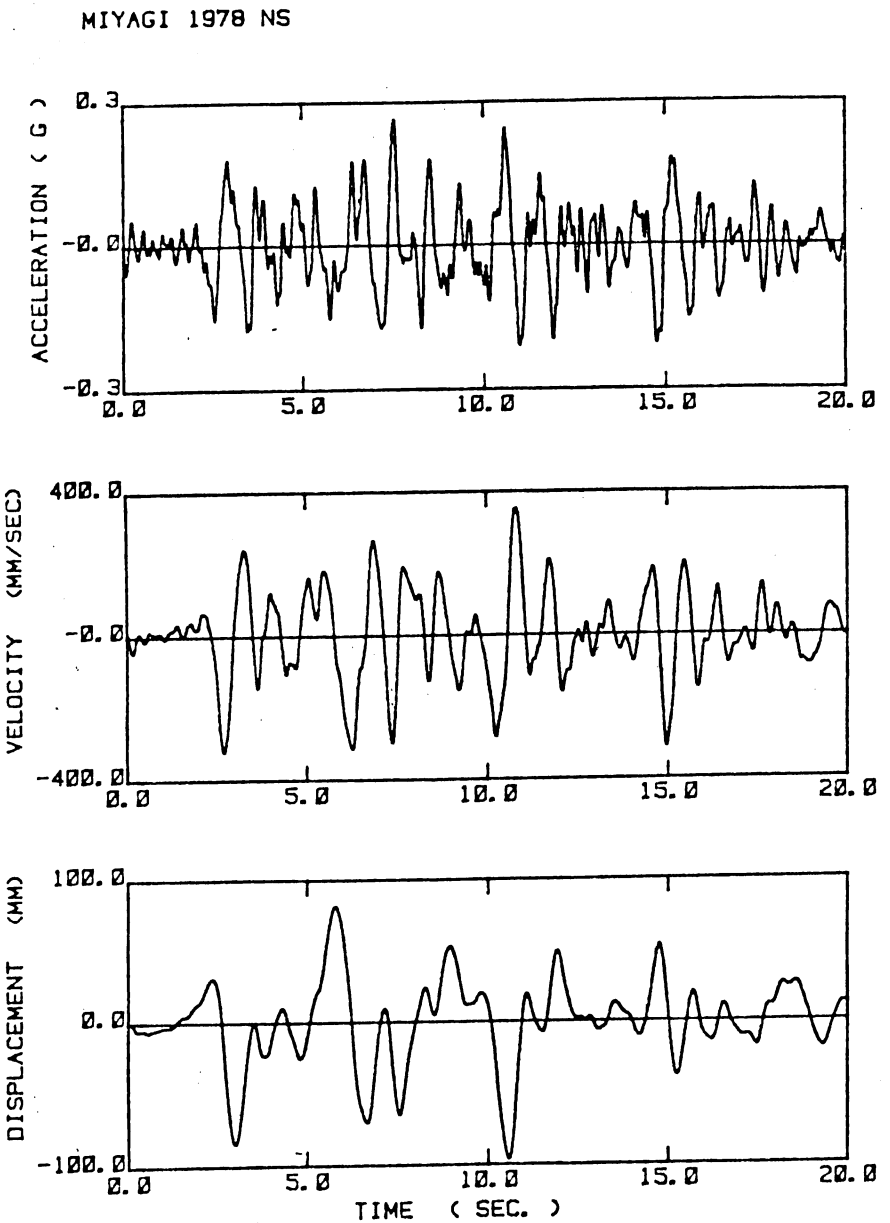


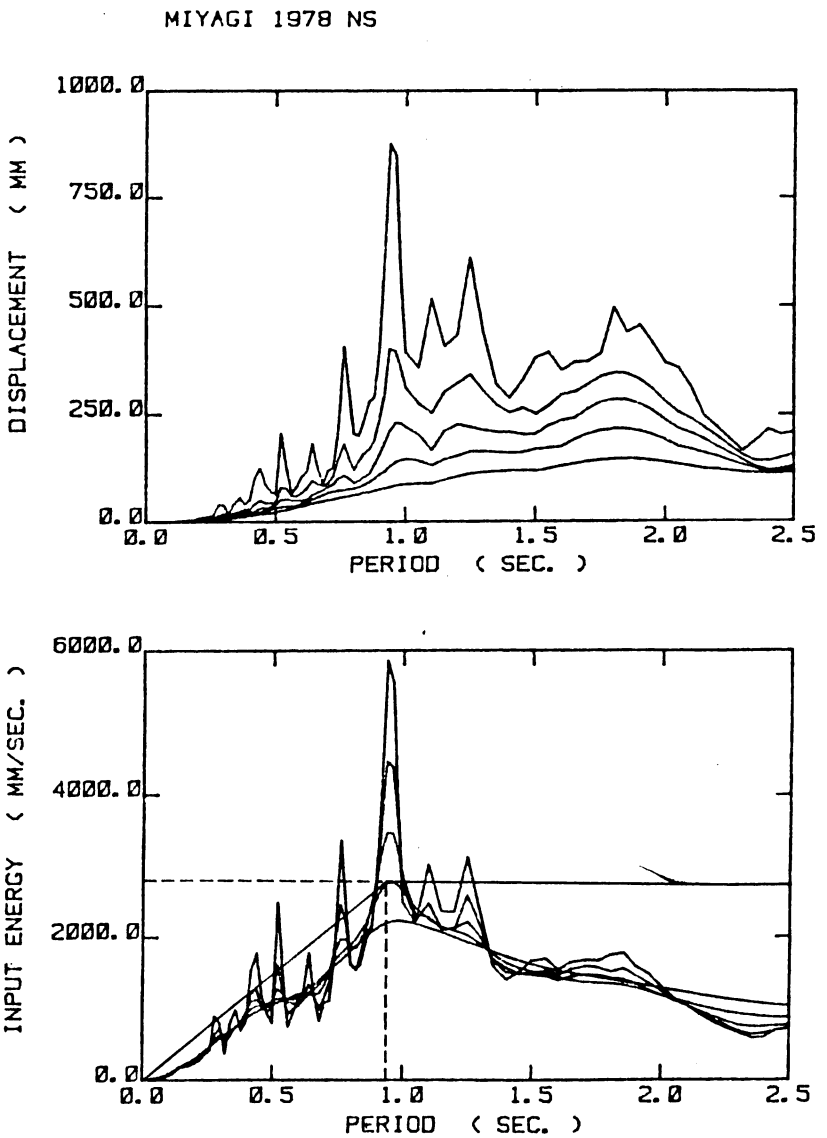


Fig. 2.9 Miyagi 1978 NS Ground Motion Record and Response Spectra

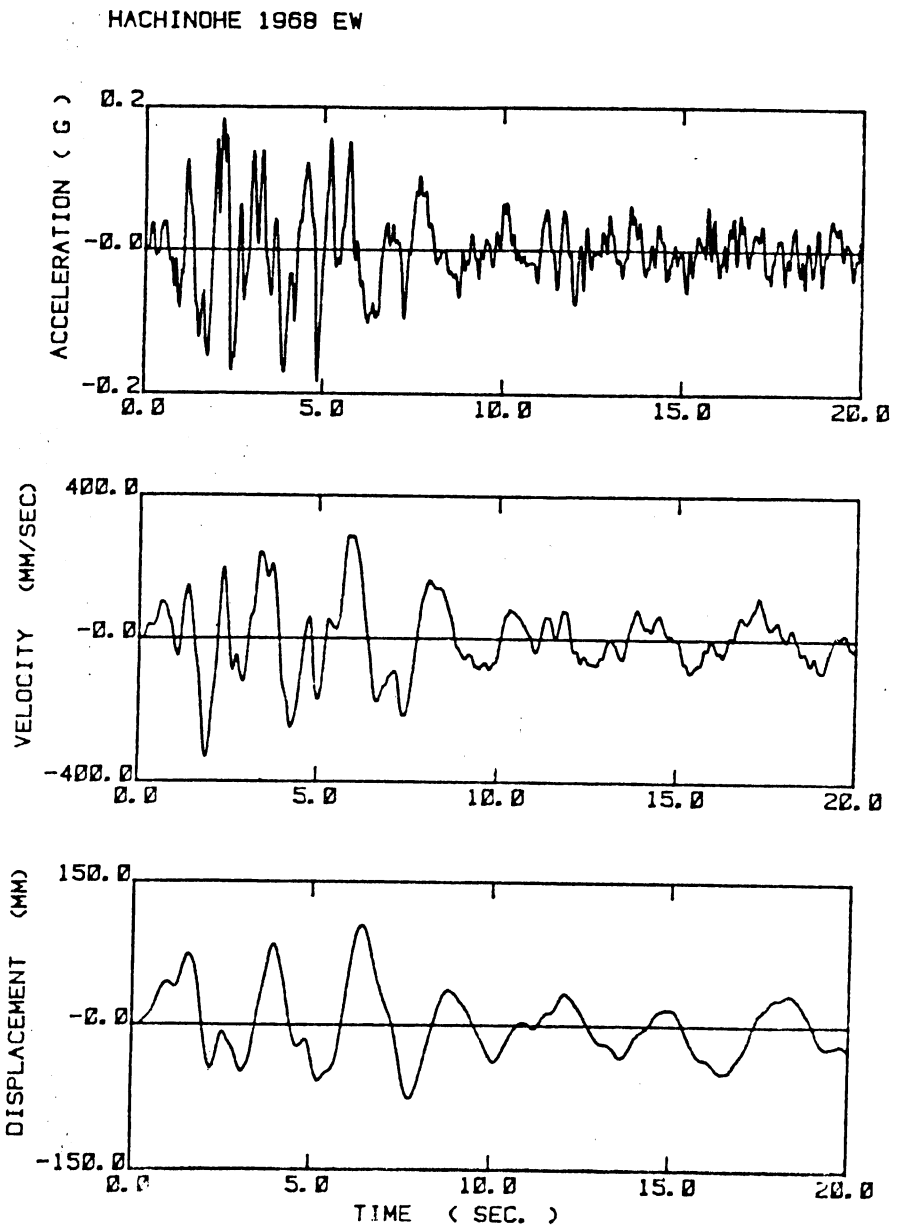


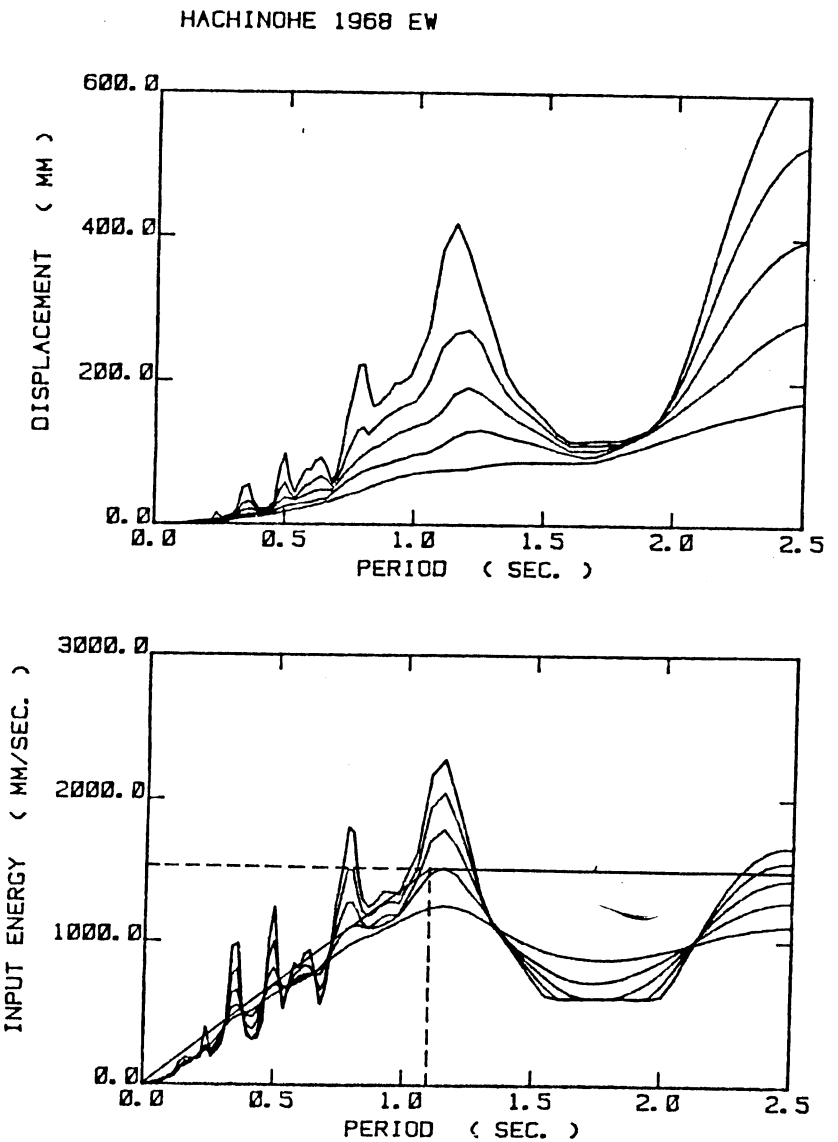


Fig. 2.10 Hachinohe 1968 EW Ground Motion Record and Response Spectra

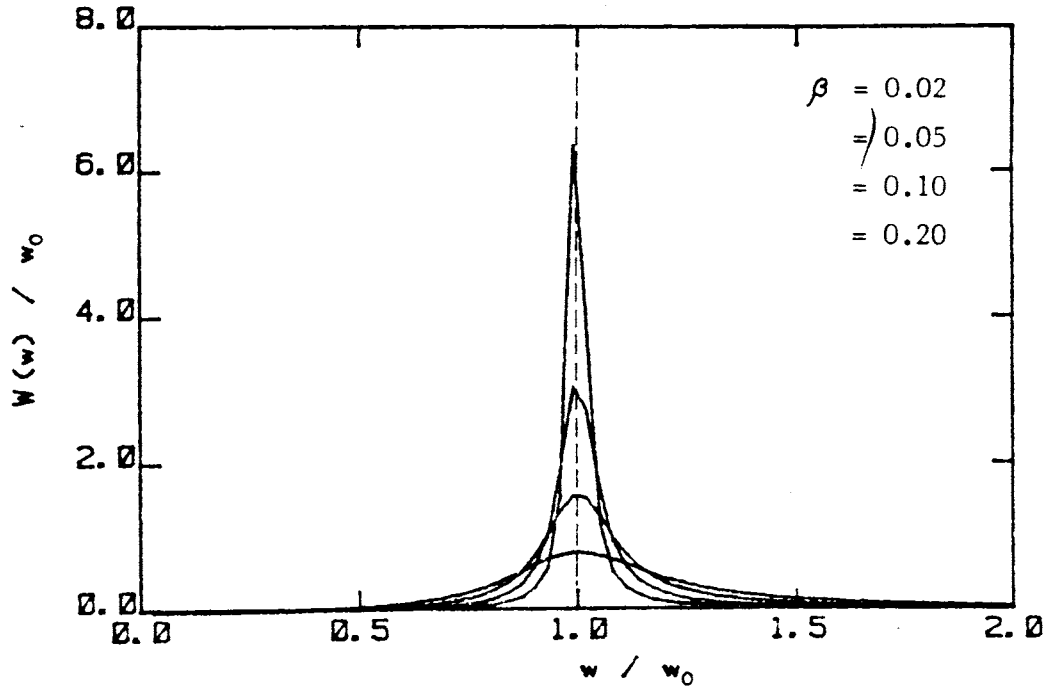


Fig. 2.11 Weighting Function for Energy Spectrum

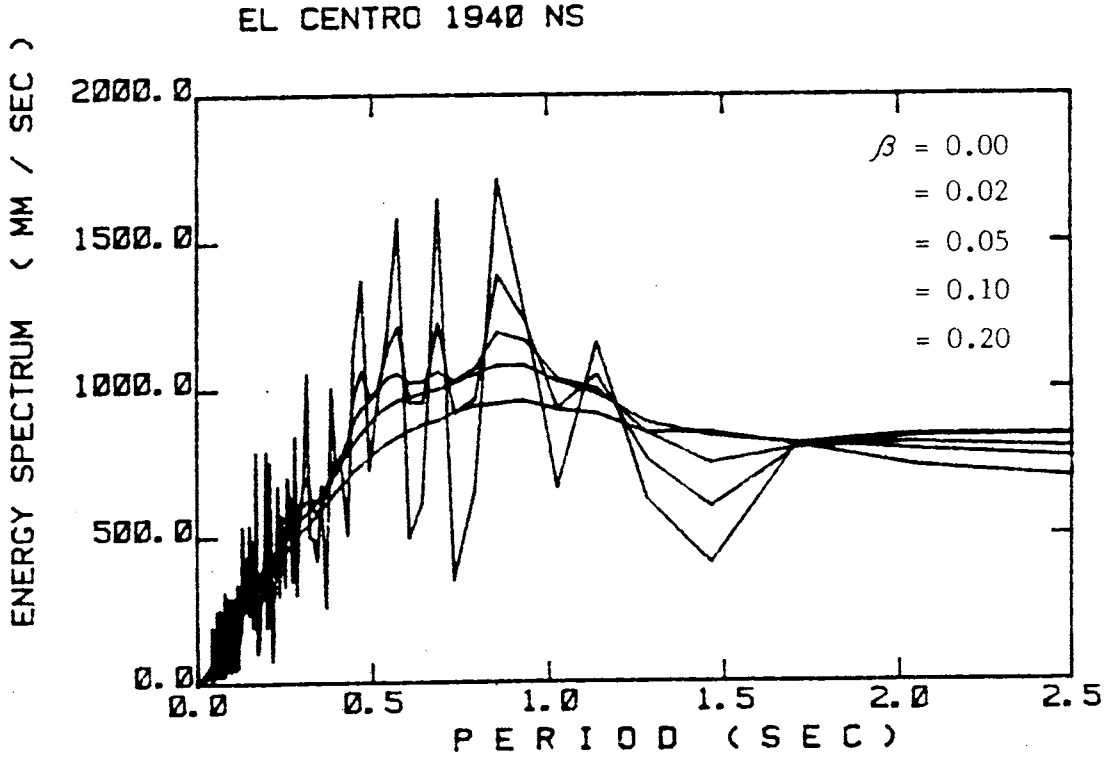


Fig. 2.12 Energy Spectra Obtained from Fourier Spectrum

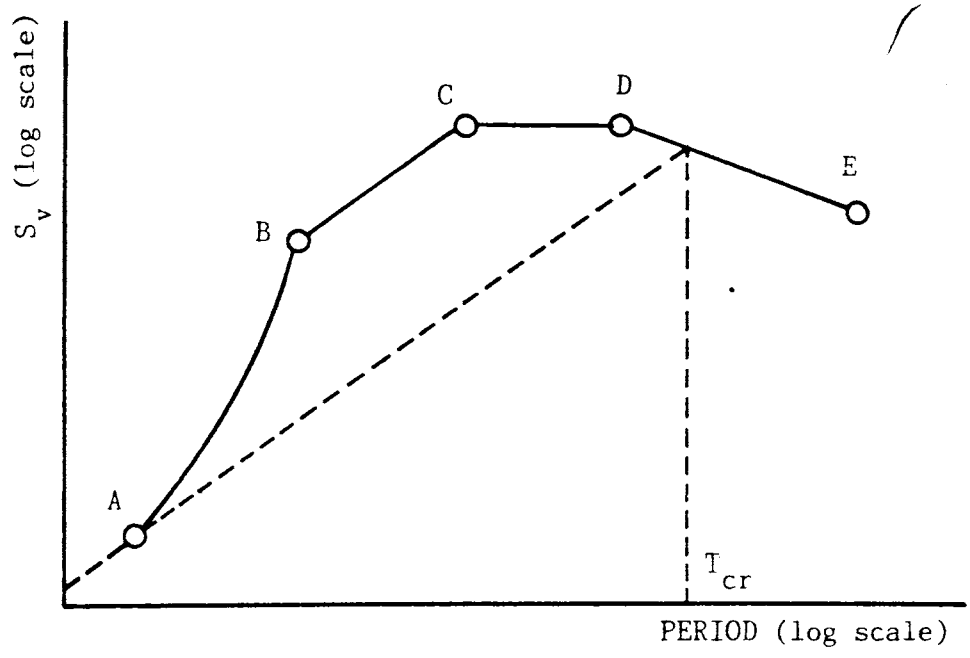


Periods T in sec. and velocity responses $S_v$ in cm/sec. at cotrol points A, B, C, D, and E are listed below for horizontal acceleration at free rock surface normalized to a ground velocity of 10 cm/sec. All velocity responses refer to a damping factor of 0.05.

| Field | Magnitude, M | Epicentral Distance (km) | Control Points | | | | | | | | | |
|---|---|---|---|---|---|---|---|---|---|---|---|---|
| | | | A | | B | | C | | D | | E | |
| | | | $T_A$ | $S_v$ | $T_B$ | $S_v$ | $T_C$ | $S_v$ | $T_D$ | $S_v$ | $T_E$ | $S_v$ |
| Near | 8 | 25 | 0.02 | 0.6 | 0.10 | 10 | 0.30 | 30 | 0.50 | 30 | 2.0 | 12 |
| | 7 | 10 | | 0.7 | 0.10 | 11 | 0.23 | 24 | 0.45 | 24 | | 7 |
| | 6 | 5 | | 1.2 | 0.10 | 17 | 0.13 | 21 | 0.35 | 21 | | 3 |
| Intermediate | 8 | 120 | | 0.5 | 0.20 | 18 | 0.35 | 32 | 1.00 | 32 | | 26 |
| | 7 | 45 | | 0.5 | 0.13 | 11 | 0.33 | 28 | 0.80 | 28 | | 19 |
| | 6 | 15 | | 0.6 | 0.10 | 10 | 0.25 | 24 | 0.60 | 24 | | 12 |
| Far | 8 | 350 | | 0.5 | 0.22 | 26 | 0.37 | 44 | 1.20 | 44 | | 42 |
| | 7 | 150 | | 0.5 | 0.14 | 15 | 0.36 | 38 | 0.90 | 38 | | 32 |
| | 6 | 60 | | 0.5 | 0.10 | 10 | 0.33 | 33 | 0.70 | 33 | | 20 |

Fig. 2.13 Ohsaki Spectra

Alluvium Model

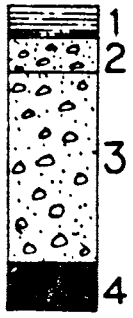


| soil | H(m) | $\rho$(t/m$^3$) | Initial Values | | Modified Values*1 | |
|---|---|---|---|---|---|---|
| | | | $V_s$(m/s) | $\beta$ | $V_s$(m/s) | $\beta$ *2 |
| 1. fill, silt | 3 | 1.4 | 100 | 0.05 | 70 | 0.15 |
| 2. gravel | 4 | 1.9 | 200 | 0.02 | 160 | 0.10 |
| 3. gravel | 23 | 1.9 | 300 | 0.02 | 240 | 0.10 |
| 4. rock | | 2.0 | 600 | 0.02 | 540 | 0.05 |

*1 Values are modified to be compatible with strains calculated from response analysis of the models subjected to incident seismic waves,

*2 complex damping factor.

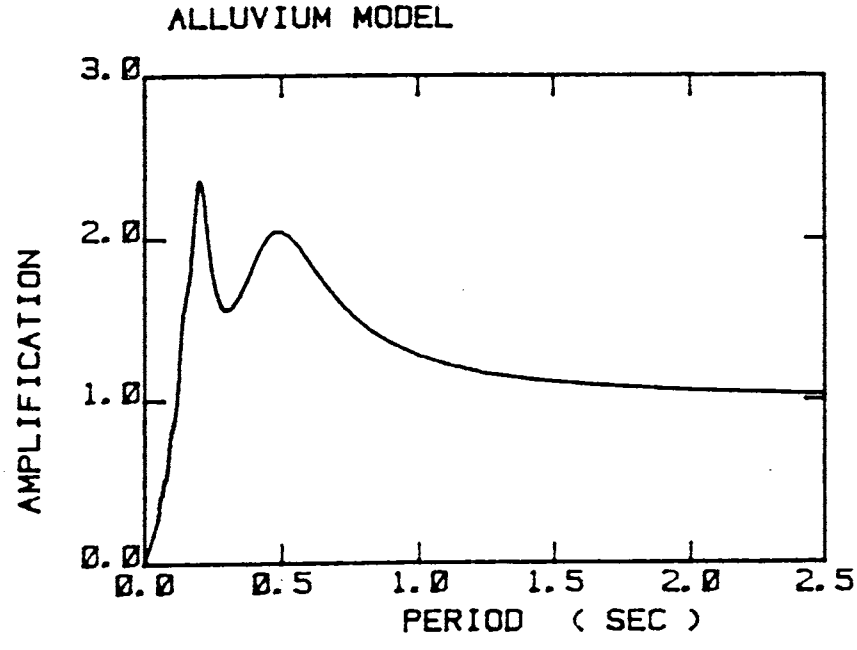


Fig. 2.14 Calculated Amplification Factor for a Site in Sendai, Japan ( after Shibuya et al, 1980 )

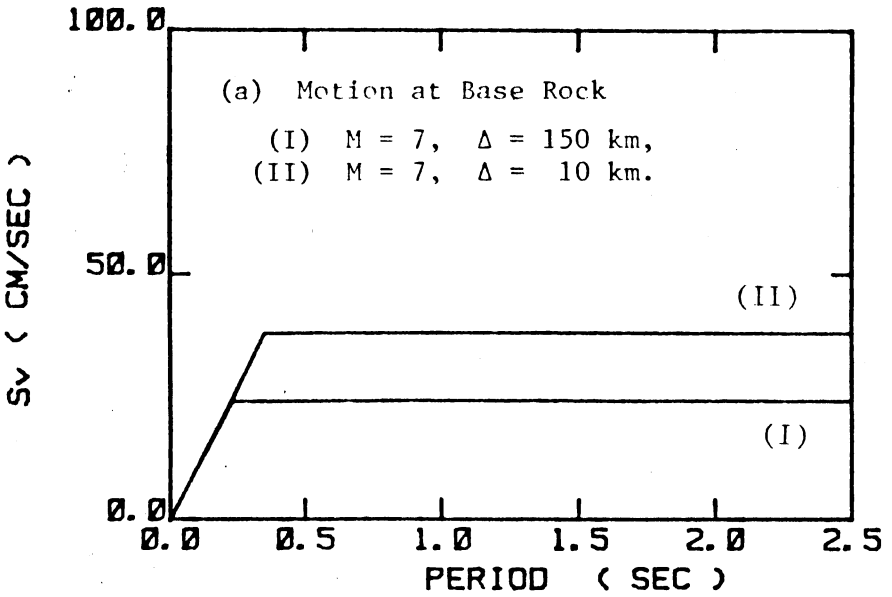


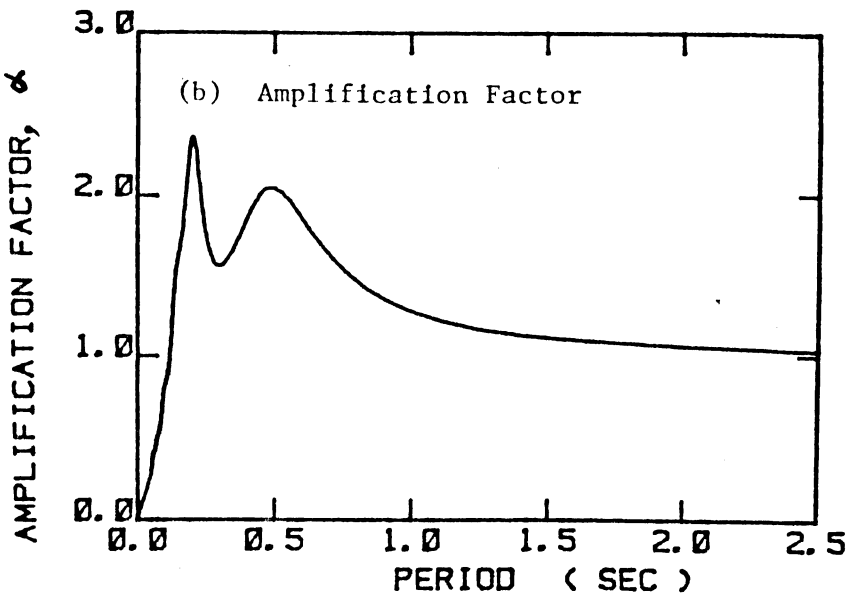


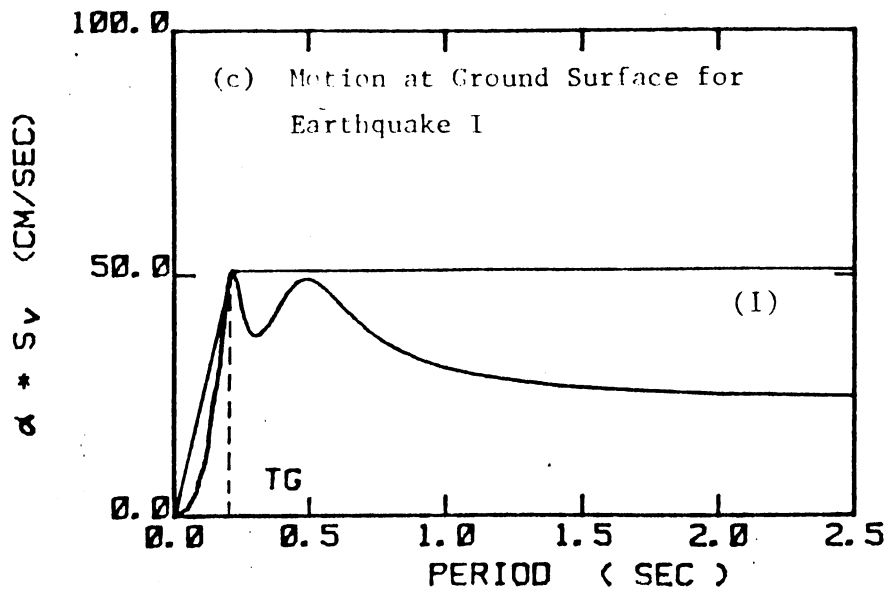


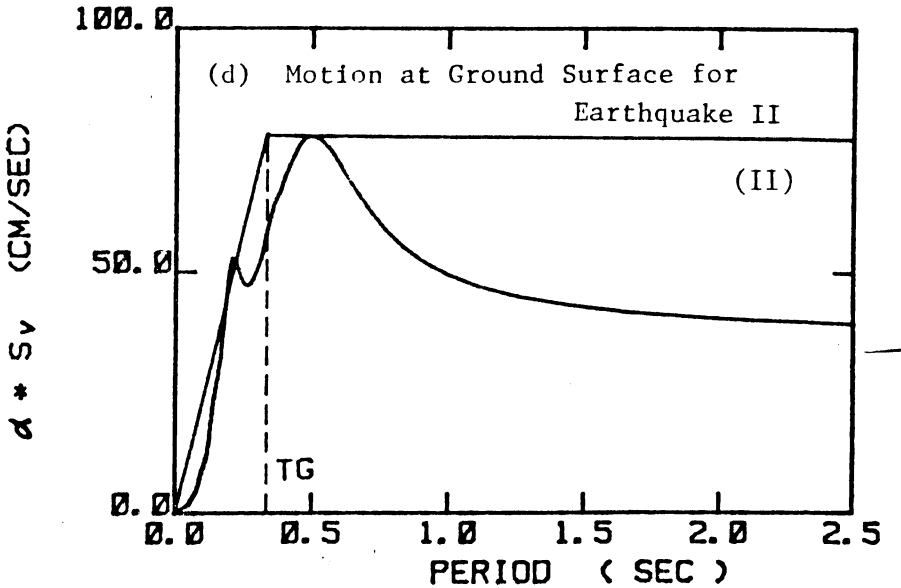


Fig. 2.15 An Illustration of Differences in Characteristic Period for Ground Motions

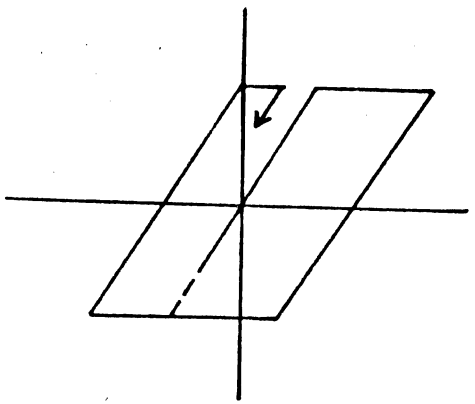

MODEL 1

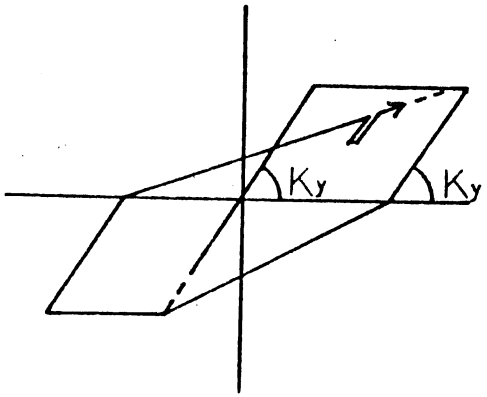


MODEL 2

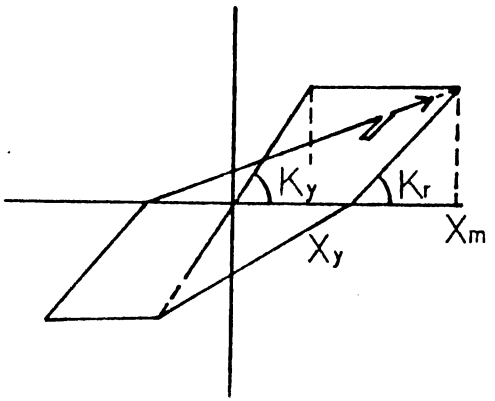


MODEL 3

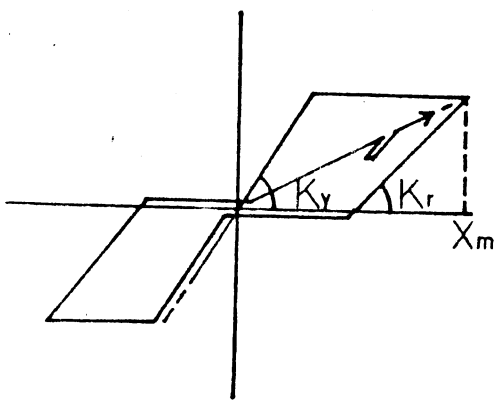


MODEL 4

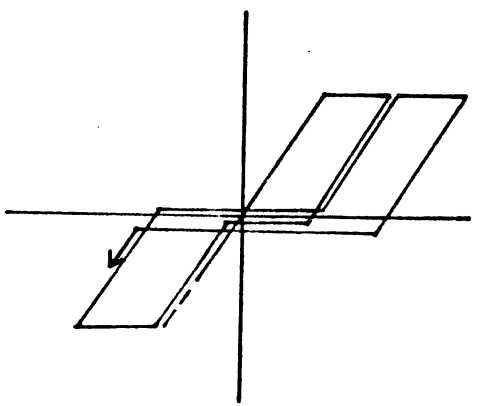

MODEL 5

$$K_r = K_y \sqrt{X_y / X_m}$$

Fig. 3.1 Hysteresis Models

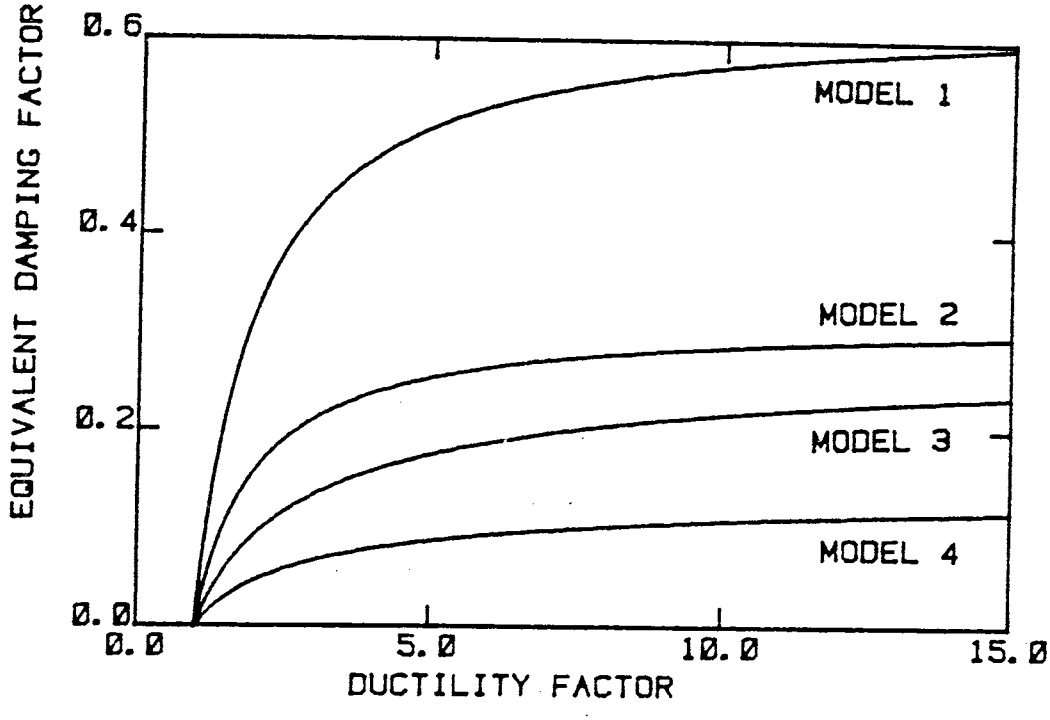


Fig. 3.2 Equivalent Damping Factor

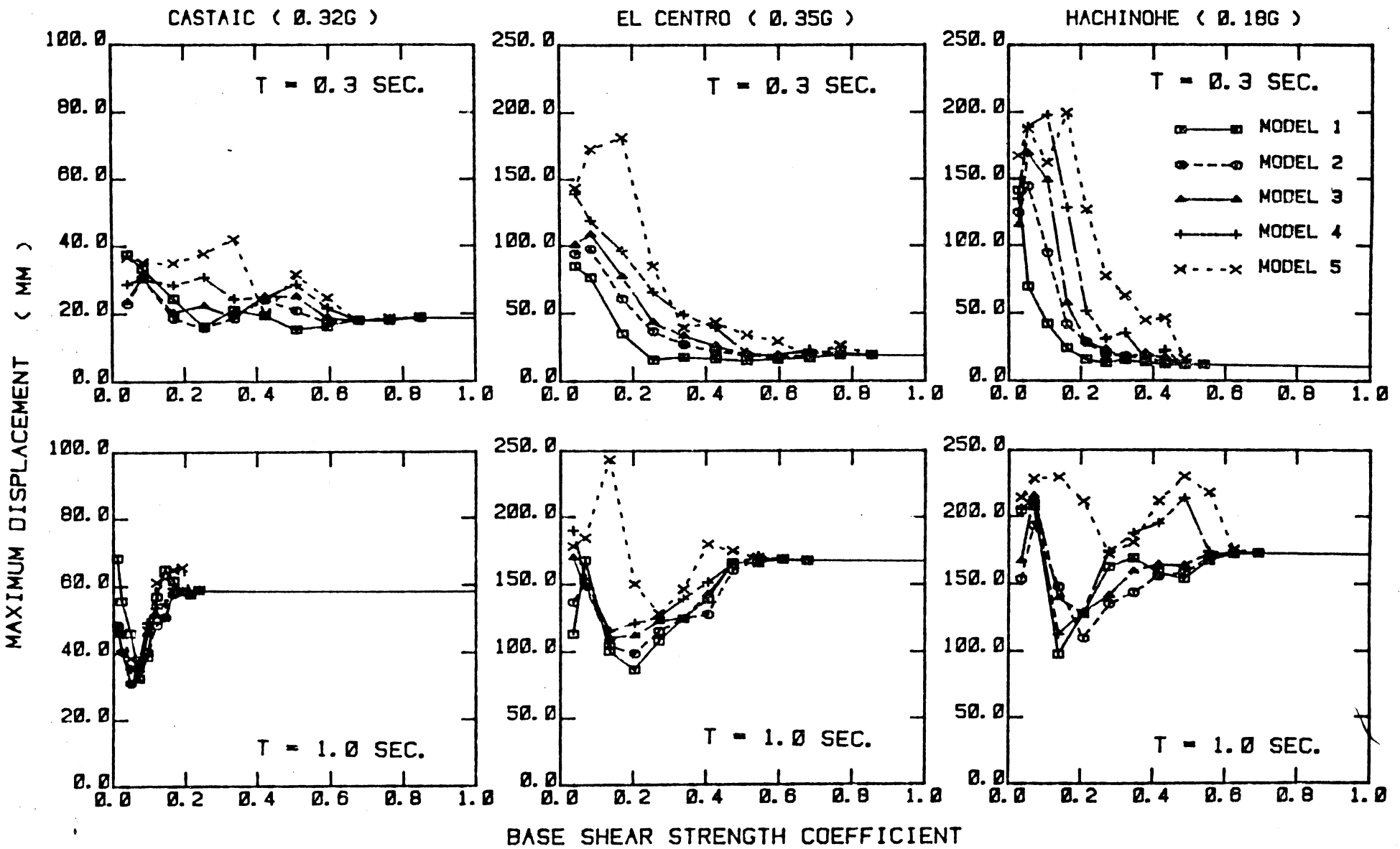


Fig. 4.1 Calculated Nonlinear Response for Various Hysteresis Models, Ground Motions and Initial Periods

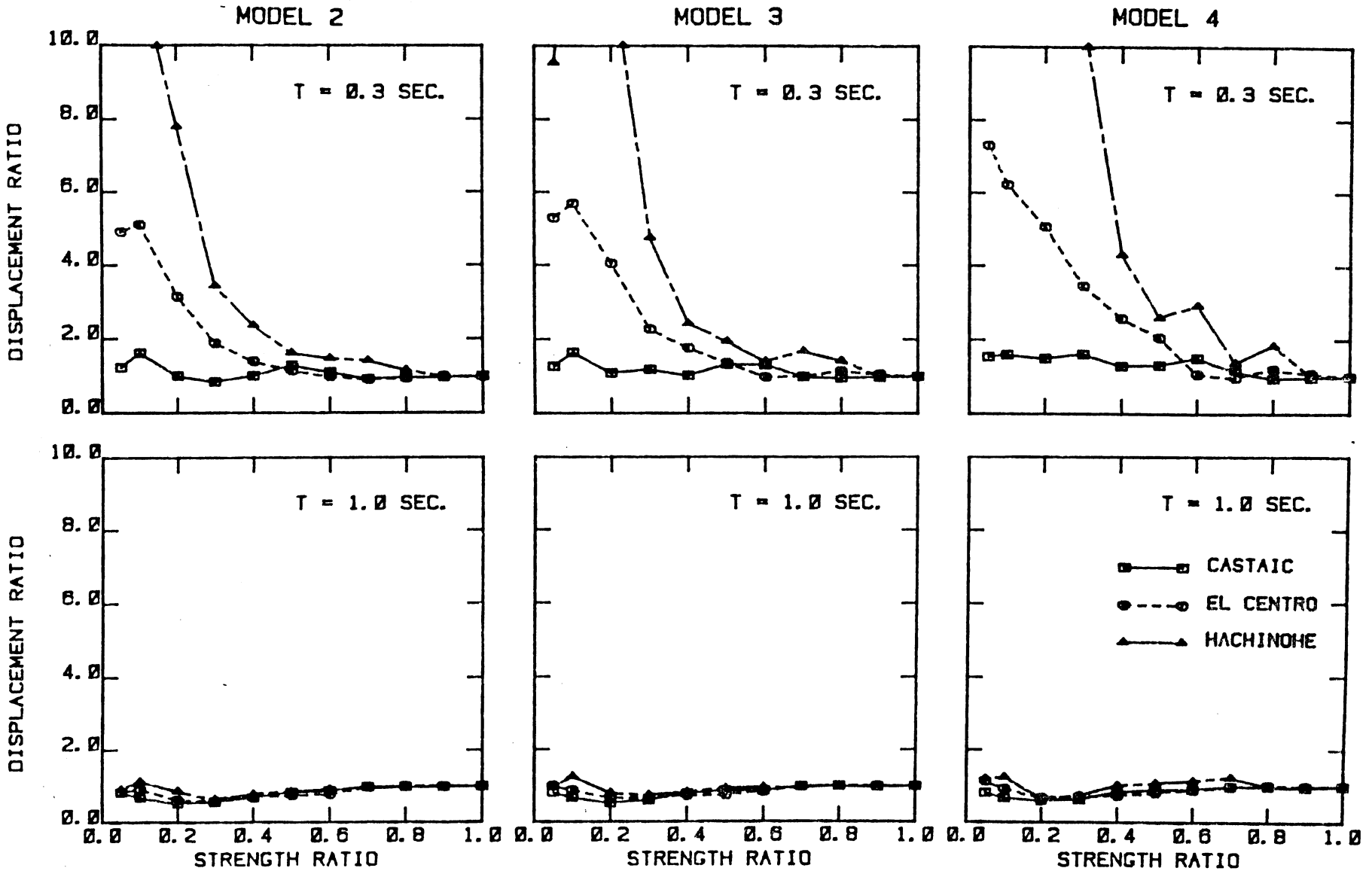


Fig. 4.2 Variation of Nonlinear Displacement Response with the Type of Ground Motion and Hysteresis Model

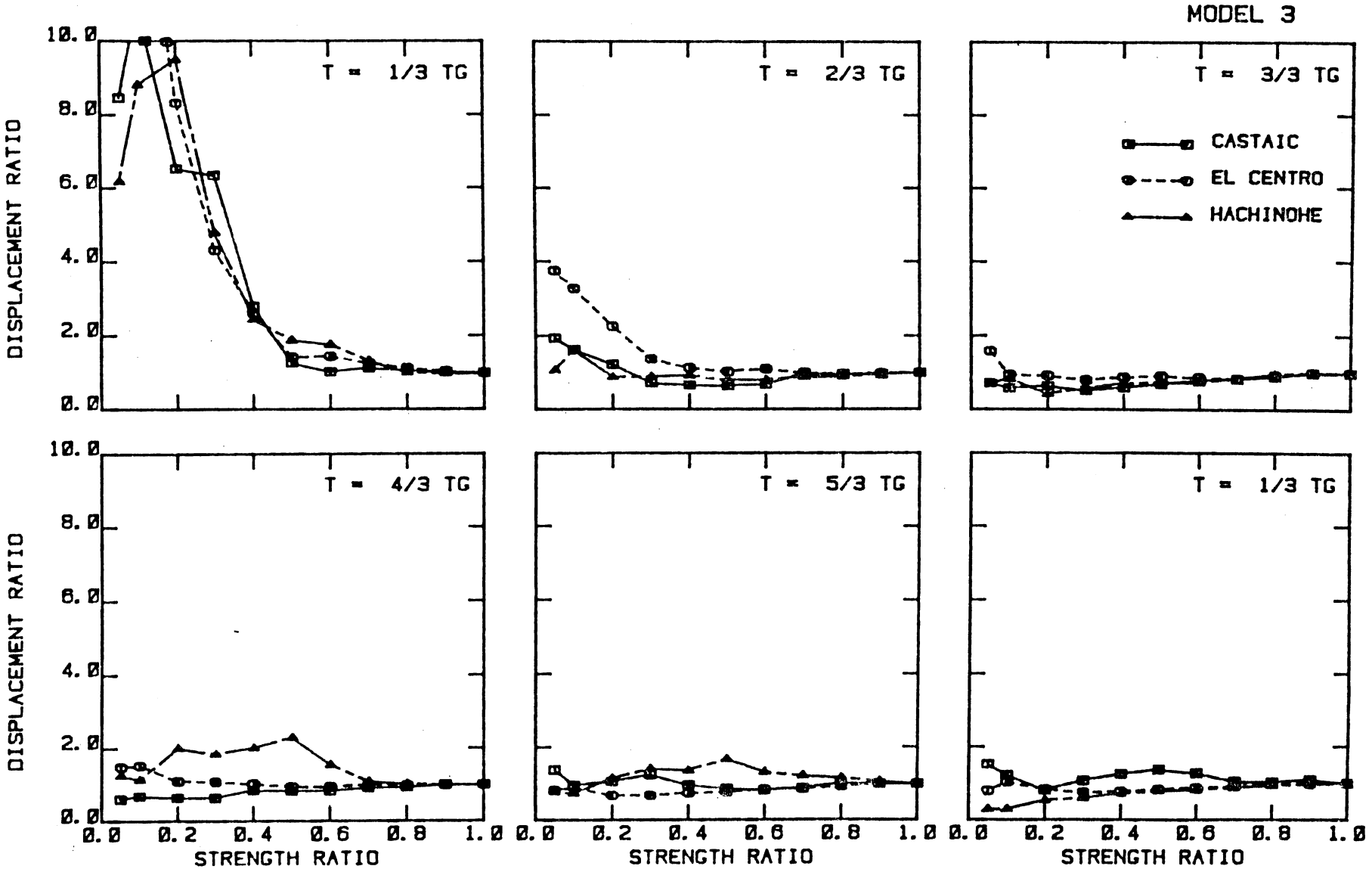


Fig. 4.3 Normalized Nonlinear Displacement Response

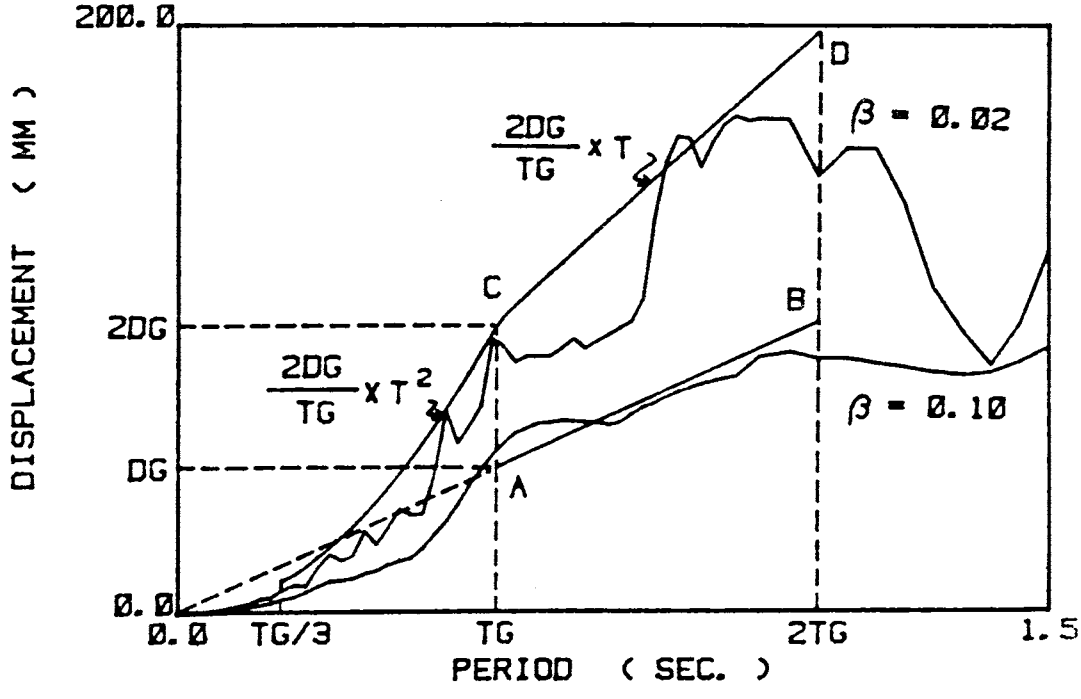


Fig. 4.4 Construction of the Idealtzed Displacement Response Spectrum for a Dumping Factor of 0.02

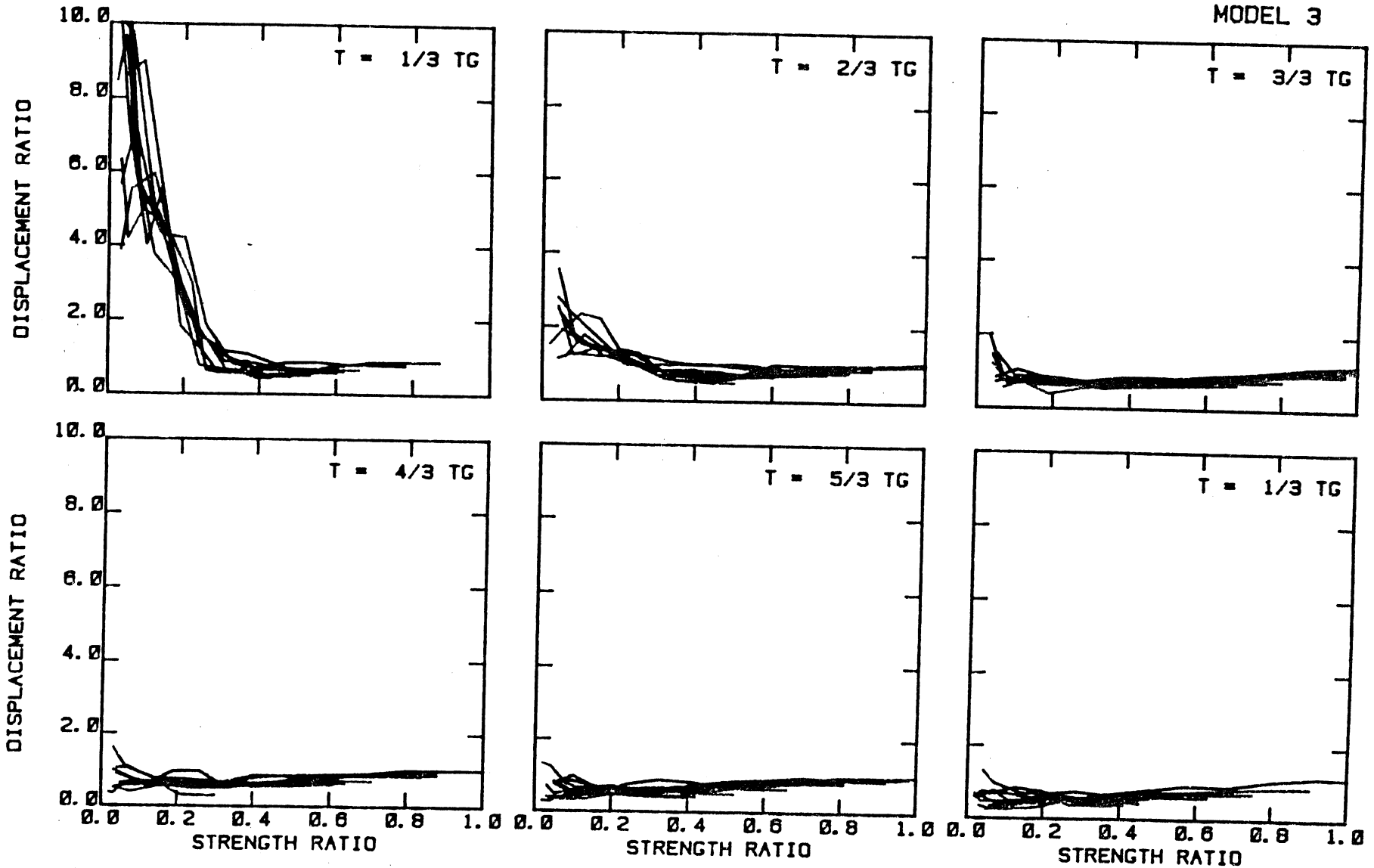


Fig. 4.5 Normalized Nonlinear Displacement Response Based on Ldealized Displacement Response Spectra ( Model 3 )

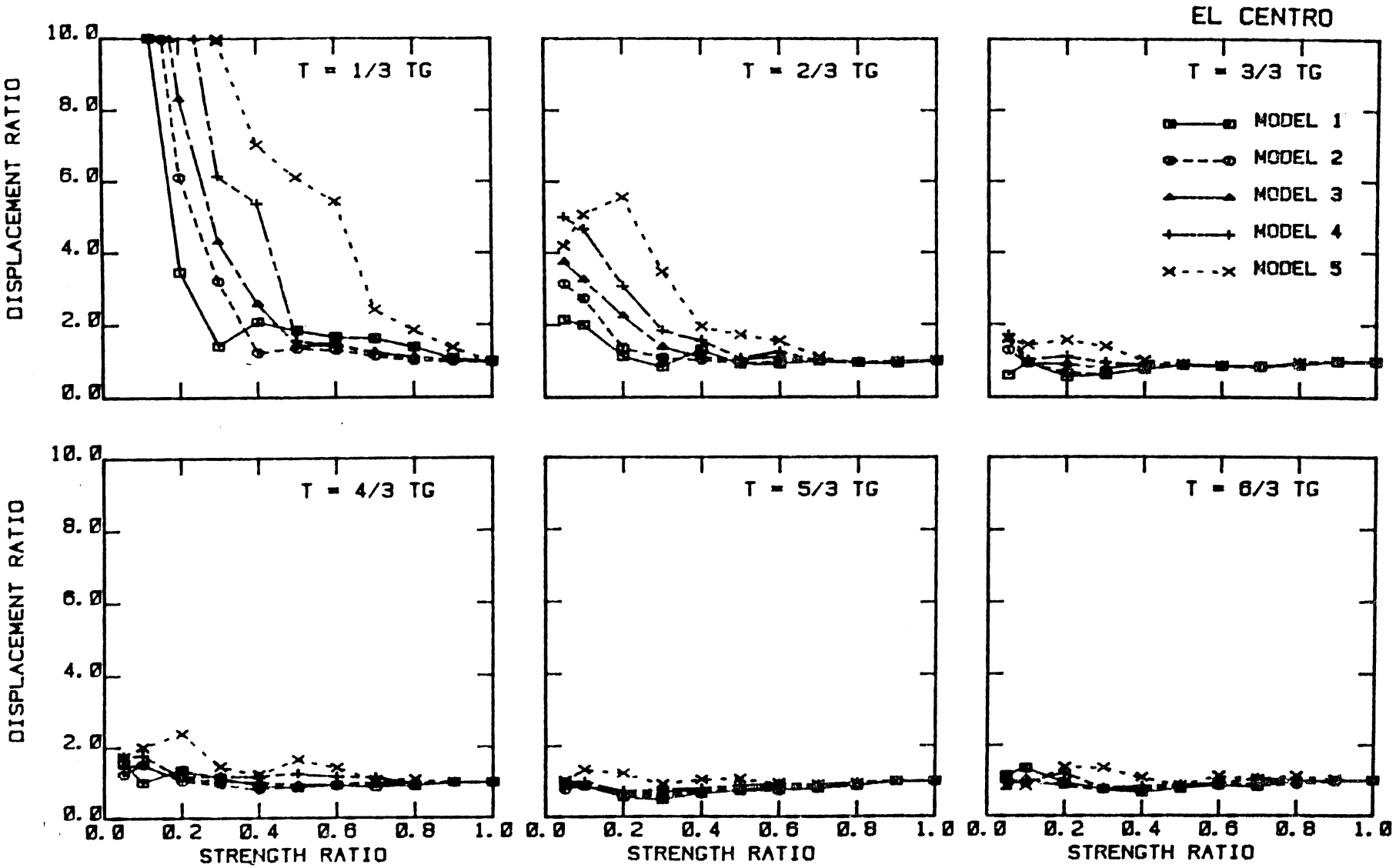


Fig. 4.6 Variation of Nonlinear Displacement Response with Type of Hysteresis Model ( Response to El Centro )

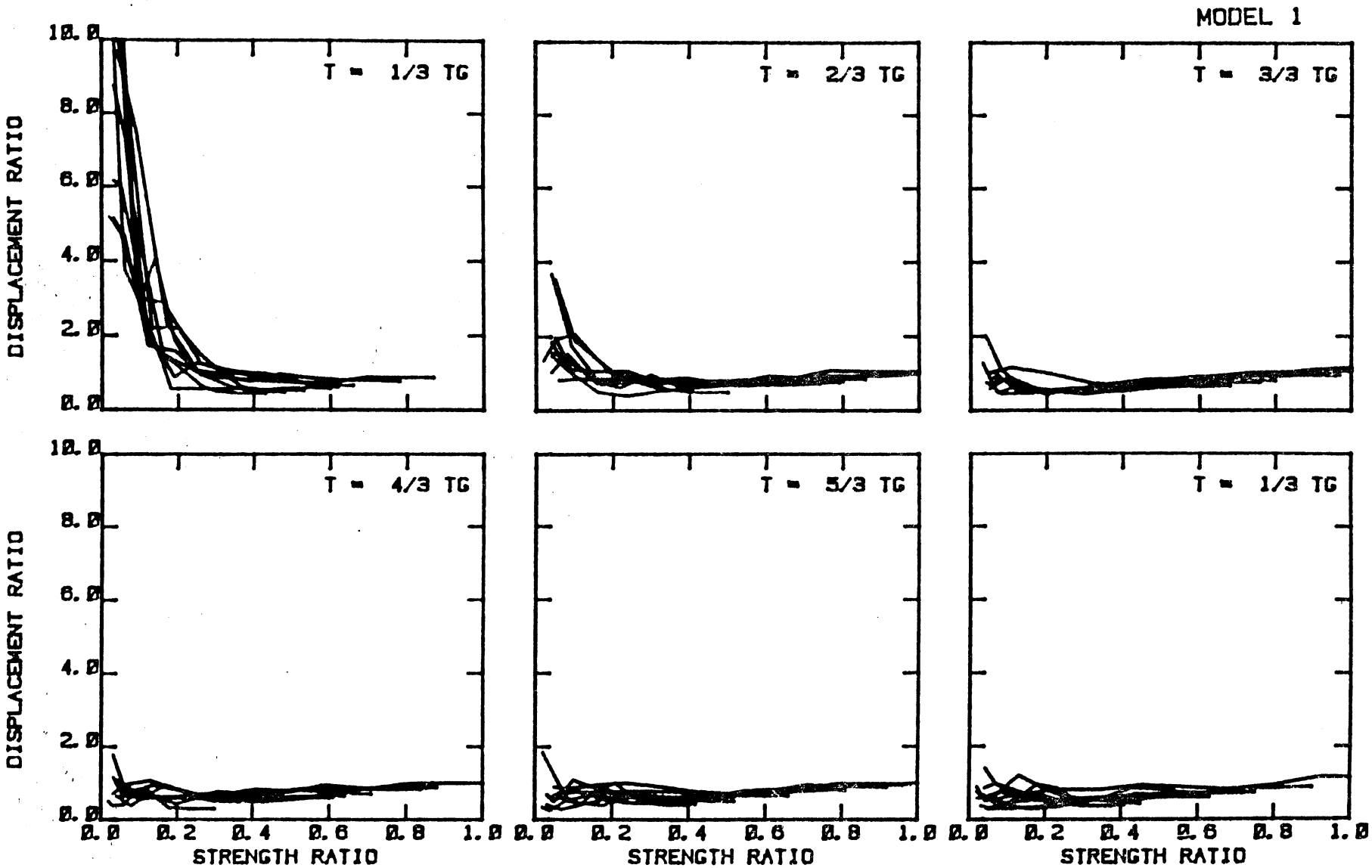


Fig. 4.7 Normalized Nonlinear Displacement Response Based on Idealized Displacement Response Spectra ( model 1 )

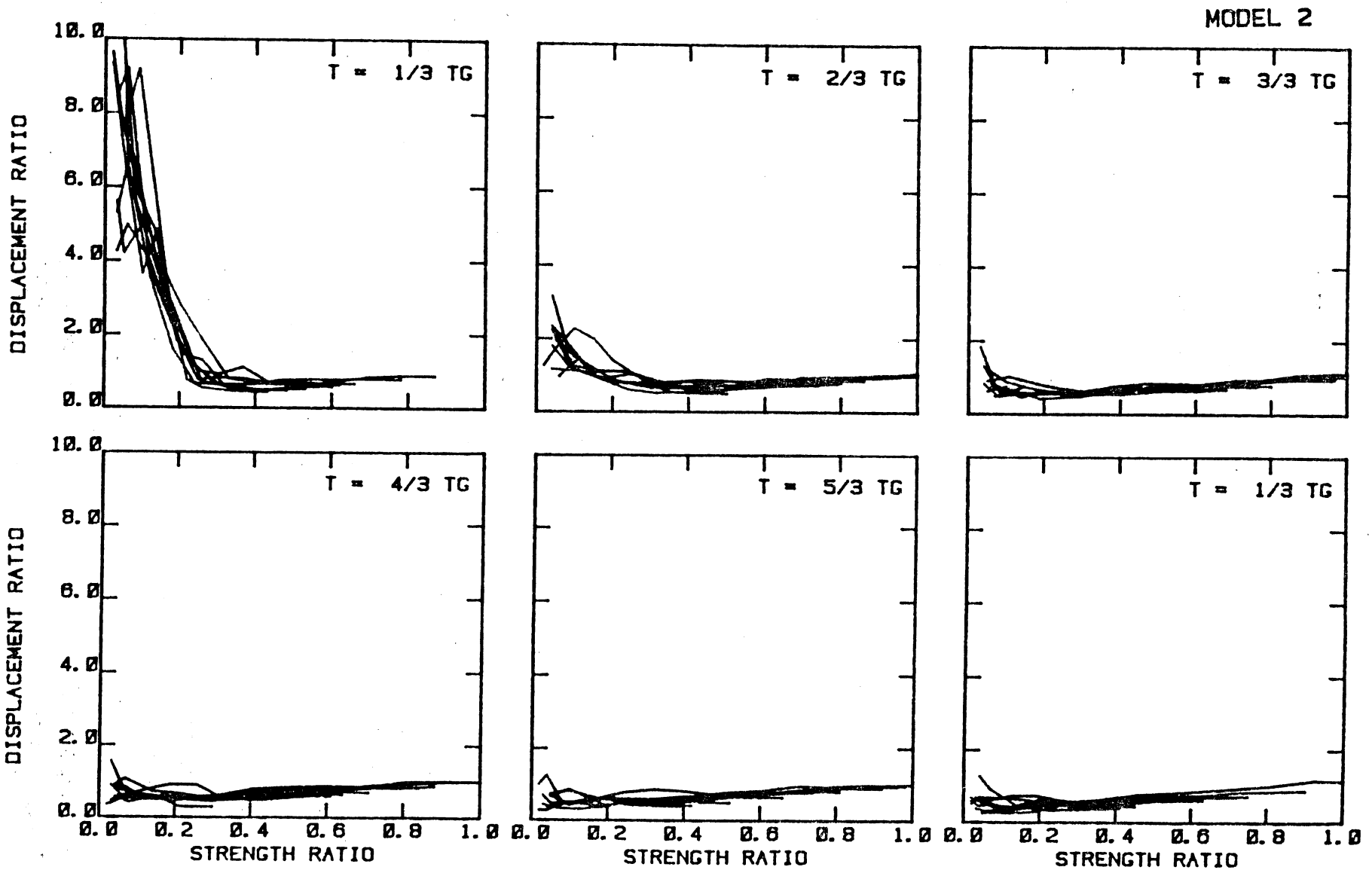


Fig. 4.8 Normalized Nonlinear Displacement Response Based on Idealized Displacement Response Spectra ( Model 2 )

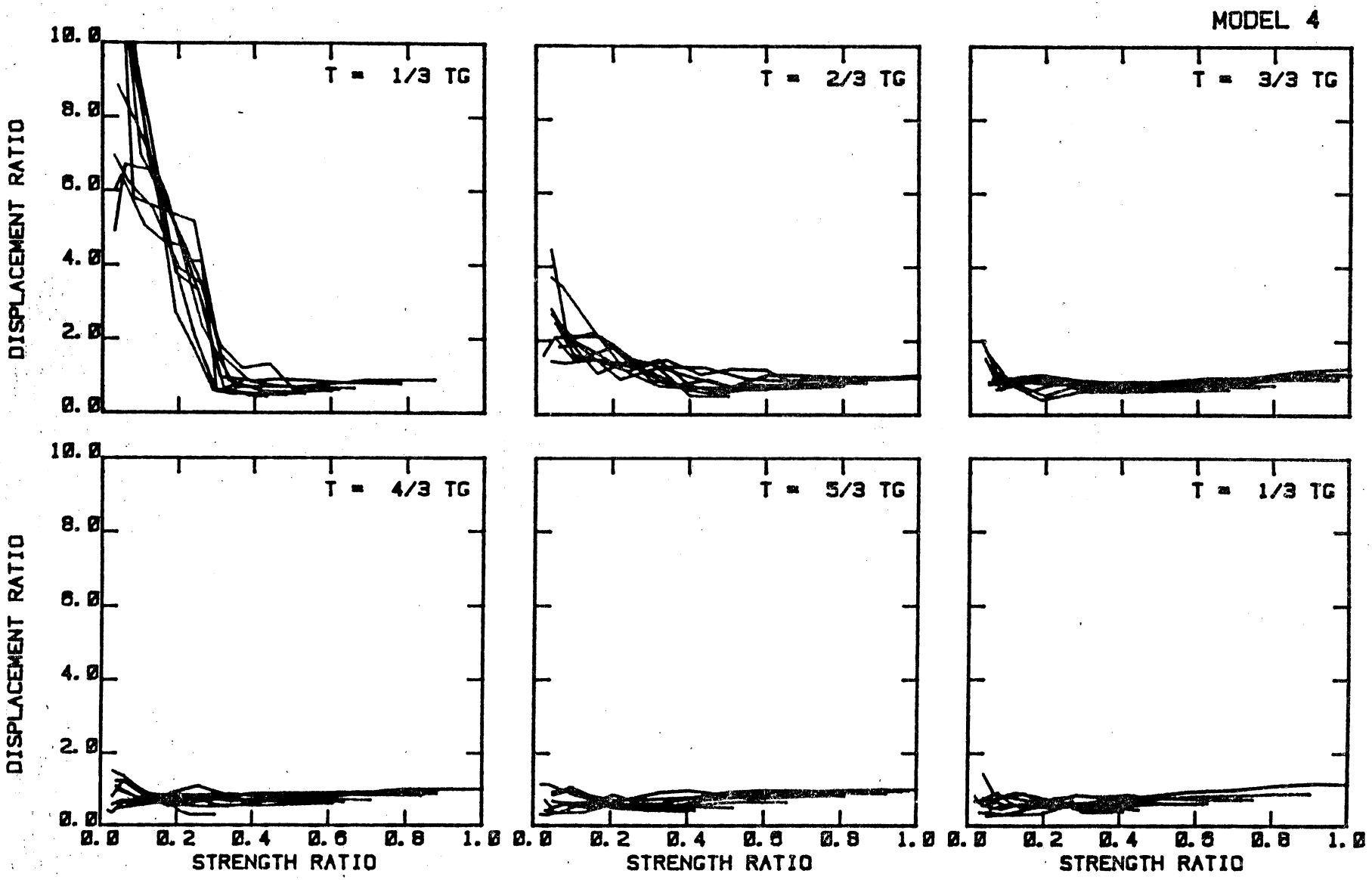


Fig. 4.9 Normalized Nonlinear Displacement Response Based on Idealized Displacement Response Spectra ( Model 4 )

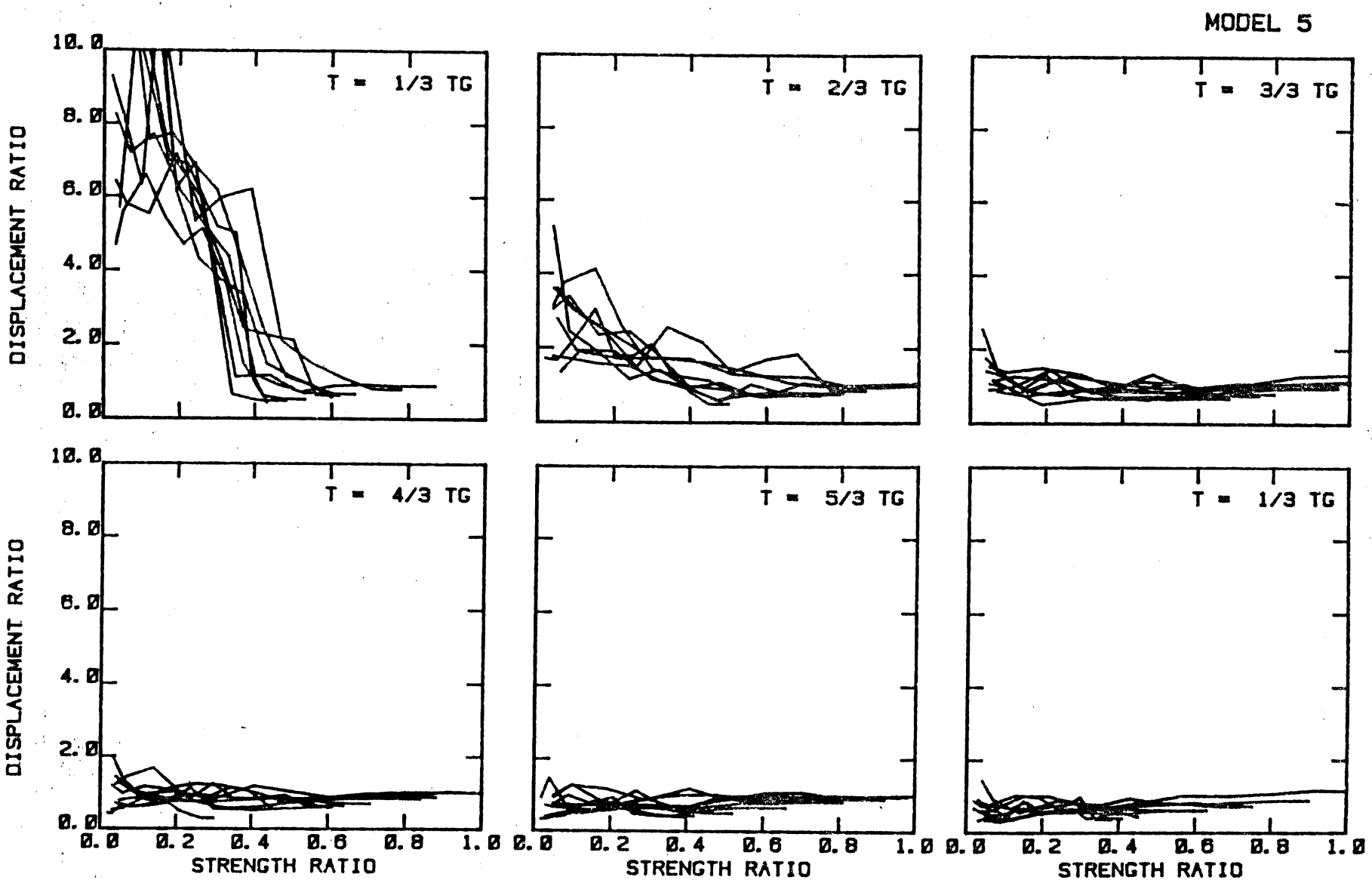


Fig. 4.10 Normalized Nonlinear Displacement Response Based on Idealized Displacement Response Spectra ( Model 5 )

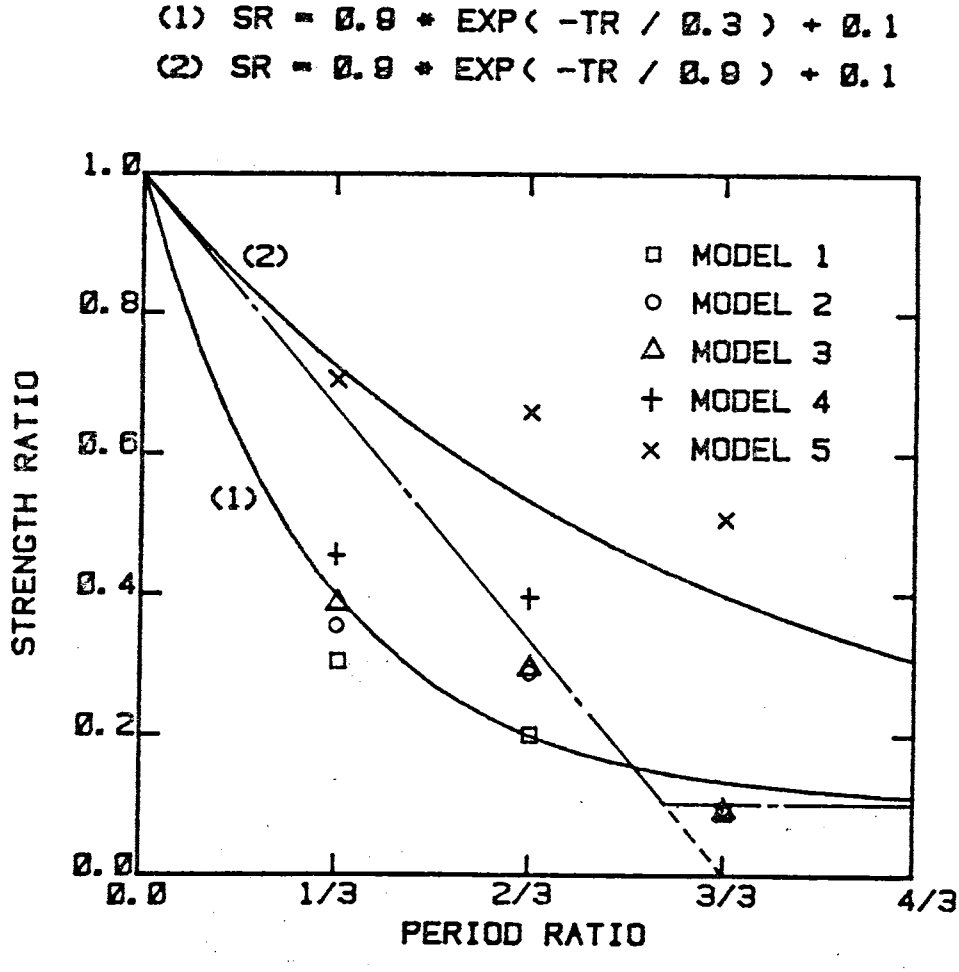


Fig. 4.11 Effect of Strength Ratio, SR, and Period Ratio, TR, on Region when Displacement Ratio, DR, does not exceed unity

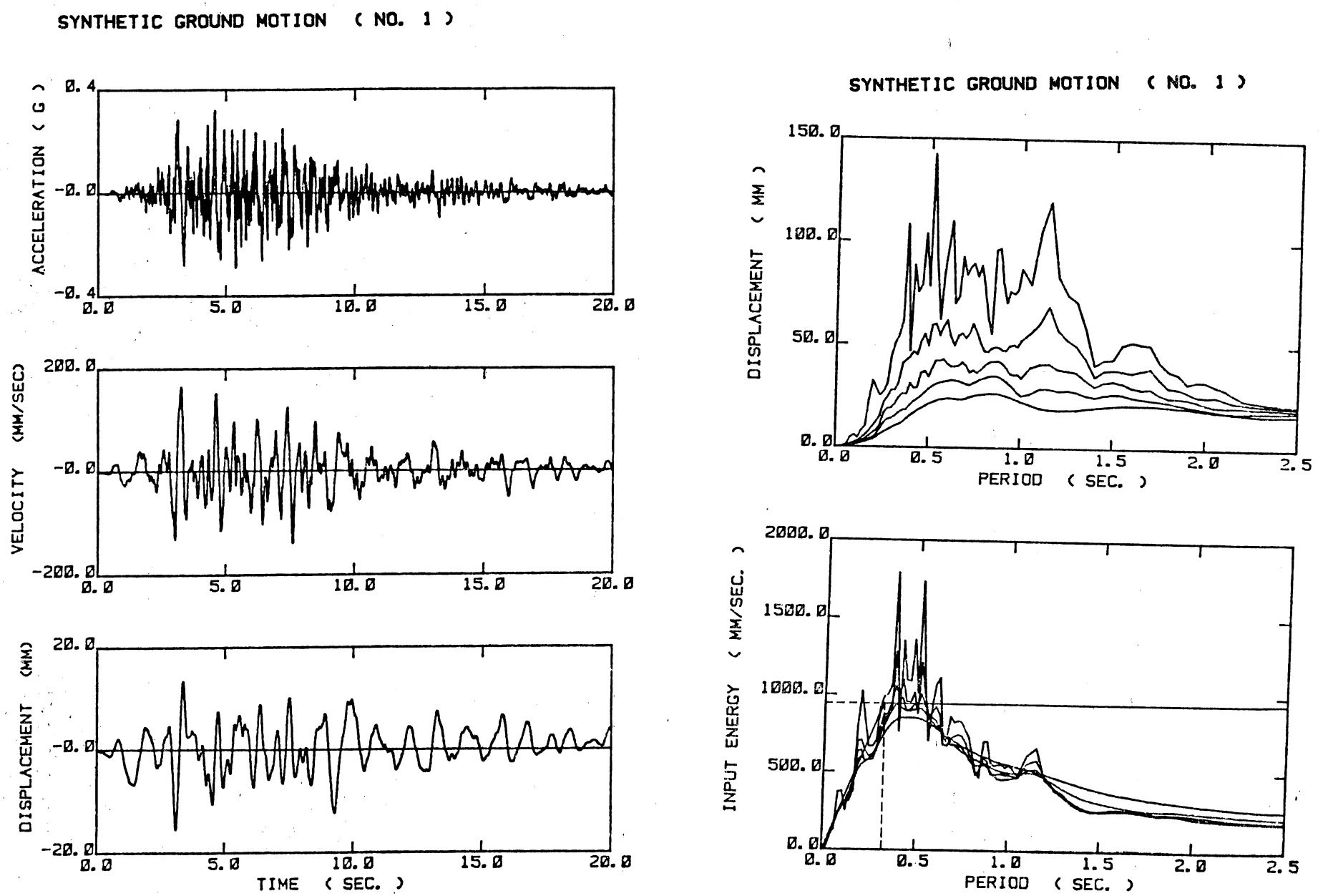


Fig. 4.12 Ground Motion Generated to Fit Specified Response Parameters ( NO. 1 )

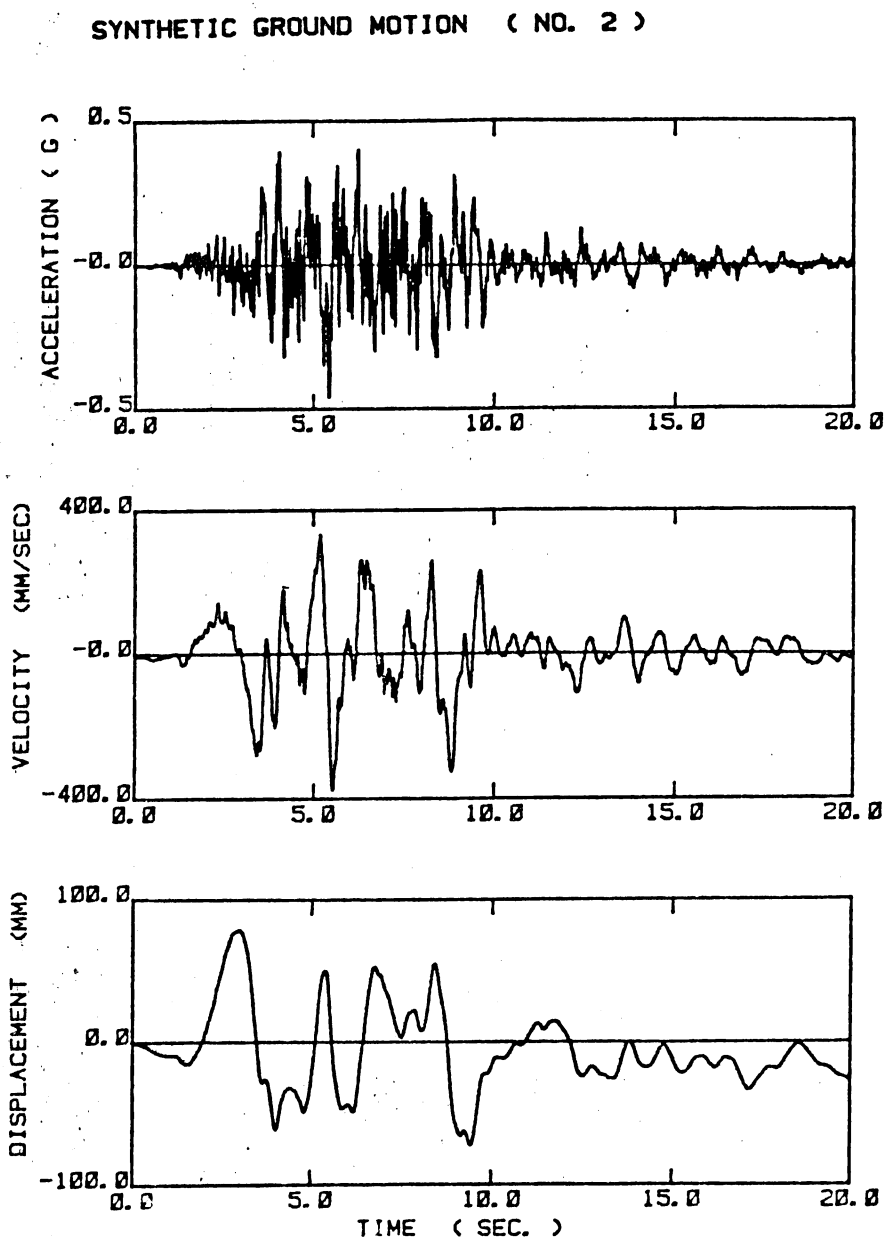


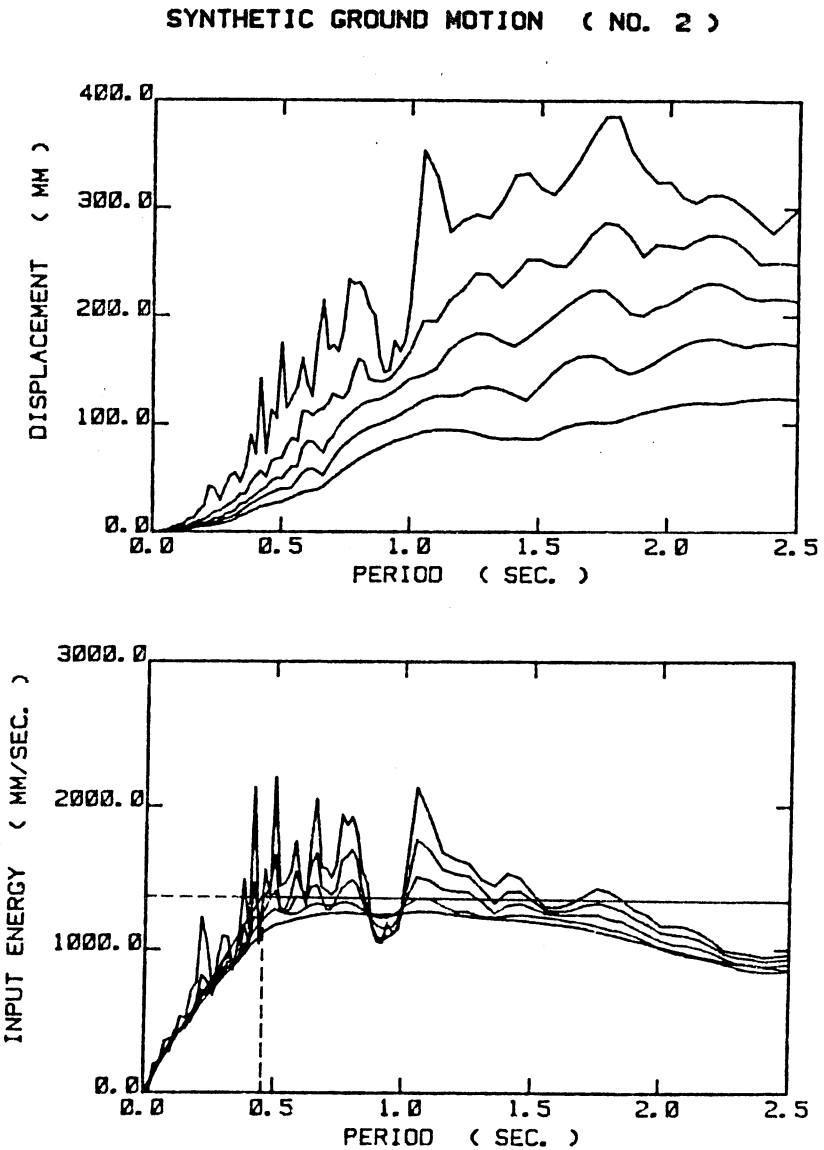


Fig. 4.13 Ground Motion Generated to Fit Specified Response Parameters ( No. 2 )

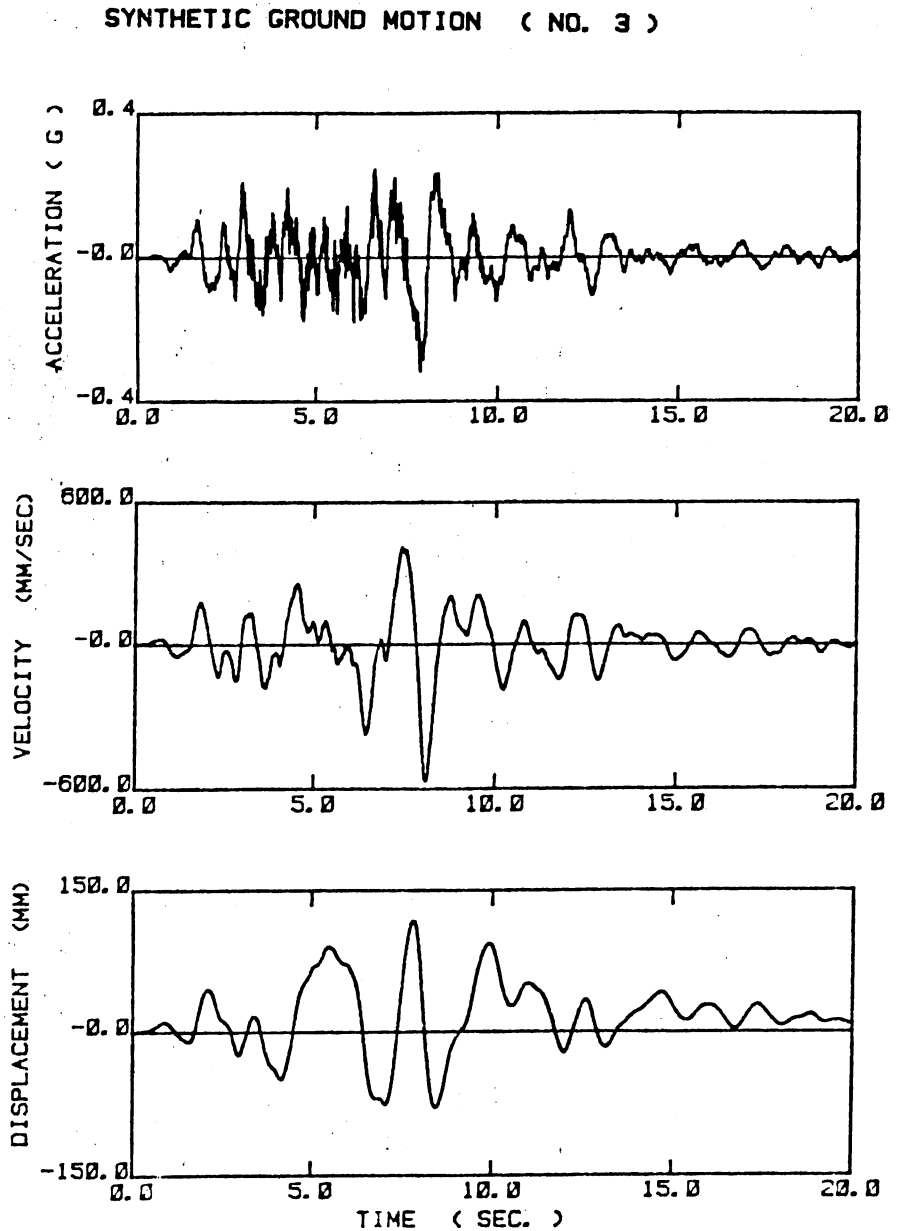


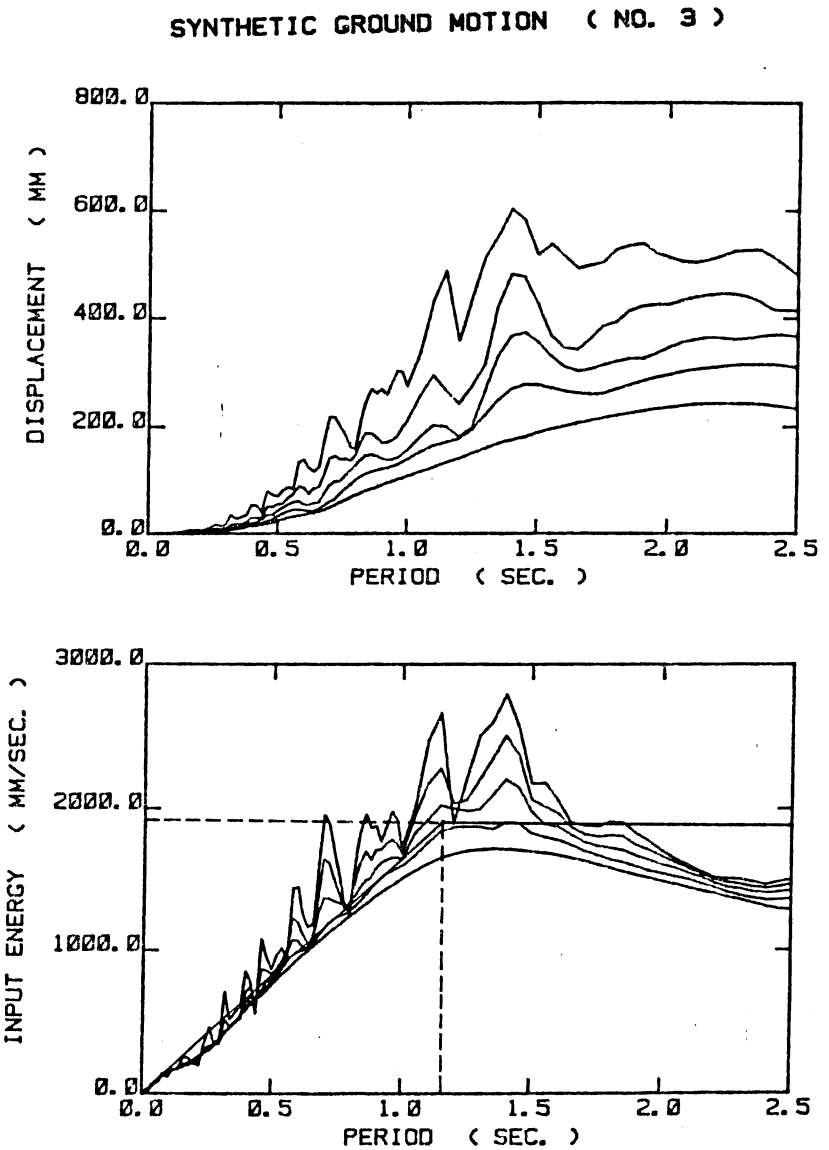


Fig. 4.14 Ground Motion Generated to Fit Specified Response Parameters ( No. 3 )

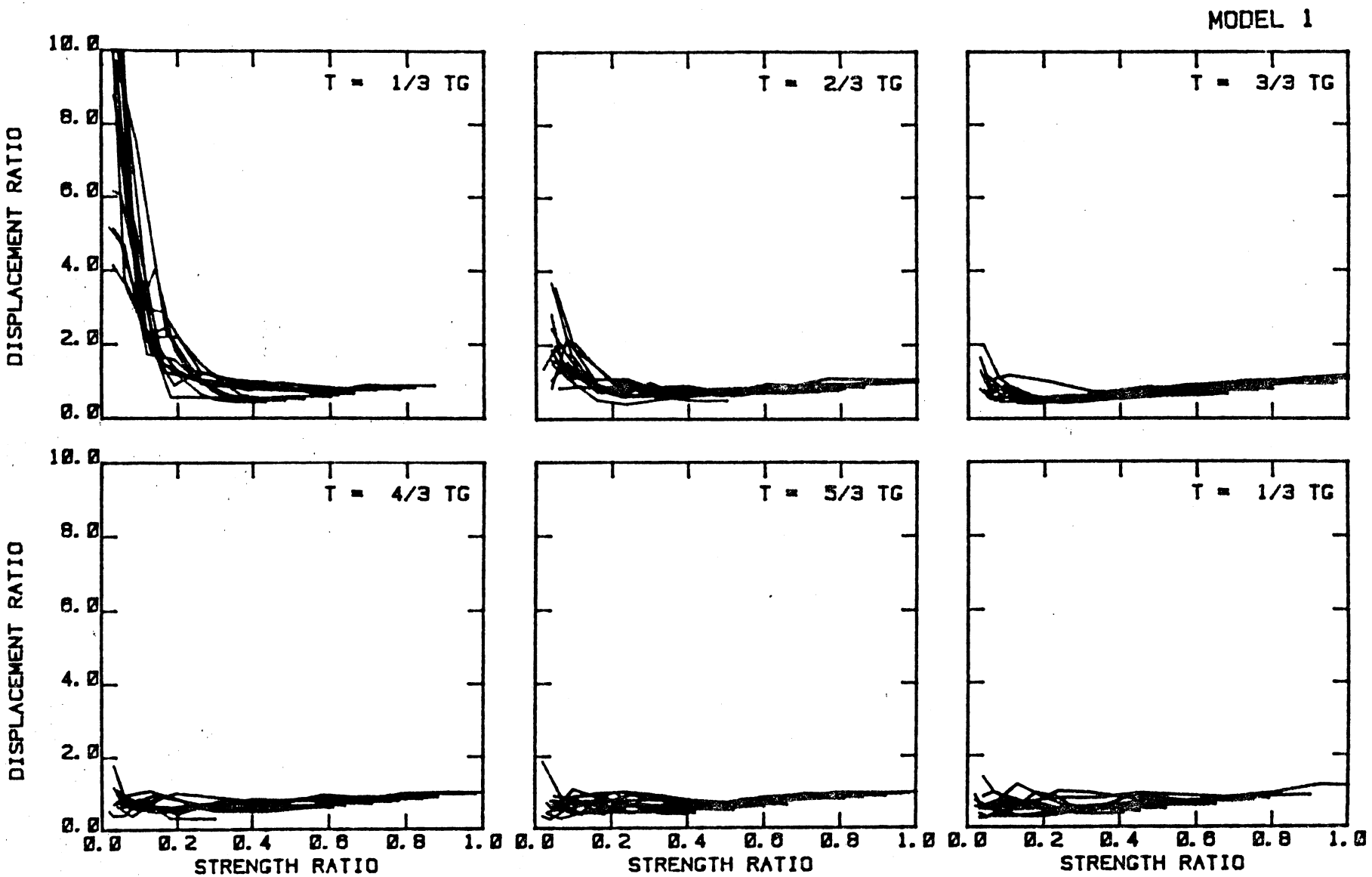


Fig. 4.15 Normalized Nonlinear Displacement Response for Groud Motions and Synthetic Ground Motions ( Model 1 )

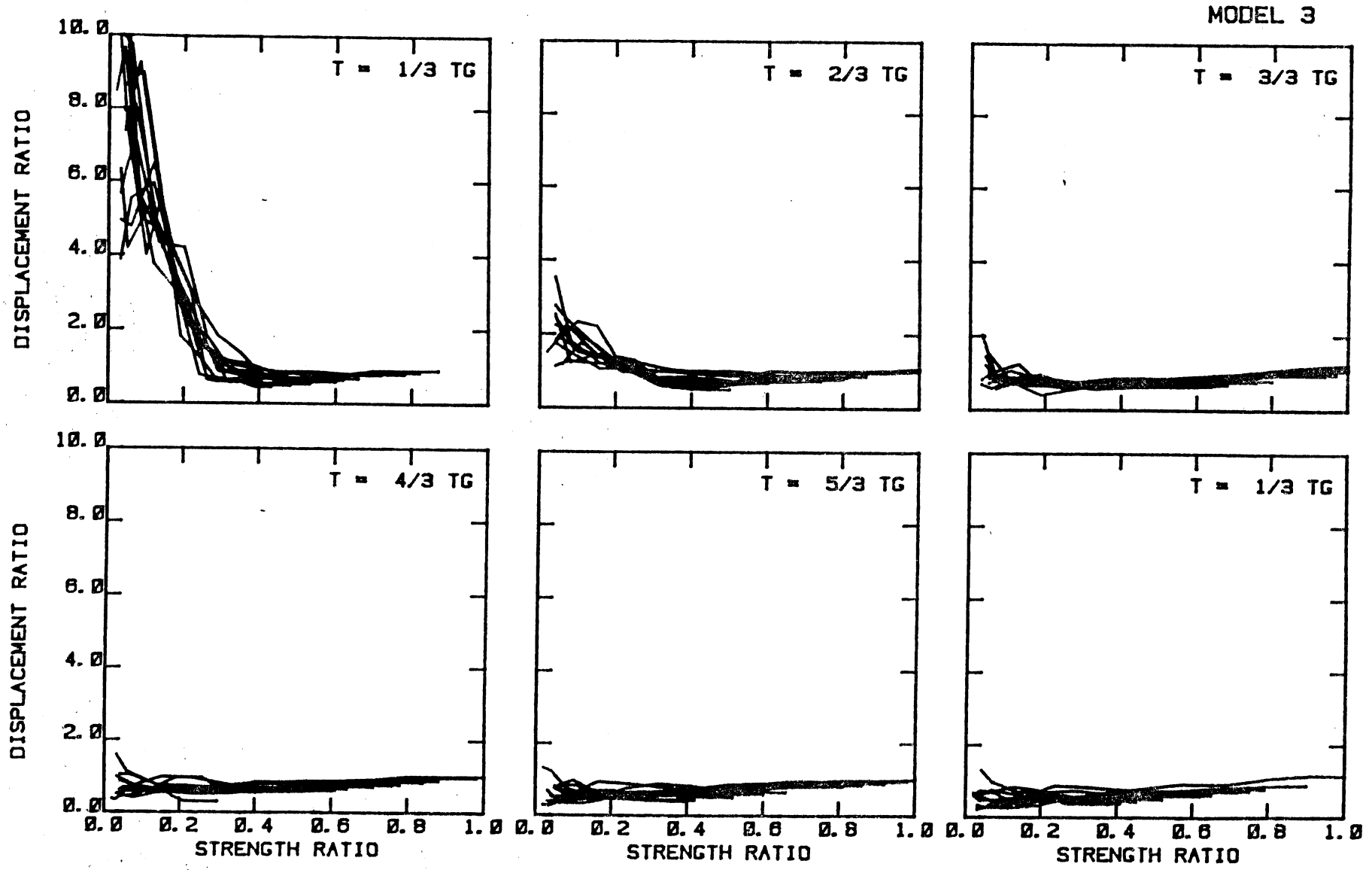


Fig.4.16 Normalized Nonlinear Displacement Response for Ground Motions and Synthetic Ground Motions ( Model 3 )

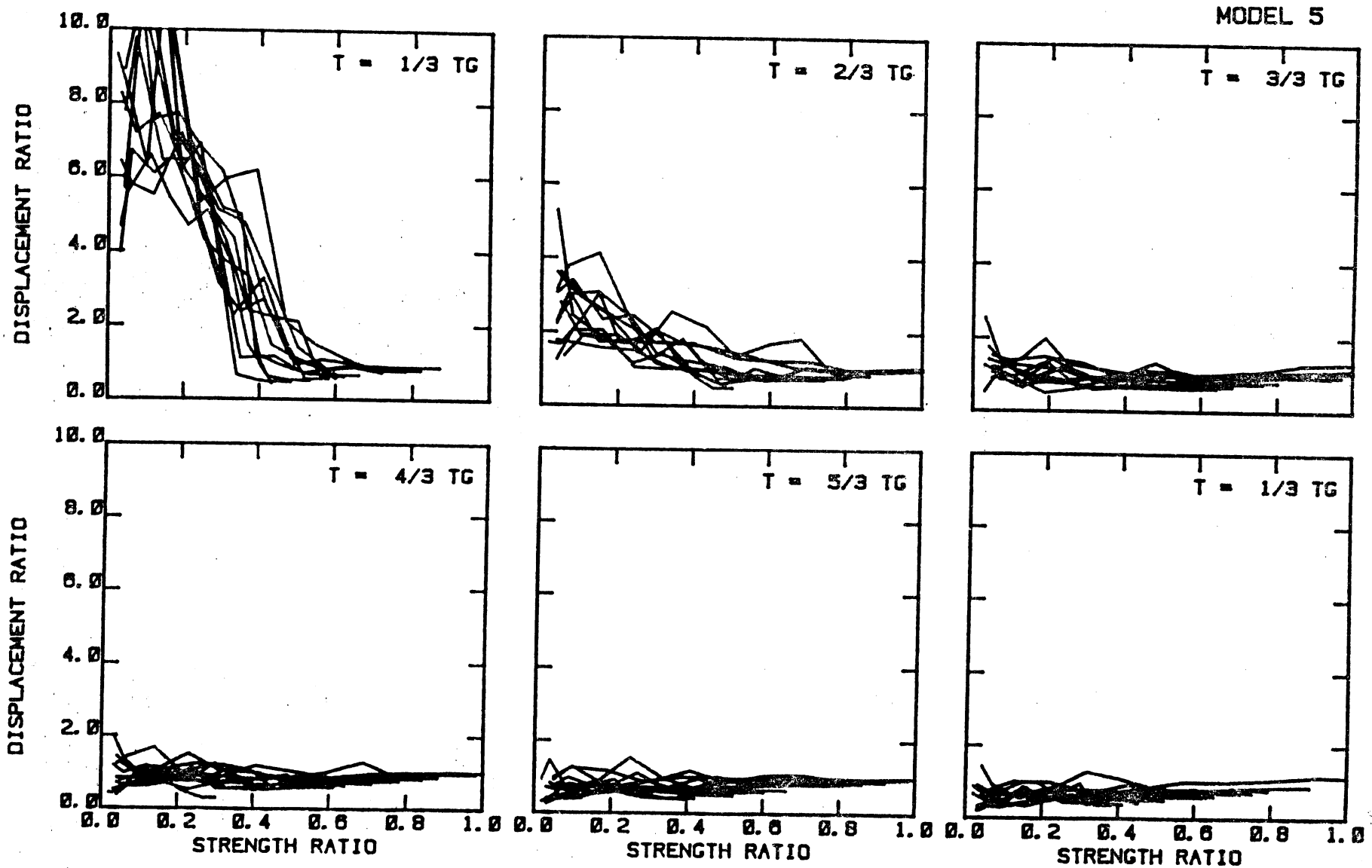


Fig. 4.17 Normalized Nonlinear Displacement Response for Ground Motions and Synthetic Ground Motions ( Model 5 )

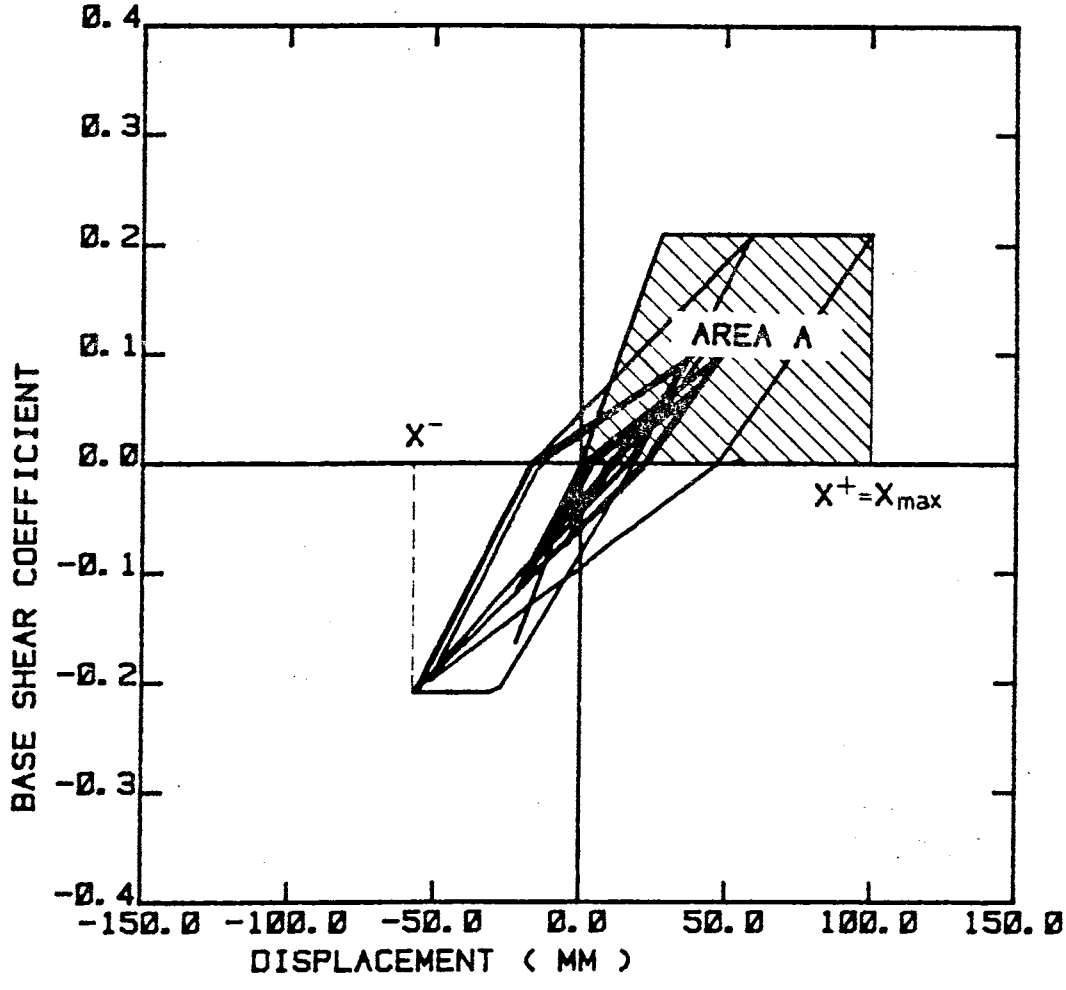


Fig. 4.18 Definition of Apparent Maximum Energy ( Area A )

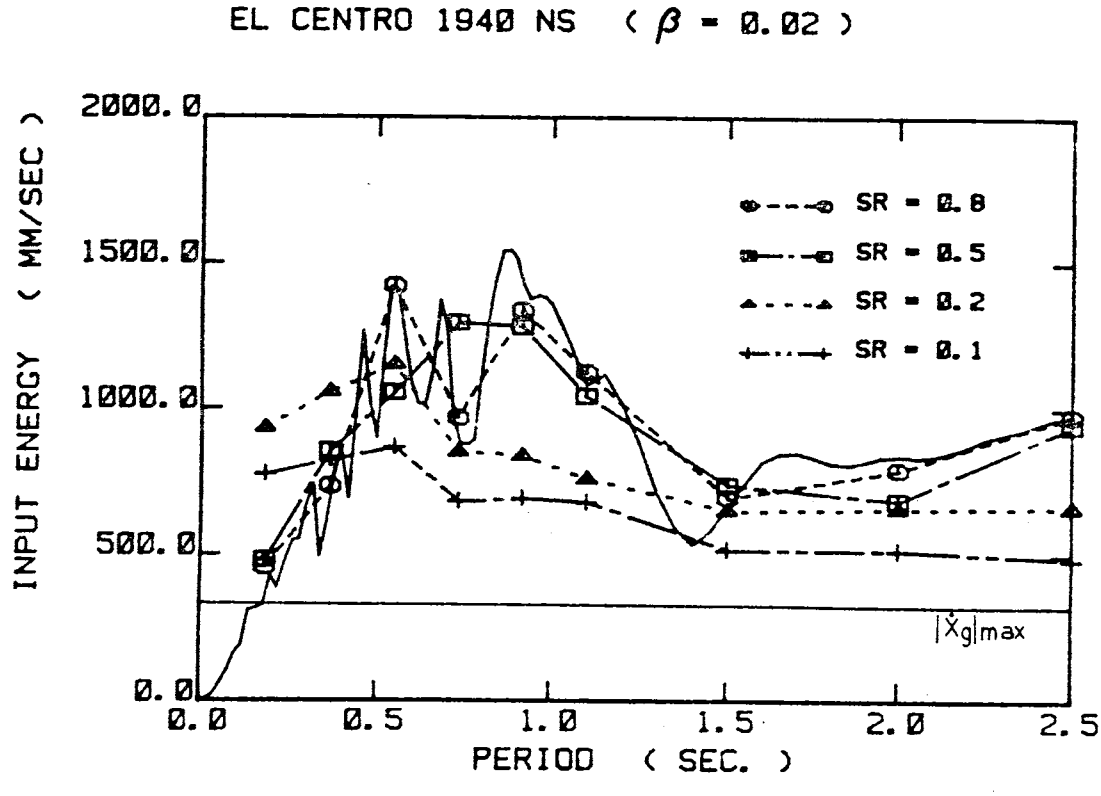


Fig. 4.19 Changes of Input Energy with Strength Ratio

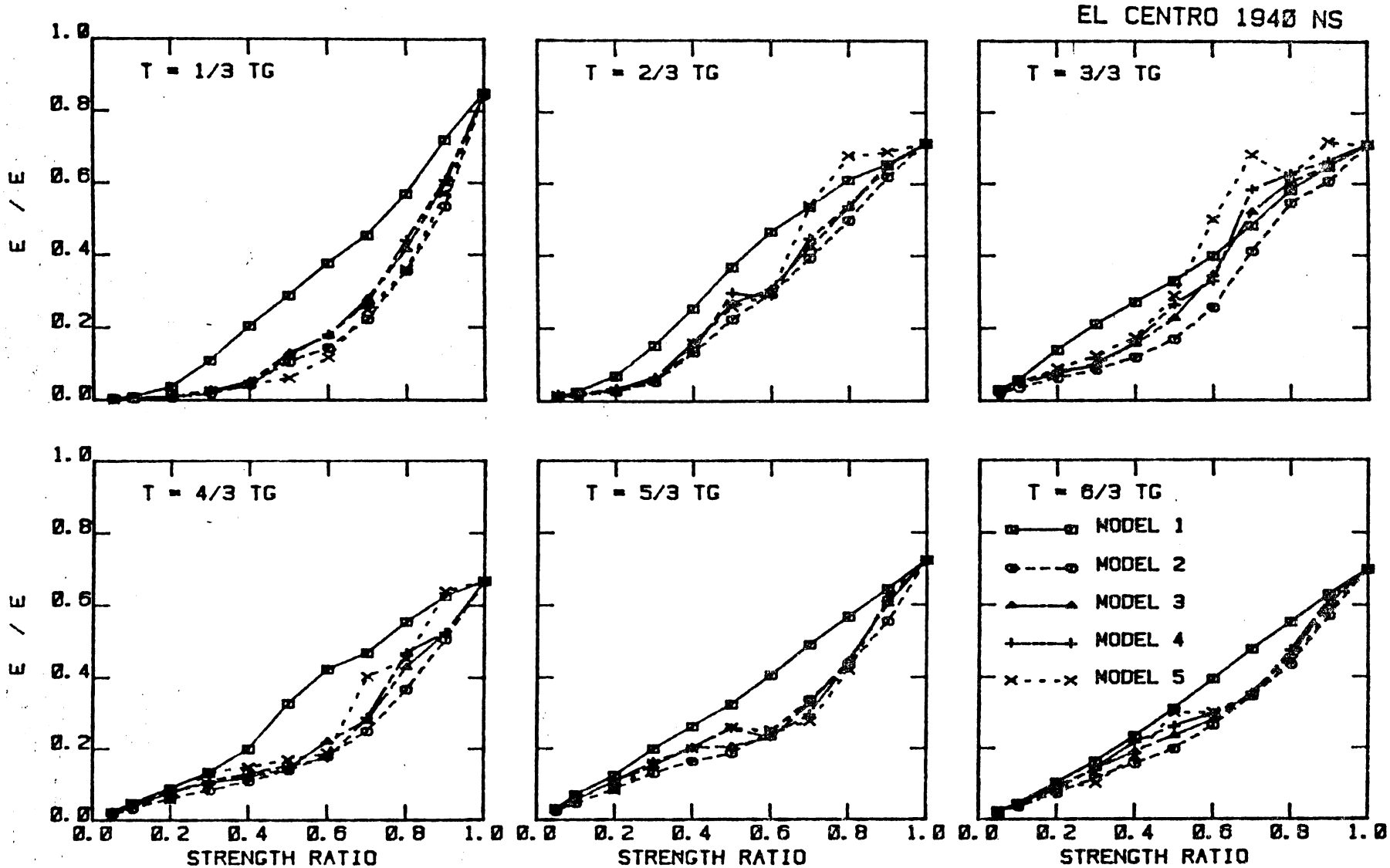


Fig. 4.20 Variation of Energy Ratio ( Damping Energy / Input Energy ) with Strength Ratio

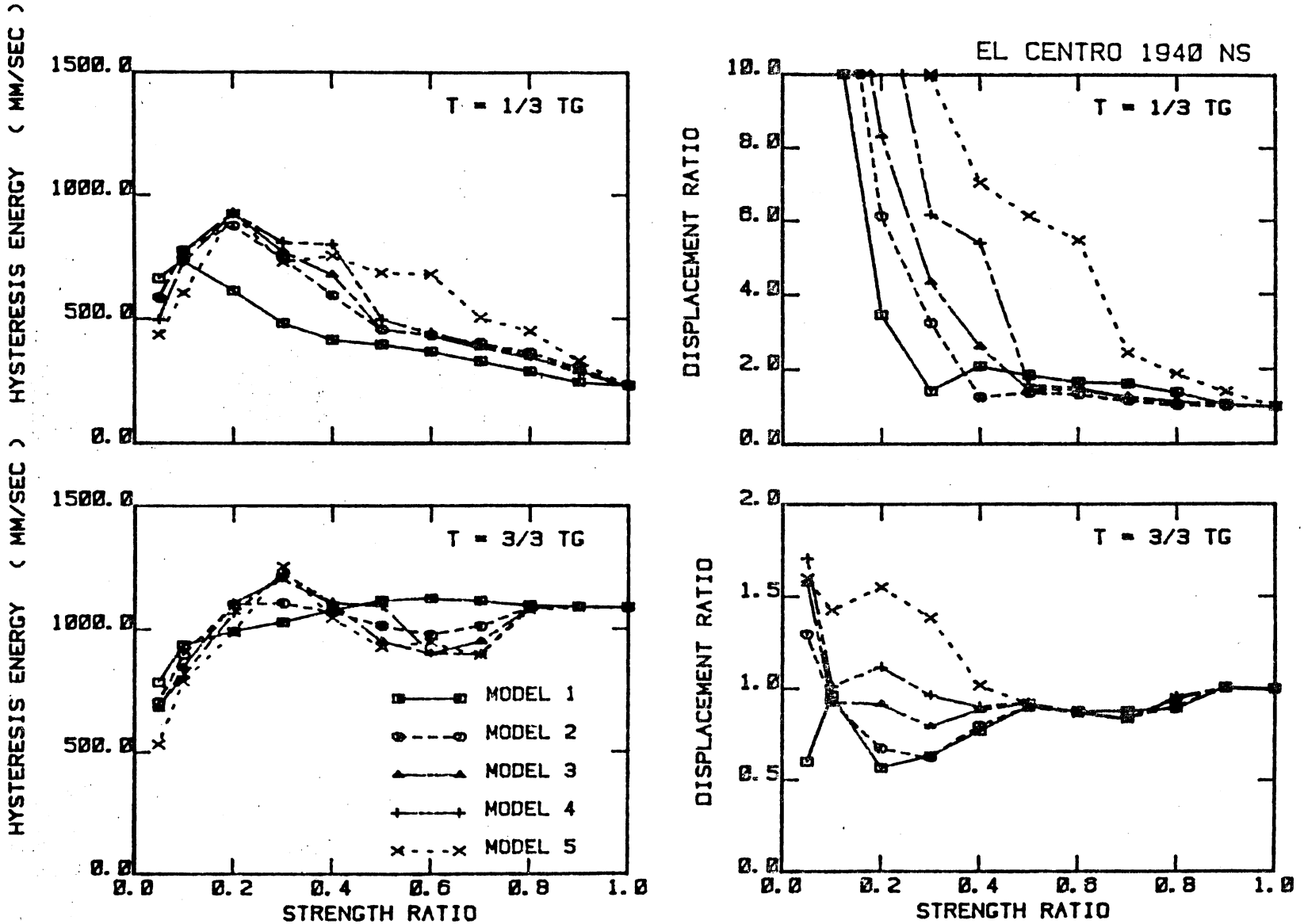


(a) Hysteresis Energy

(b) Displacement Ratio

Fig. 4.21 Hysteresis Energy

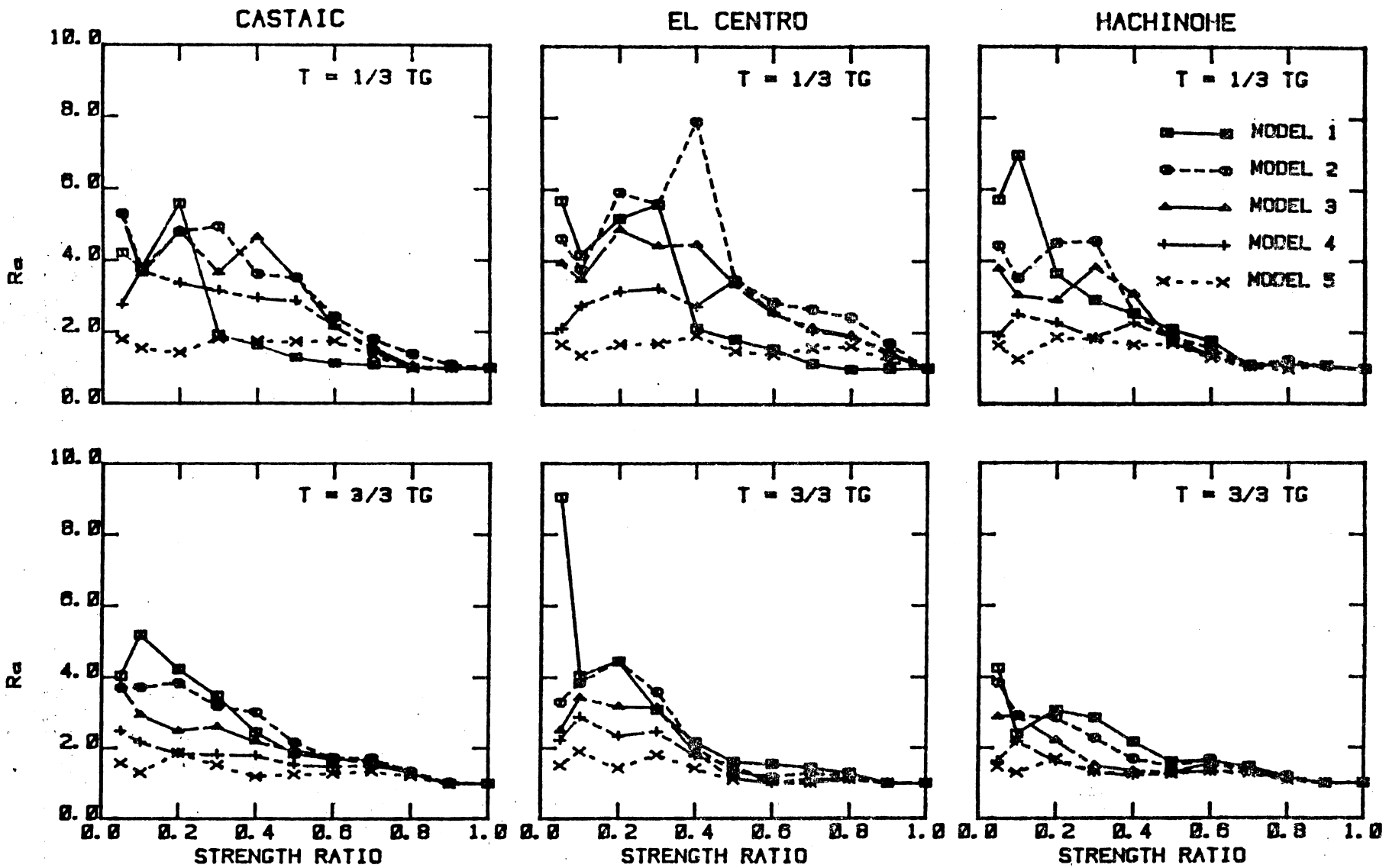


Fig. 4.22 Variation of Accumulation Ratio with Strength Ratio

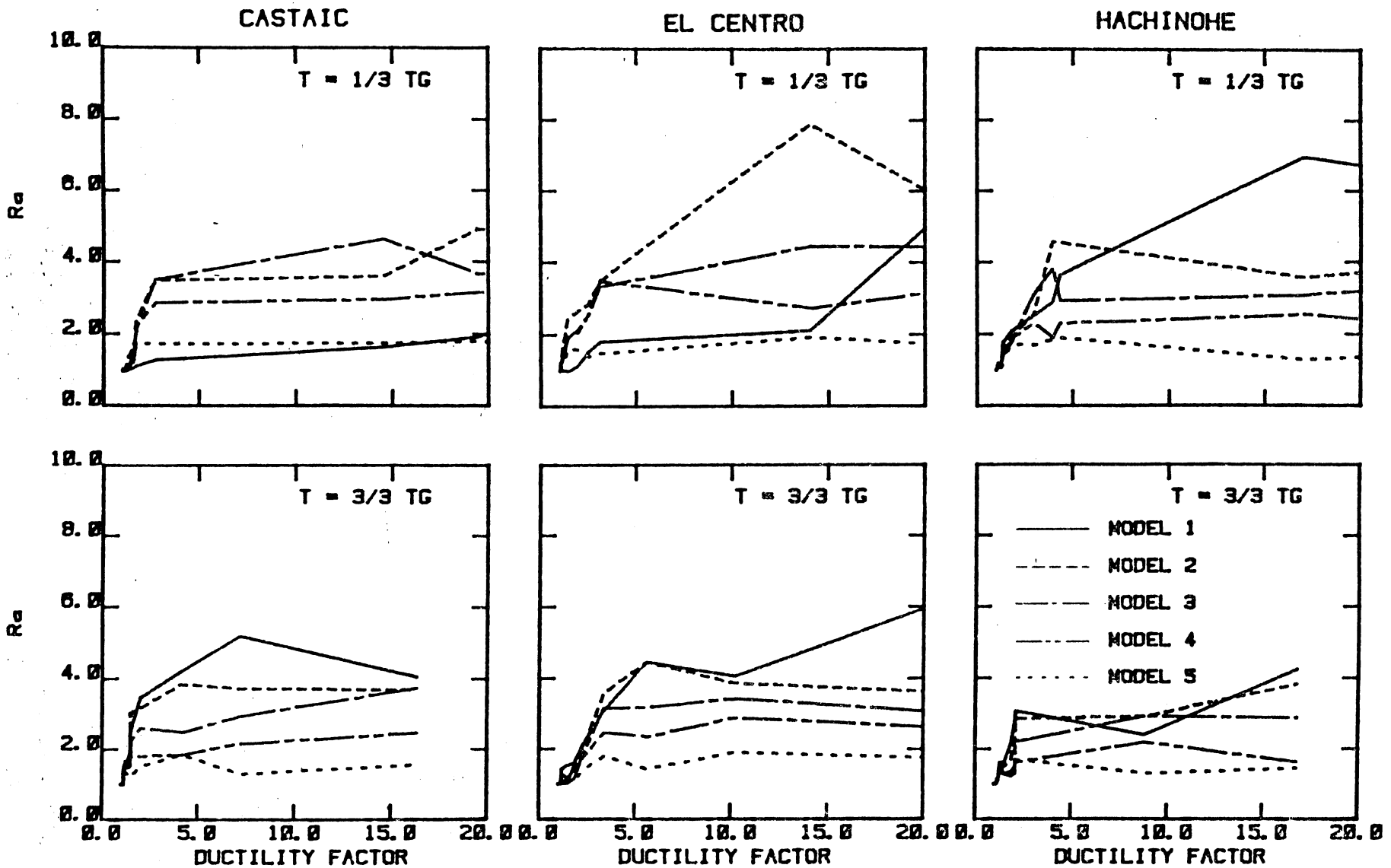


Fig. 4.23 Variation of Accumulation Ratio with Ductility Factor

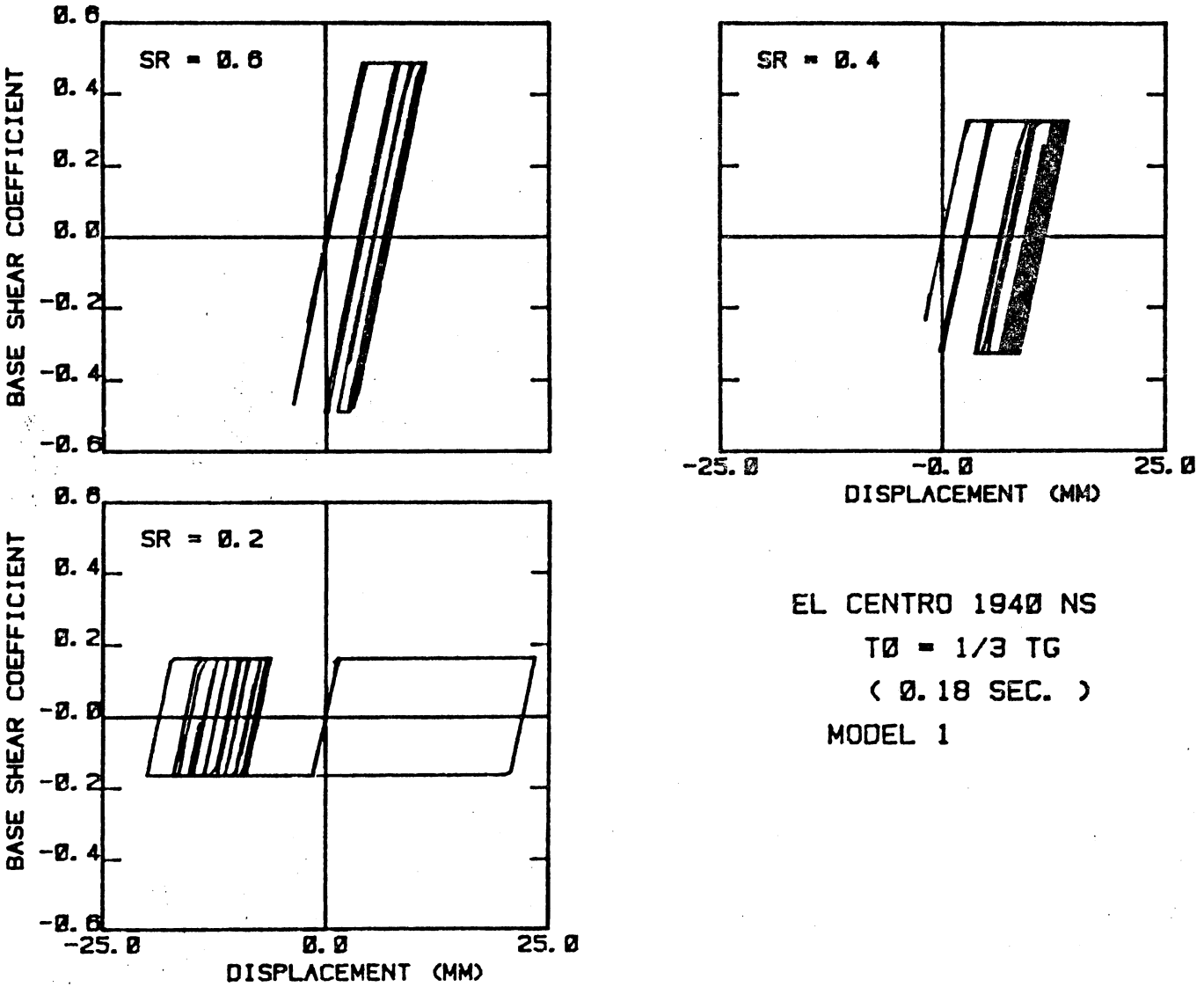


Fig. 4.24 Hysteretic Response Calculated for Various Strength Ratio
( $T_o$ = 1/3 TG, Model 1 )

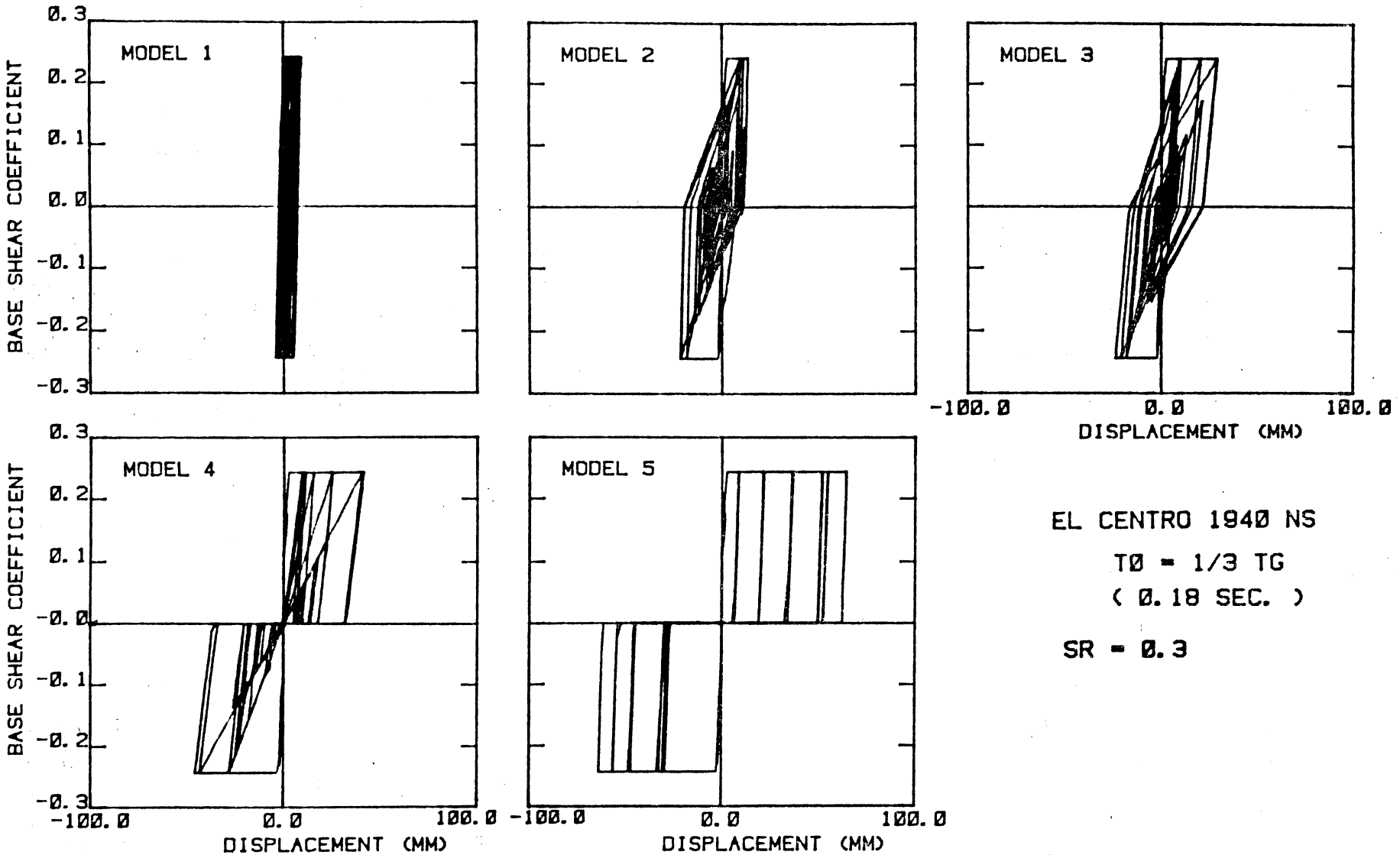


Fig. 4.25 Hysteretic Response Calculated for Various Hysteresis Models
( $T_o$ = 1/3 TG, SR = 0.3 )

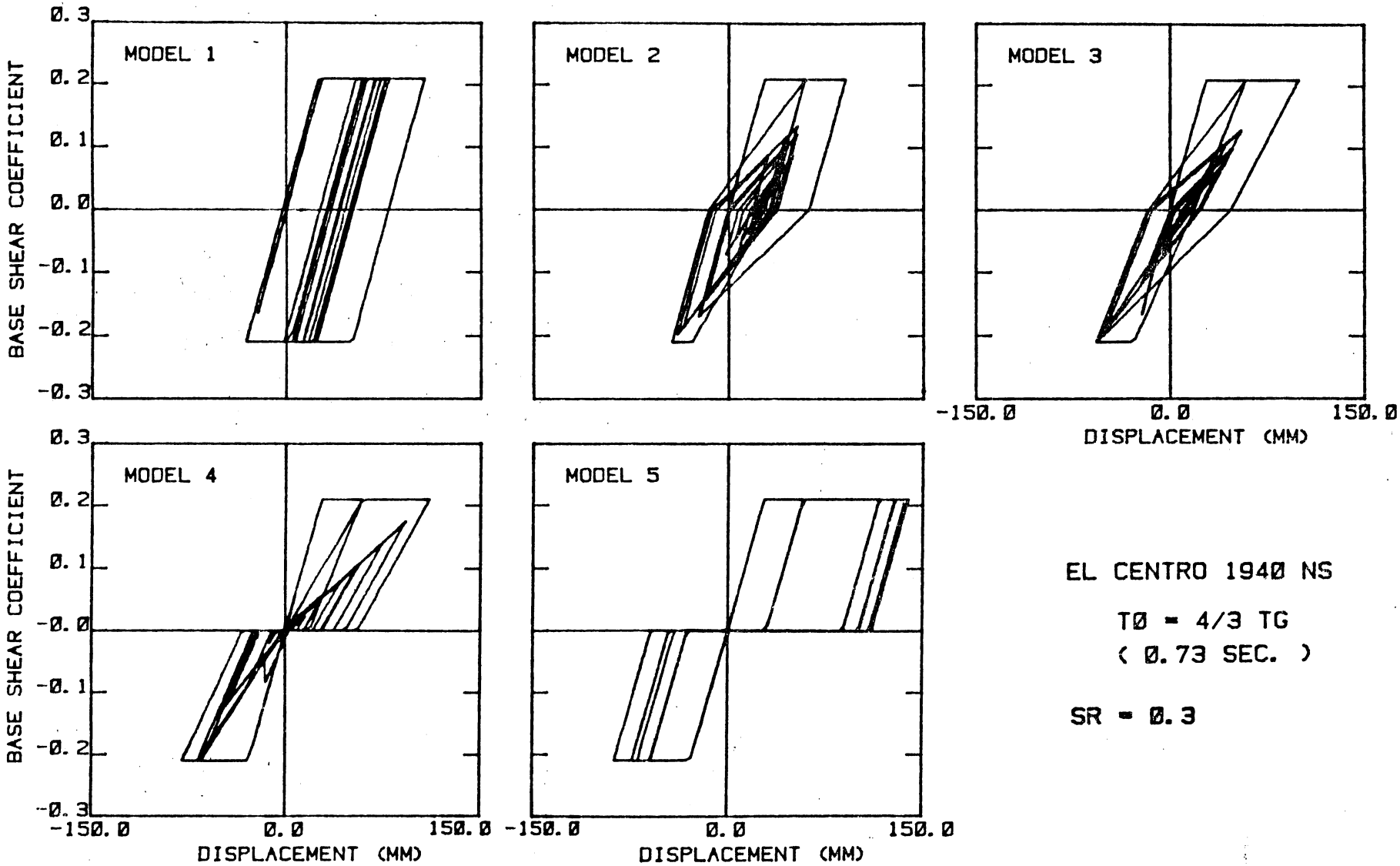


Fig. 4.26 Hysteretic Response Calculated for Various Hysteresis Models
( $T_o$ = 4/3 TG, SR = 0.3 )

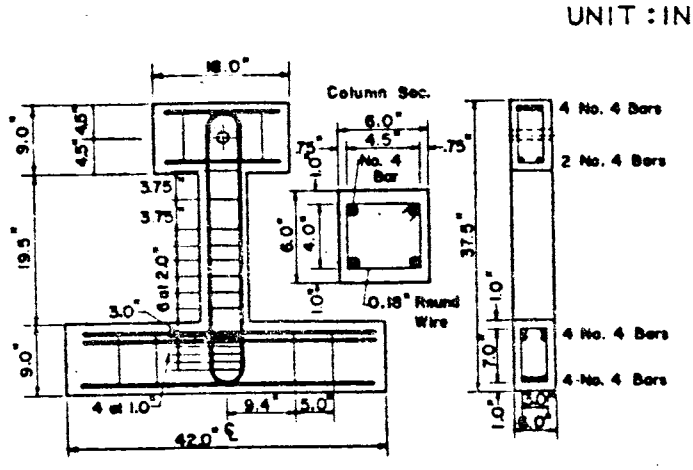


Fig. 5.1 Dimensions for Test Specimen T2 and T5

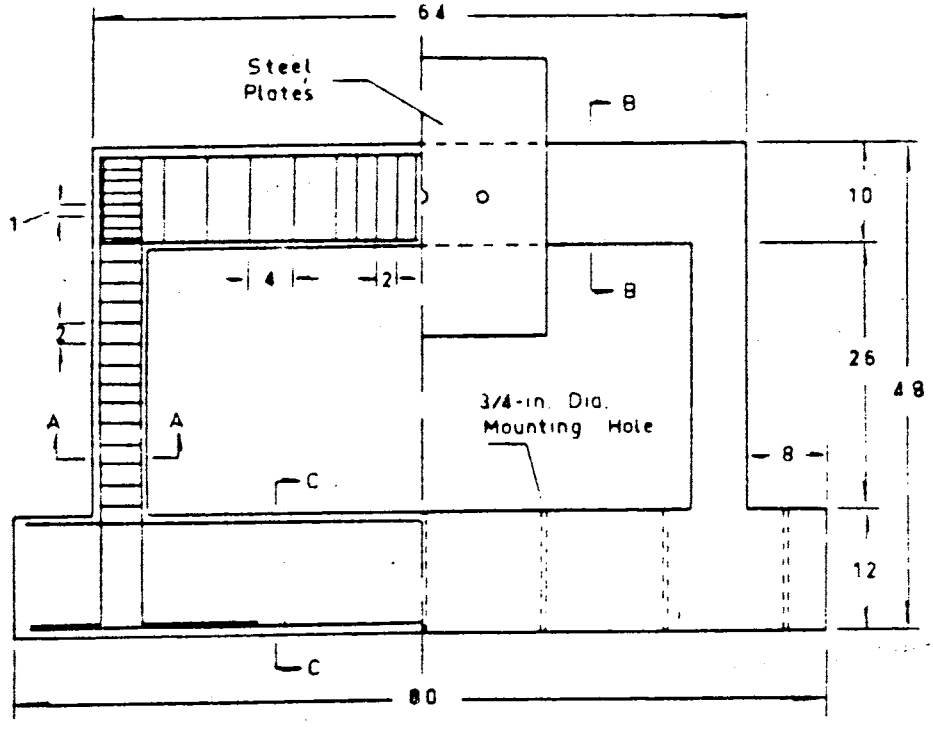


Fig. 5.2 Dimensions for Test Structures FE1 and FE2

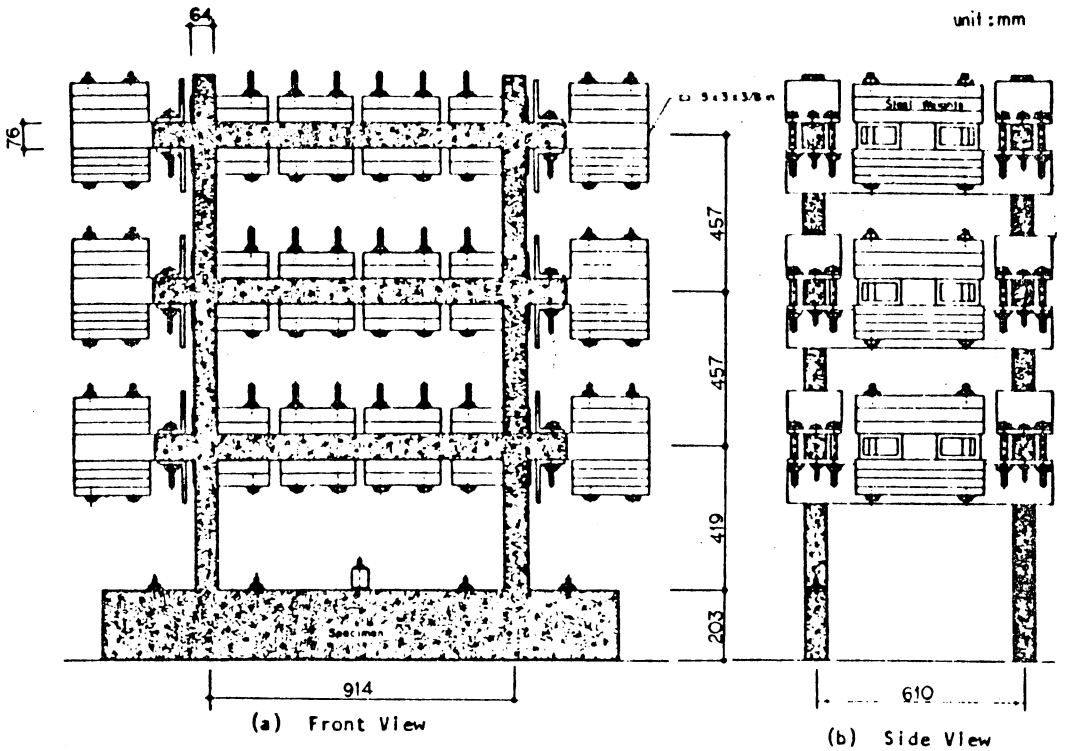


Fig. 5.3 Dimensions for Test Structures O-D1, O-D2 and O-D3

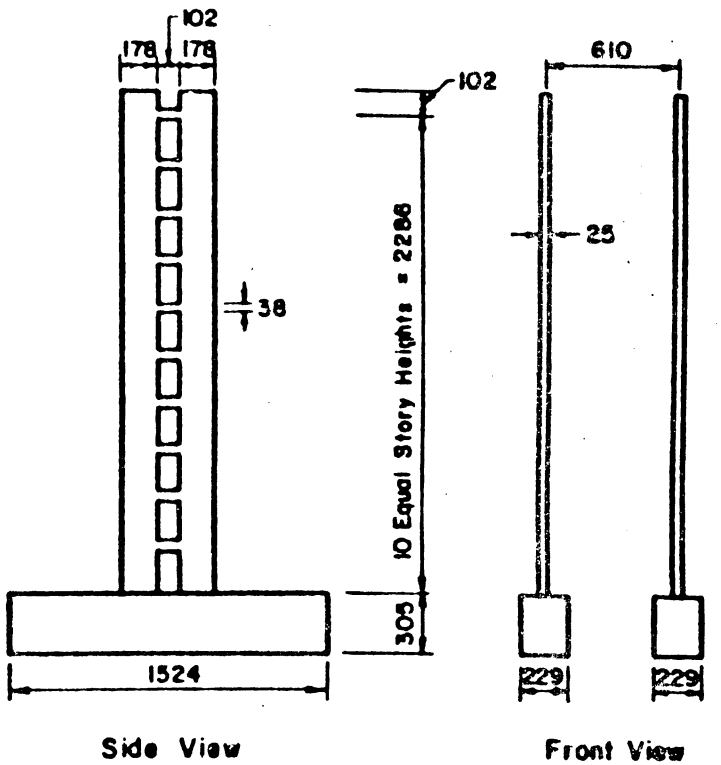


Fig. 5.4 Dimensions for Test Structures A-D1, A-D2, A-D3 and A-M1

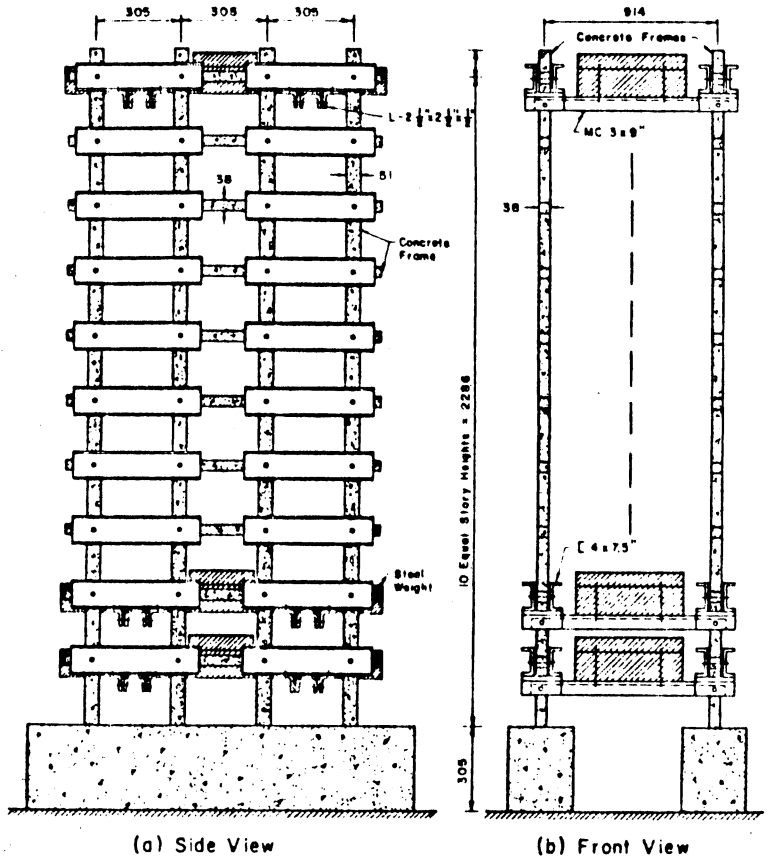


Fig. 5.5 Dimensions for Test Structures H-1 and H-2

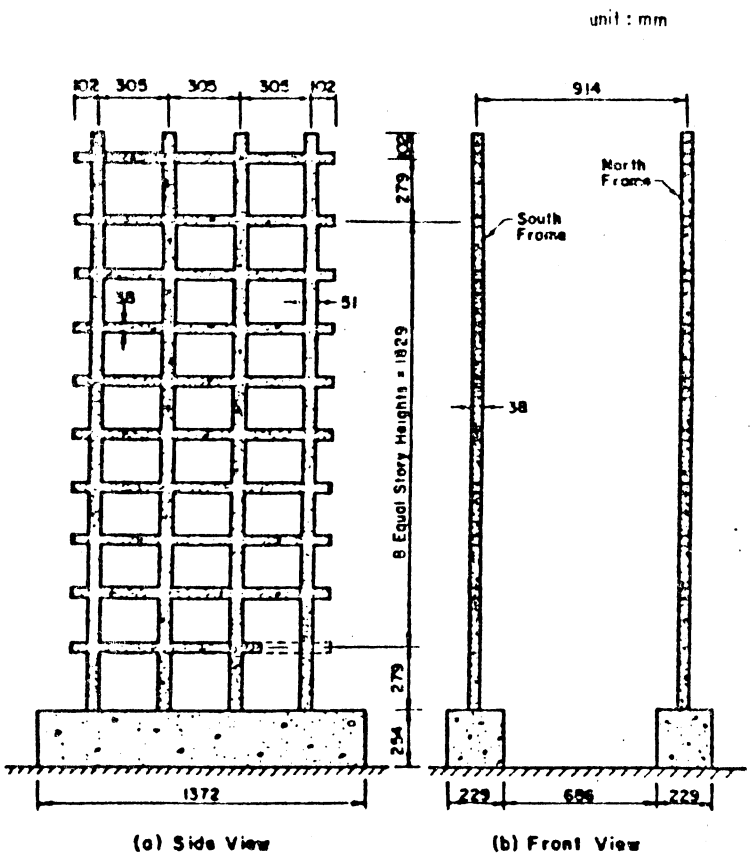


Fig. 5.6 Dimensions for Test Structures MF1 and MF2

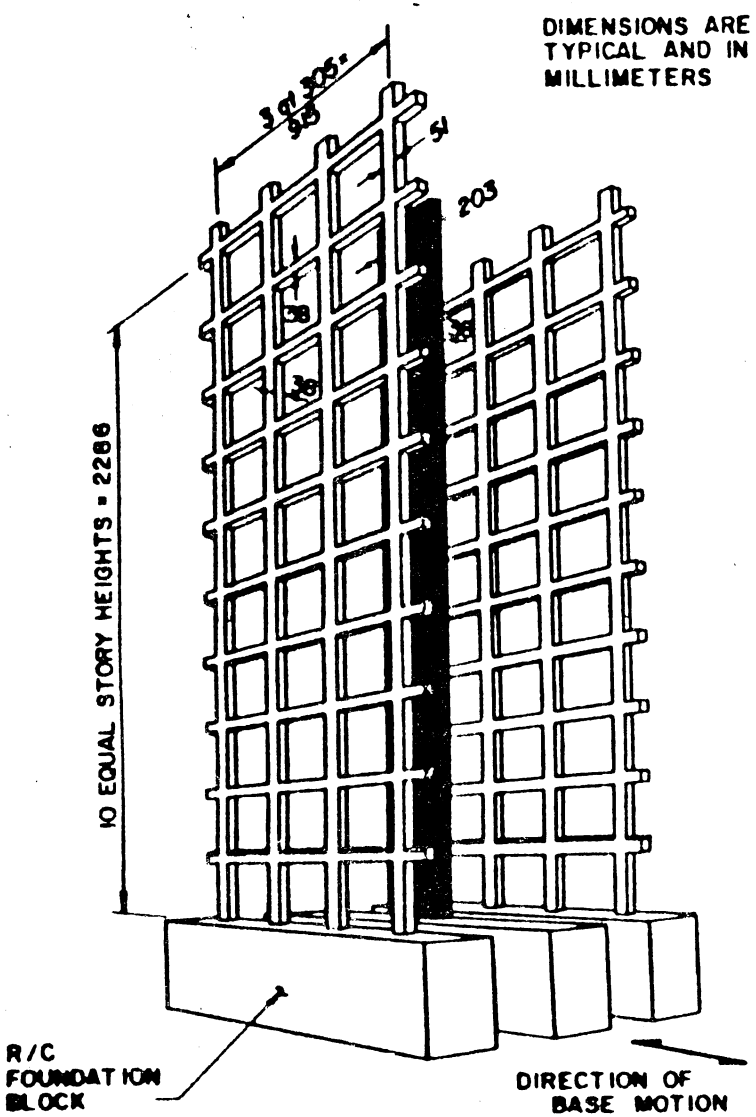


Fig. 5.7 Dimensions for Test Structures
FW Series

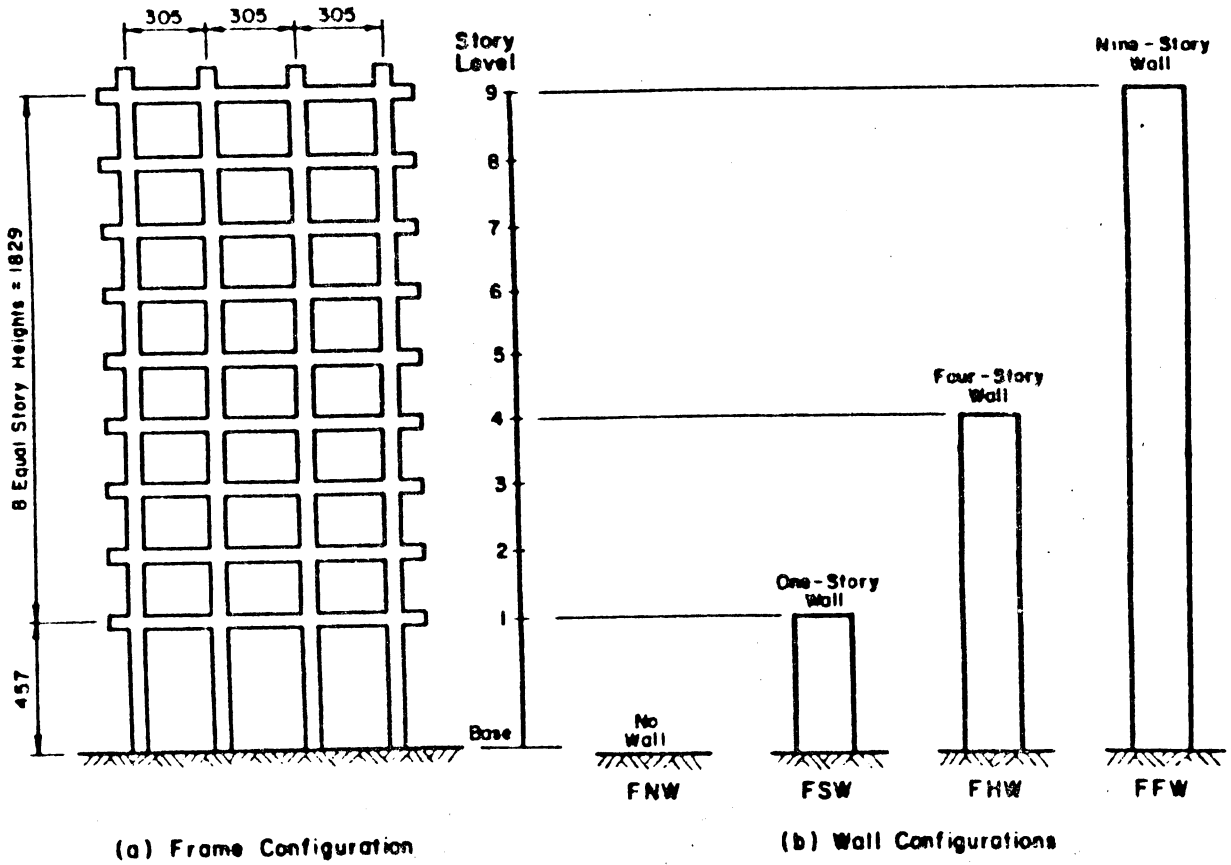


Fig. 5.8 Dimensions for Test Structures
F*W Series

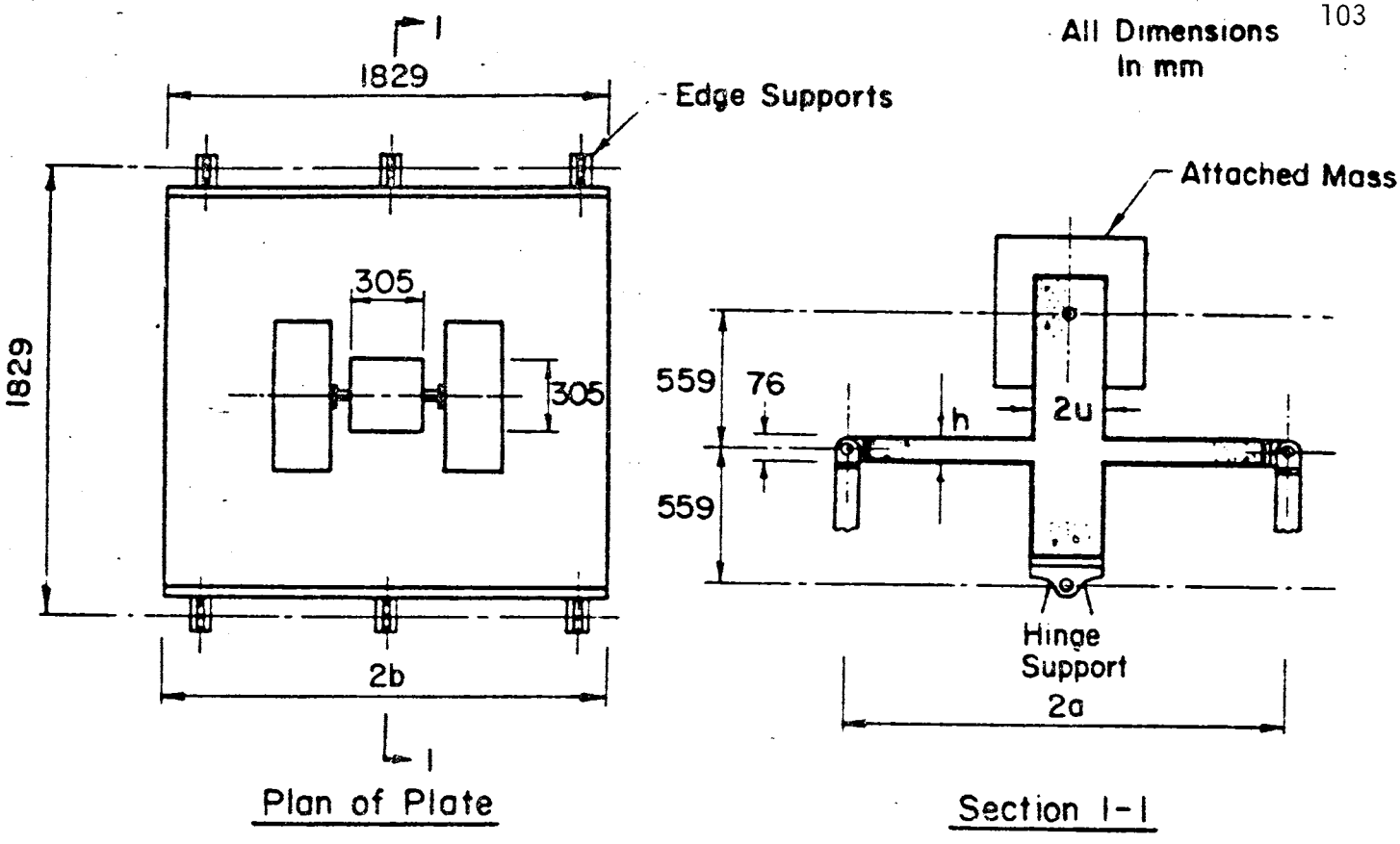


Fig. 5.9 Dimensions for Test Specimen M-D1, M-D2 and M-D3

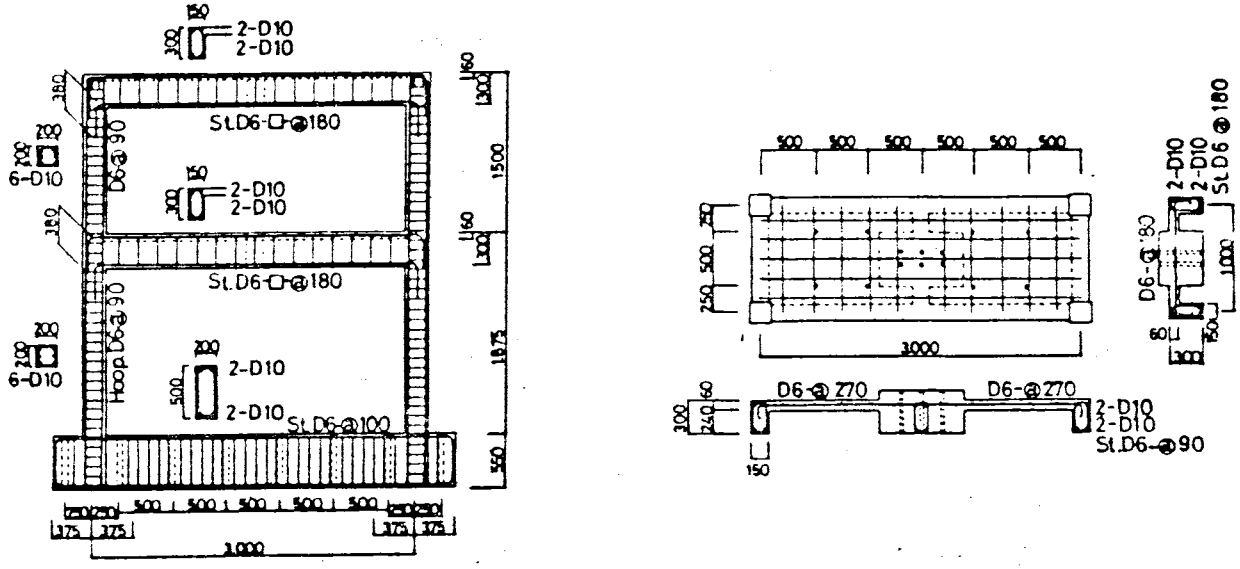


Fig. 5.10 Dimensions for Test Structure DR20

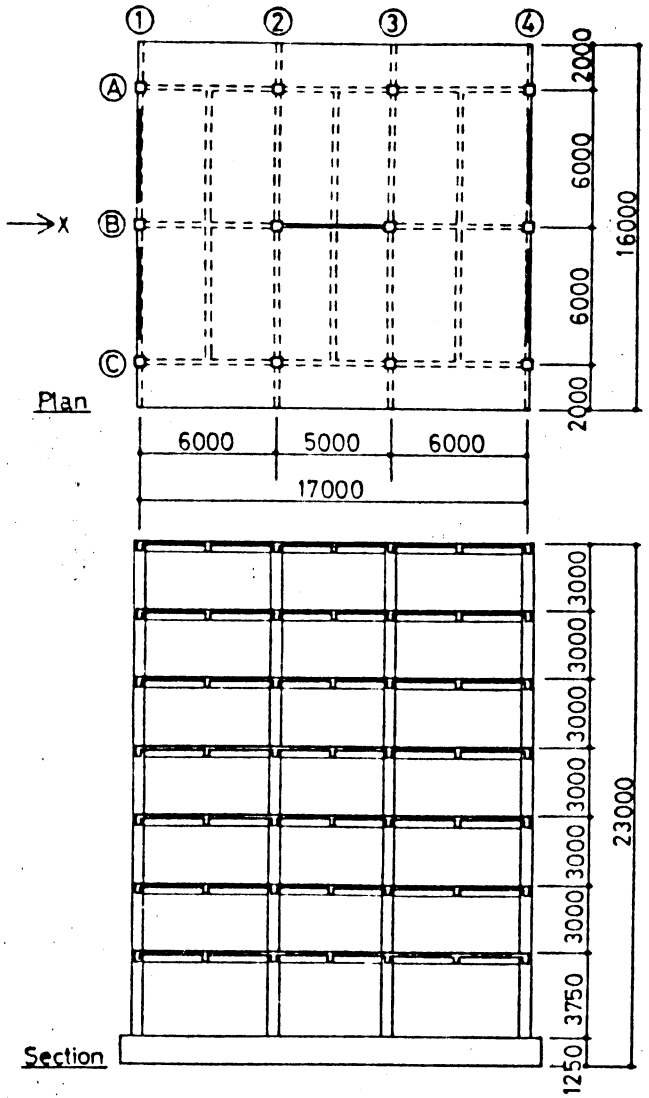


Fig. 5.11 Dimensions for Test Structure PSD3

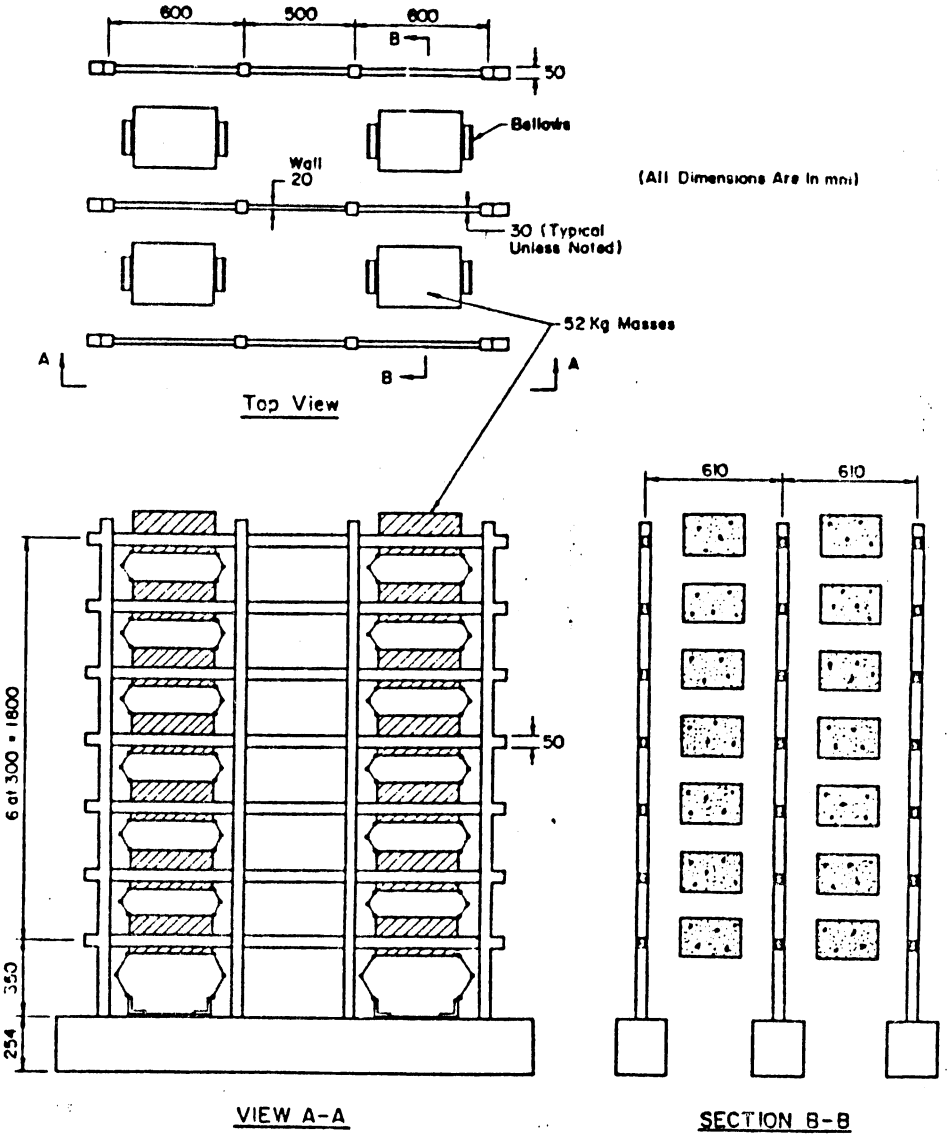


Fig. 5.12 Dimensions for Test Structures NS-1, NS-2 and NS-3

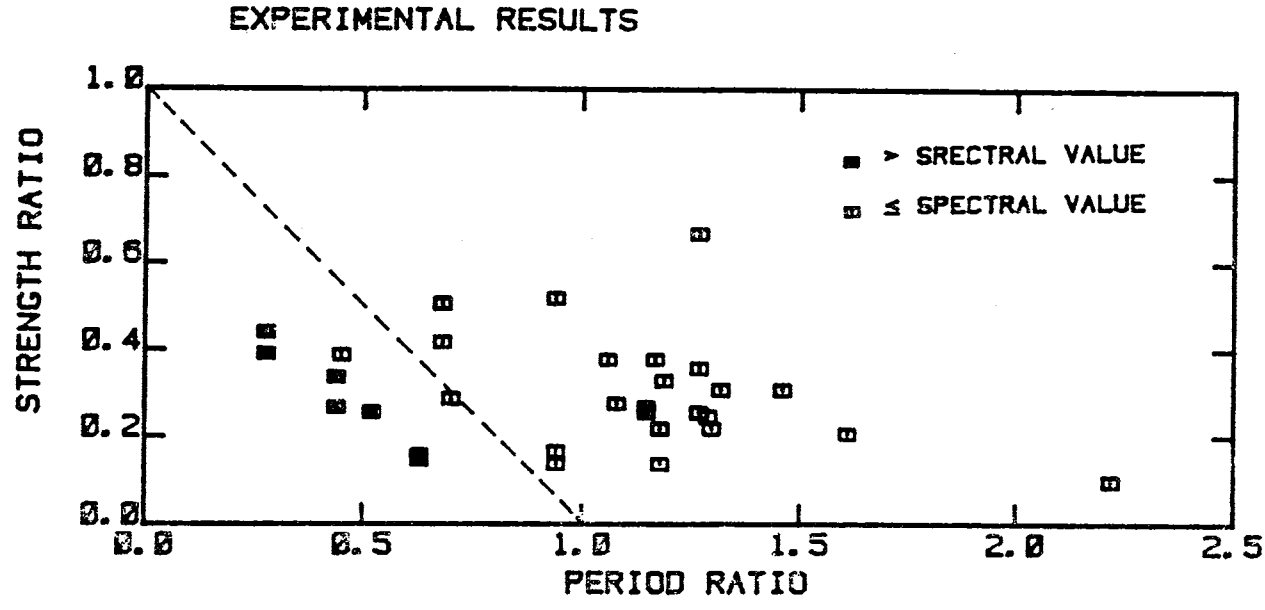


(a) Distribution of Test Structures

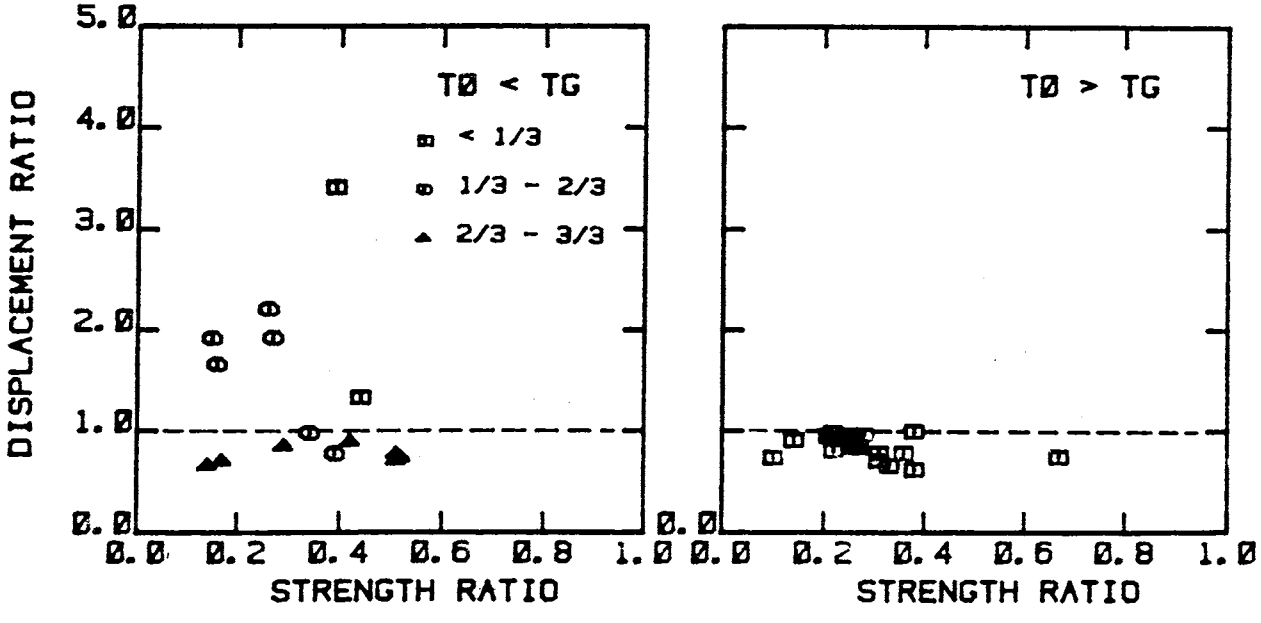


(b) Normalized Displacement Response ( $T_o$ < TG )

(c) Normalized Displacement Response ( $T_o$ > TG )

Fig. 5.13 Experimental Results

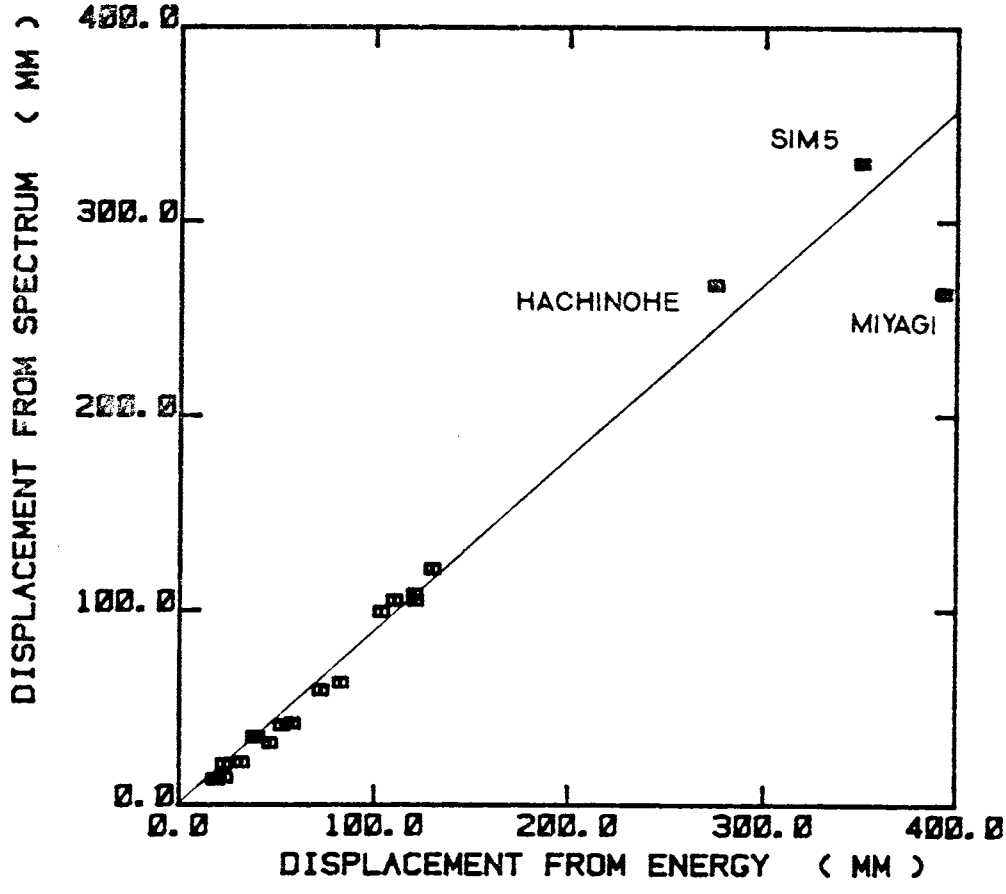


Fig. 6.1 Relationship between Idealized Displacement Response Spectrum and Energy Spectrum at TG

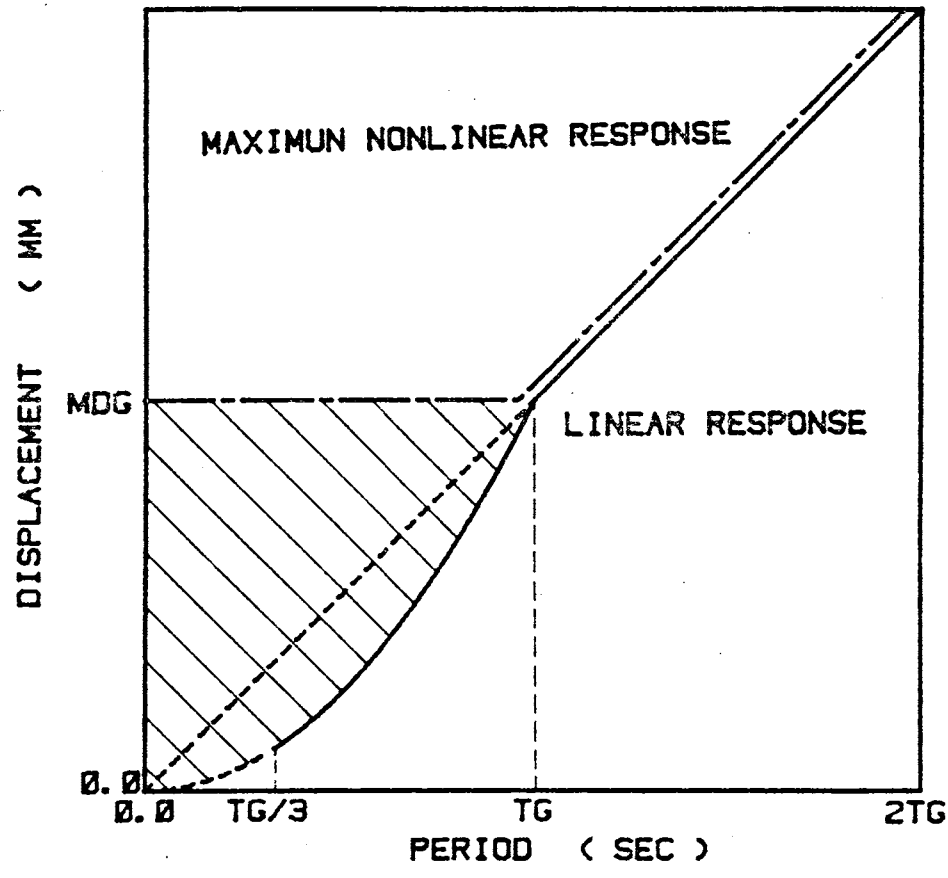


Fig. 6.2 Maximum Displacement Response

# APPENDIX A

## EVALUATION OF NONLINEAR DISPLACEMENT RESPONSE CALCULATED USING EQUIVALENTLINEAR MODELS

One of the simple procedures to obtain estimates of maximum nonlinear response displacements for reinforced concrete structures is the method based on "equivalent linear system" which considers nonlinear effects by modifying effective period and damping (Shibata 1975, Moehle 1984). Recently, Moehle (1984) has reported that the method based on the equivalent linear system and smoothed response spectrum produced good results for variety of structural systems and over a wide range of response. In this Appendix, the results of the procedure used by Moehle are compared with those of the method developed in this report.

Main points of the equivalent or substitute structure method are : (1) Increase of the displacement response caused by incresing effective period, and (2) decrease of the displacement response caused by increasing equivalent viscous damping. The former can be estimated by a function of the effective period based on the expected level of nonlinear response. The effective period can be obtained as a function of an assumed ductility ratio, $\mu$, which is defined as the ratio of the maximum displacement ($D_2$) divided by the "yielding displacement ($D_y$)." If the force-displacement response is elasto-plastic (Fig. A.1a), the effective period $T_e$ is related to $T_o$ as defined by Eq. A.1.

$$T_e = T_o * \sqrt{\mu} \qquad (A.1)$$

The equivalent damping was assumed by Shibata to be descrived by the function proposed by Gulkan.

$$\beta_{eq} = 0.2 * ( 1 - 1/\sqrt{\mu} ) + 0.02 \qquad ( A.2 )$$

The displacement response spectrum for the damping ratio, $\beta_{eq}$, is approximated by Eq. A.3 (Shibata 1975).

$$\frac{[ S_d ]_{eq}}{[ S_d ]_{2\%}} = \frac{8}{6 + 100\beta_{eq}} \qquad ( A.3 )$$

Combining Eqs. A.2 and A.3 leads to,

$$\frac{[ S_d ]_{eq}}{[ S_d ]_{2\%}} = \frac{0.4\sqrt{\mu}}{1.4\sqrt{\mu} - 1} = \frac{0.4}{1.4 - 1/\sqrt{\mu}} \qquad ( A.4 )$$

(1) $T_O > TG$

As smoothed displacement response spectrum is given by a straight line shown in Fig. A.1b, an increase of the response caused by an increase of period is,

$$D_1 = D_0 * \frac{T_{ef}}{T_0} = D_0 * \sqrt{\mu} \qquad ( A.5 )$$

However, an increase in displacement is accompanied by a increase in equivalent damping. Therefore, the displacement response is calculated by multiplying Eqs. A.4 and A.5.

$$D_2 = D_1 \frac{0.4\sqrt{\mu}}{1.4\sqrt{\mu} - 1} = D_0 \frac{0.4\,\mu}{1.4\sqrt{\mu} - 1} \qquad (A.6)$$

As Eq. A.6 was obtained with an assumption of a certain value of ductility ratio, $\mu$, this value should be equal to $D_y * \mu$. Accordingly,

$$D_y * \mu = D_0 \frac{0.4\mu}{1.4\sqrt{\mu} - 1} \qquad (A.7)$$

Refering Fig. A.1a, $D_y$ can be obtained from $D_0$ using a strength ratio, SR, as follows,

$$D_y = D_0 * SR \qquad (A.8)$$

Combining Eqs. A.7 and A.8 leads to,

$$\mu = \frac{(0.4/SR + 1)^2}{2} \qquad (A.9)$$

Hence, the displacement ratio is given by,

$$DR = \frac{D_2}{D_0} = \frac{D_y}{D_0} = \frac{(SR + 0.4)^2}{2SR} \qquad (A.10)$$

(2) $T_0 < TG$

In this range of periods, displacement depends on whether $T_{ef}$ remains below TG or exceed it.

i) $T_{ef} < TG$

In this case, the smoothed displacement response spectrum is a function of the square of period, so that $D_1$ is given by Eq. A.11 instead of Eq. A.5

(Fig. A.1c).

$$D_1 = D_0 \left(\frac{T_{ef}}{T_0}\right)^2 = D_0 * \mu \qquad (A.11)$$

The displacement ratio of this case can be obtained in the same way as shown in case (1), Accordingly,

$$DR = \frac{SR}{(1.4 - 0.4 / SR)^2} \qquad (A.12)$$

ii) $T_{ef} > TG$

In order to simplify the derivation, an imaginary displacement response spectrum is drawn by extending the strait response spectrum into the region below TG. The relation between the linear response ($D_0$) and that on the imaginary displacement response spectrum ($D_3$) is given by Eq. A.13 as a function of the period ratio, TR (Fig. A.1d).

$$\frac{D_3}{D_0} = \frac{1}{TR} \qquad (A.13)$$

The relation of $D_2$ to $D_3$ is given by Eq. A.10 by replacing $D_0$ with $D_3$, so that the displacement ratio is given by Eq. A.14.

$$DR = \frac{D_2}{D_0} = \frac{D_3}{D_0}\frac{D_2}{D_3} = \frac{(SR + 0.4)^2}{2SR}\frac{1}{TR} \qquad (A.14)$$

The smaller of Eq. A.12 and A.14 is the displacement ratio for the case of $T_0 <$ TG.

Fig. A.2 shows the relationship between the strength ratio, SR, and the

displacement ratio, DR, at some period ratio points. In case of $T_0 > TG$, the displacement ratio is almost unity similar to this study, while it is larger than one in case of $T_0 < TG$. Comparing with the displacement ratio shown in Fig. 4.5, the value calculated by the "equivalent linear method" is smaller than the value obtained from this study for combination of lower strength and period ratios. It follows that the equivalent-linear-model method functions well in regions where the nonlinear displacement response is calculated successfully using the linear model with 2-percent damping and period $T_0$. This study suggests that for combinations of low period and strength ratios, use of the equivalent-linear-model is likely to lead to underestimates of the response displacement.

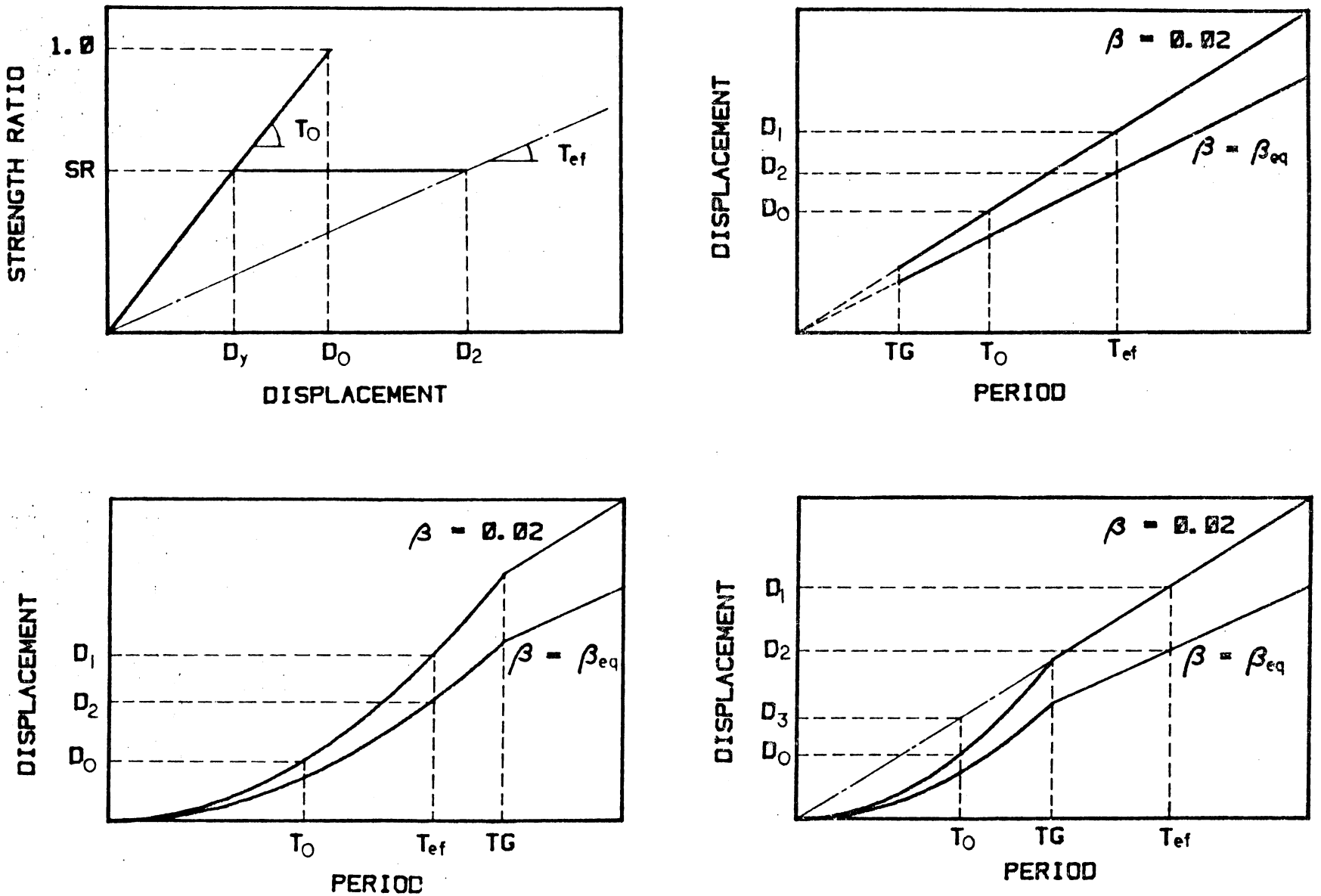


Fig. A.1 Displacement Response Based on "Equivalent Linear Method"

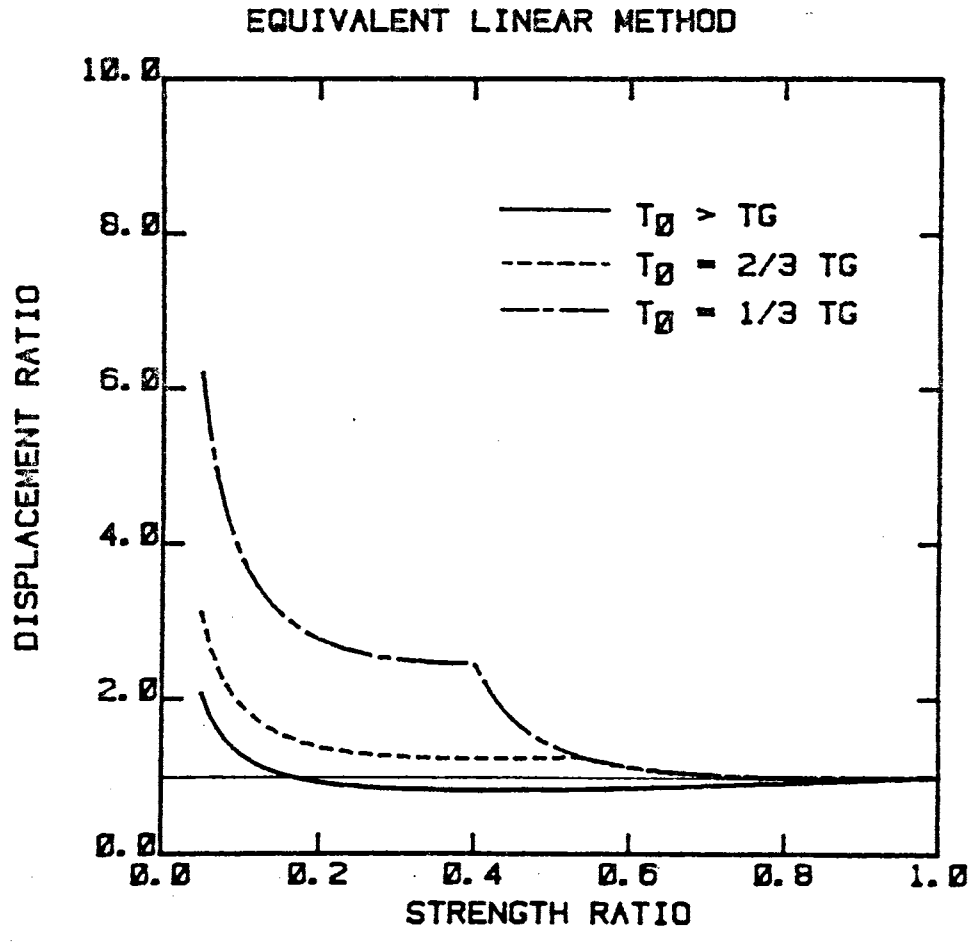


Fig. A.2 Displacement Ratio Based on "Equivalent Linear Method"